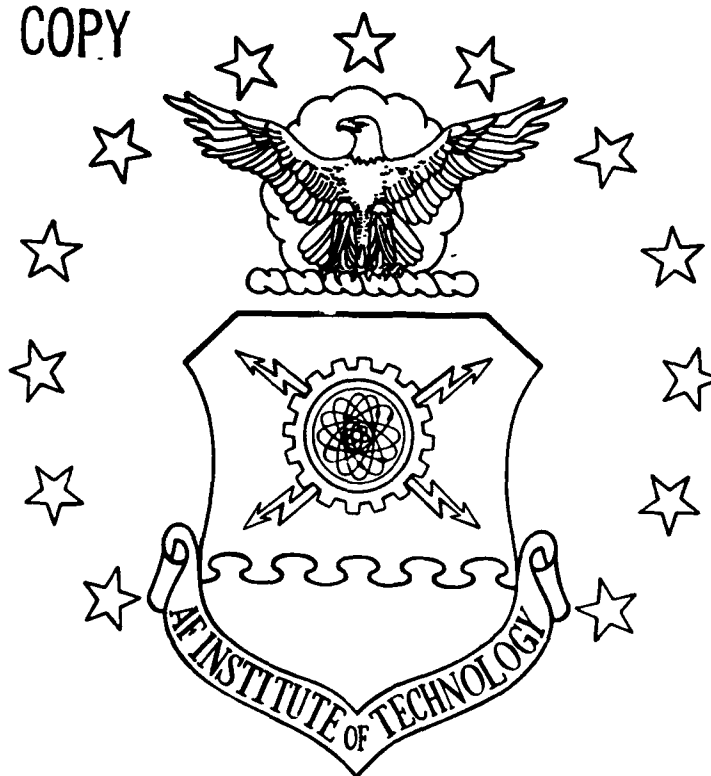


DTIC FILE COPY

(P)

AD-A229 848



DEVELOPMENT OF A PIEZOELECTRIC POLYMER  
FILM PRESSURE TRANSDUCER FOR LOW  
FREQUENCY AND DYNAMIC PRESSURE  
MEASUREMENT

THESIS

Ted H. Halley  
Captain, USAF  
AFIT/GAE/ENY/90D-09

DTIC  
FLECTE  
JAN 08 1991  
S D D

DISTRIBUTION STATEMENT A

Approved for public release  
Distribution Unlimited

DEPARTMENT OF THE AIR FORCE  
AIR UNIVERSITY

**AIR FORCE INSTITUTE OF TECHNOLOGY**

Wright-Patterson Air Force Base, Ohio

91 1 3 192

AFIT/GAE/ENY/90D-09

1

DTIC  
ELECTE  
JAN 08 1991  
S D

DEVELOPMENT OF A PIEZOELECTRIC POLYMER  
FILM PRESSURE TRANSDUCER FOR LOW  
FREQUENCY AND DYNAMIC PRESSURE  
MEASUREMENT

THESIS

Ted H. Halley  
Captain, USAF  
AFIT/GAE/ENY/90D-09

Approval for public release; distribution unlimited

AFIT/GAE/ENY/90D-09

DEVELOPMENT OF A PIEZOELECTRIC POLYMER FILM PRESSURE TRANSDUCER  
FOR LOW FREQUENCY AND DYNAMIC PRESSURE MEASUREMENT

THESIS

Presented to the Faculty of the School of Engineering  
of the Air Force Institute of Technology  
Air University  
In Partial Fulfillment of the  
Requirements for the Degree of  
Master of Science in Aeronautical Engineering

Ted H. Halley. B.M.E.

Captain, USAF

December 1990

Accession For	
NTIS	OSACI
DTIC	TRB
Unannounced	
Justification	
By	
Distribution	
Availability	
Dist	Availability
A-1	

Approval for public release; distribution unlimited



### Acknowledgements

Throughout this effort, many people have provided me with assistance in various ways. Among them has been my thesis advisor, Dr. Paul I. King. His ideas and technical direction were crucial to the progress of this research. I also appreciate the advise given to me by the other members of my committee, Dr. William Elrod and Lt Col Edward Kolesar. I would like to thank Mr. Jay Anderson for his assistance in writing the data collection programs and for his understanding of electronics. I am grateful for the assistance of Mr. Leroy Cannon.

Finally, I want to thank my loving wife, Deborah, for her patience, understanding, encouragement, and typing of this thesis. And to my son, Jonathan, for patiently awaiting the return of his father. Last, but not least, I thank the Lord.

## Table of Contents

Acknowledgements .....	ii
Table of Contents .....	iii
List of Figures .....	v
List of Tables .....	viii
List of Symbols .....	ix
Abstract .....	xiii
I. Introduction .....	1-1
Motivation .....	1-1
Summary of Current Knowledge .....	1-2
Problem Statement .....	1-3
Assumptions .....	1-4
Scope .....	1-5
Approach .....	1-5
Order of Presentation .....	1-6
II. Background .....	2-1
History .....	2-1
Piezoelectricity .....	2-4
Piezoelectric Properties .....	2-10
Piezoelectric Materials .....	2-16
PVDF Pressure Transducers .....	2-21
Summary .....	2-22
III. Experimental Design, Development, and Evaluation Procedures .....	3-1
Reset Circuit Design .....	3-1
Sampling and Reset Operation .....	3-8
Reset Circuit Characteristics .....	3-13
Circuit Implementation .....	3-19
Design Calculations .....	3-22
Time History Reconstruction .....	3-27
Circuit Layout .....	3-28
PVDF Transducer .....	3-29
Test and Evaluation .....	3-32
Time History Reconstruction Test .....	3-37
System Testing .....	3-38
Summary .....	3-41

IV. Experimental Data and Analysis .....	4-1
Introduction .....	4-1
Film Characterization .....	4-1
Circuit Characterization .....	4-3
Time History Reconstruction Process .....	4-8
System Testing .....	4-10
Observations .....	4-16
Conclusion .....	4-17
V. Conclusions and Recommendations .....	5-1
Conclusions .....	5-1
Recommendations .....	5-1
Appendix A: Materials and Equipment .....	A-1
Appendix B: Recommended Materials .....	B-1
Appendix C: Data Collection and Analysis Programs .....	C-1
Appendix D: Sample Cost Data .....	D-1
Appendix E: Digital Filter Data .....	E-1
Appendix F: Sample Time History Reconstruction .....	F-1
References .....	REF-1
Vita .....	VIT-1

## List of Figures

Figure		Page
2-1.	Barium Titanate: A Piezoelectric .....	2-3
2-2.	Concept of a Center of Inversion in a Crystalline Structure. (a) Crystal with a center of Inversion, and (b) Crystal without a center of Inversion .....	2-6
2-3.	Simple Dipole .....	2-7
2-4.	Example of (a) Unstressed and (b) Stressed Crystal with Angular Rotations .....	2-9
2-5.	Axis System for a Piezoelectric Material ....	2-11
2-6.	Types of Deformation, Defining Piezoelectric Constants $d$ and $e$ .....	2-15
2-7.	Piezoelectric Film Dipole Alignment During the Poling Process .....	2-19
2-8.	Crystalline Form of PVDF Before and After Poling .....	2-20
2-9.	Metallized Film Surfaces for Poling and Film Axes .....	2-21
3-1.	Equivalent Electrical Circuit for the Piezoelectric Film as a Charge Generator .....	3-2
3-2.	Equivalent Electrical Circuit for the Piezoelectric Film as a Current Generator .....	3-3
3-3.	Charge Decay of a Piezoelectric Device .....	3-4
3-4.	Equivalent Electrical Circuit for the Piezoelectric Film, Cable, and Amplifier .....	3-5
3-5.	Voltage Follower Circuit .....	3-6
3-6.	Charge Amplifier Circuit .....	3-7
3-7.	Sampling and Reset Operation .....	3-9
3-8.	Charge Amplifier Reset and Sampling Scheme ..	3-10
3-9.	Sampling and Reset Pulse Terminology .....	3-12

Figure		Page
3-10.	Charge Amplifier with a Low-Leakage Reset Switch .....	3-20
3-11.	Charge Amplifier with Instrumentation Amplifier Gain Set to 1000 .....	3-30
3-12.	General Circuit Arrangement Used for System Testing .....	3-31
3-13.	Unity Gain Voltage Follower .....	3-33
3-14.	General Arrangement of the Pressure Transducers Mounted on the Cylinder .....	3-39
3-15.	Cylinder with Pressure Transducers in the Flow Field .....	3-40
4-1.	Charge Decay of the 110 $\mu\text{m}$ Thick PVDF Film ..	4-3
4-2.	Frequency Response of the Charge Amplifier Circuit .....	4-4
4-3.	Sample Reset Period with Switching Noise and Feedback Capacitor Decay .....	4-6
4-4.	Sample DC Offset Data .....	4-7
4-5.	DC Offset as a Function of Input Voltage ....	4-8
4-6.	Reconstructed Sine Wave Showing the Sampled Data and Input Sine Wave .....	4-9
4-7.	PSD of Dynamic Pressure Gage Time History Data .....	4-12
4-8.	PSD of PVDF Film Time History Data .....	4-12
4-9.	Filtered Data for the Dynamic Pressure Gag ..	4-14
4-10.	Filtered and Corrected PVDF Film Gage Data ..	4-14
4-11.	Filtered Dynamic Pressure Gage Data .....	4-15
4-12.	Filtered and Corrected 52 Micron Thick PVDF Film Gage Data .....	4-15
E-1.	Random Noise Signal with Embedded 60 Hz Sine Wave .....	E-6
E-2.	PSD of the Unfiltered Noise Signal .....	E-6



Figure		Page
E-3.	Desired Response of the Stopband Filter ....	E-7
E-4.	Response of the Butterworth Stopband Filter	E-7
E-5.	Response of the Chebyshev Stopband Filter ..	E-8
E-6.	Response of the Butterworth and Chebyshev Low-pass Filters .....	E-8
E-7.	PSD of the 'Noisy' Data Filtered with the Chebyshev Stopband Filter .....	E-9
E-8.	PSD of the 'Noisy' Data Filtered with the Chebyshev Stopband and low-pass Filters ....	E-9

### List of Tables

Table		Page
3-1.	Charge Error for Various Products .....	3-17
3-2.	Film Capacitance and Sensitivity .....	3-24
3-3.	Circuit Time Constant and Charge Development .....	3-25
3-4.	Reset Rate Limits .....	3-26
4-1.	PVDF Film Sensitivity .....	4-2
4-2.	Rise Rates for the Circuit's Various RC Combinations .....	4-5
4-3.	Measured and Specified Bandwidth for AD524BD Instrumentation Amplifier .....	4-7
A-1.	Materials .....	A-1
A-2.	Equipment .....	A-1
B-1.	Recommended Operational Amplifiers .....	B-1
B-2.	Recommended Transistors .....	B-1
D-1.	PVDF Film Transducer Cost .....	D-1
D-2.	Dynamic Pressure Transducer Cost .....	D-1
F-1.	Sample Numbers Used to Reconstruct Sine Data	F-4

### List of Symbols

A . . . . .	Area
A . . . . .	Displacement
A/D . . . . .	Analog to Digital
AFIT . . . . .	Air Force Institute of Technology
c . . . . .	Charge Development Rate
cm . . . . .	Centimeters
C . . . . .	Capacitance
C <sub>circuit</sub> . . . . .	Capacitance of Charge Amplifier
C <sub>f</sub> . . . . .	Capacitance of PVDF Film
C <sub>fb</sub> . . . . .	Feedback Capacitor
°C . . . . .	Degrees Celsius
d . . . . .	Piezoelectric Strain Constant
d . . . . .	Length of Dipole
D . . . . .	Derivative with Respect to Time
D . . . . .	Electric Displacement
e . . . . .	Piezoelectric Stress Constant
E . . . . .	Electric Field
e <sub>0</sub> . . . . .	Electric Field
exp . . . . .	Exponential
f . . . . .	Reset Pulse Rate
f . . . . .	Force
F . . . . .	Force
f <sub>reset min</sub> . . . . .	Minimum Reset Pulse Rate
f <sub>reset max</sub> . . . . .	Maximum Reset Pulse Rate

g . . . . .	Piezoelectric Stress Constant
gm . . . . .	Gram
Hz . . . . .	Hertz (Cycle per second)
i . . . . .	Current
IR . . . . .	Insulation Resistance
kHz . . . . .	Kilo-Hertz
k $\Omega$ . . . . .	Kilo-Ohms
k <sup>2</sup> . . . . .	Electro-Mechanical Coupling Factor
K . . . . .	Piezoelectric Sensitivity
<sup>o</sup> K . . . . .	Degrees Kelvin
l . . . . .	Length
M $\Omega$ . . . . .	Mega-Ohms
MHz . . . . .	Mega-Hertz
mm . . . . .	Millimeters
MOSFET . . . .	Metal-Oxide-Semiconductor Field Effect Transistor
n . . . . .	Number of Samples
mv . . . . .	Millivolt
NaKC <sub>4</sub> H <sub>4</sub> O <sub>6</sub> ·4H <sub>2</sub> O	Rochelle Salt
p . . . . .	Pyroelectric Constant
p . . . . .	Dipole Observation Point
P . . . . .	Polarization
pF . . . . .	Pico-Farad
PSD . . . . .	Power Spectral Density
psi . . . . .	Pounds Force per Square Inch
PVDF . . . . .	Polyvinylidene Fluoride
q . . . . .	Fundament Unit of Charge

$Q$ . . . . .	Transistor
$Q$ . . . . .	Charge
$Q_{min}$ . . . . .	Minimum Detectable Charge
$r$ . . . . .	Distance Between $p$ and the Dipole Center
$\hat{r}$ . . . . .	Polar Coordinate Unit Vector
$R$ . . . . .	Resistance
$R_f$ . . . . .	Resistance of PVDF Film
$R_{fb}$ . . . . .	Feedback Resistor
$R_{off}$ . . . . .	Off Resistance of Reset Switch
$R_{on}$ . . . . .	On Resistance of Reset Switch
sec . . . . .	Second
$S_p$ . . . . .	PVDF Film Sensitivity
$t$ . . . . .	Time
$t$ . . . . .	Thickness
$t$ . . . . .	PVDF Film Thickness
$\Delta T$ . . . . .	Temperature Change
$T$ . . . . .	Time Period
$T_{reset}$ . . . . .	Reset Time Period
$V$ . . . . .	Volts
$V_{min}$ . . . . .	Minimum Detectable Voltage
$V_o$ . . . . .	Output Voltage
$V_{sat}$ . . . . .	Saturation Voltage
$w$ . . . . .	Width
$x$ . . . . .	Strain
$X$ . . . . .	Observation
$X$ . . . . .	Stress

$x_t$	. . . . .	Deflection Along PVDF Film Thickness
$\epsilon$	. . . . .	Dielectric Constant (Permittivity)
$\epsilon_f$	. . . . .	Ferroelectric Axis
$\epsilon_0$	. . . . .	Permittivity of Free Space
$\theta$	. . . . .	Angle Between the Axis of a Dipole and the Radial to the point of Observation
$\hat{\theta}$	. . . . .	Polar Coordinate Unit Vector
$\mu F$	. . . . .	Micro-Farad
$\mu m$	. . . . .	Microns
$\mu s$	. . . . .	Micro-Second
$\pi$	. . . . .	Pi
$\sigma$	. . . . .	Standard Deviation
$\tau$	. . . . .	Time Constant
$\tau_{circuit}$	. . . . .	Time Constant of Charge Amplifier
$\tau_{reset}$	. . . . .	Reset Time Constant
$\phi$	. . . . .	Dipole Potential
$\Omega$	. . . . .	Ohms

Abstract

The purpose of this research was to investigate the characteristics of a small and inexpensive pressure transducer made from piezoelectric film. The pressure transducer was designed to be small and surface mountable so that the pressure distribution could be measured on an aerodynamic body. A charge reset technique was used to overcome the traditional limitations, low frequency measurements and charge decay, of a piezoelectric device. The resulting time history had to be integrated, so a method was developed to integrate the data and remove sources of error. The time history reconstruction technique was tested with a known input and found to accurately reassemble the original input. The piezoelectric film pressure transducer was tested in a flow field along side a commercial pressure transducer. The piezoelectric transducer's frequency response showed agreement with the frequency response of the commercial transducer. Also, the time history response of the piezoelectric transducer gave evidence that low frequency pressure measurements are possible with a piezoelectric pressure transducer.

# **Development of a Piezoelectric Polymer Film Pressure Transducer for Low Frequency and Dynamic Pressure Measurement**

## 1. Introduction

### Motivation

With increasing cost for full-scale testing, more model testing and simulation is being done. Some of the typical wind tunnel data collected are pressure and force measurements. The instrumentation or transducers needed to make these measurements requires input and output through tubing and wires. In some cases, an accurate model may require many transducers. As a result, the transducers occupy a large portion of the model. If high resolution measurements are needed, a model sufficiently large to encompass all the transducers may be bigger than the available testing facility. To accurately obtain data, either the test facility would need to be larger or the model would need to be smaller and more tests run. These facts increase the cost and complexity of testing the model.

If a smaller and cheaper pressure transducer were available, model size and cost could be reduced. Potentially, a small surface mounted pressure transducer could be developed



to cover a model in adequate density to map the entire surface pressure field. To date, no transducer has been developed that is small, surface mountable and inexpensive.

#### Summary of Current Knowledge

In the late 1960's a new piezoelectric polymer film material was developed (1:328). Researchers found that polyvinylidene fluoride (PVDF) could be processed to act as a piezoelectric material. Piezoelectric materials convert physical motion or mechanical stress to an electrical signal; the inverse process can also be realized (1:328-329; 4:22-33). Since pressure exerts a force on the body on which it acts, piezoelectric film could be used as a pressure transducer (5:5). The piezoelectric film would output an electrical signal in response to a pressure.

Since the inception of PVDF piezoelectric film in the late 1960's (1:328-329), it has been used in hundreds of different applications. Piezoelectric film has been used to detect heat, act as a switch, to pick up sound from musical instruments, as a pressure sensor, and even to generate electricity (4:22-33). As a pressure sensor, PVDF film has found applications by organizations such as NASA, the US Navy, German and American researchers, and many others.

In the mid 1970's, the National Bureau of Standards (NBS) developed a PVDF transducer to study impact pressures in car crashes (3). They developed two transducers: 1) a 1 cm diameter sensor and 2) a smaller 2 mm diameter sensor. The

1 cm sensor worked, but it produced extraneous outputs due to film flexing and stretching from an improper mounting technique. The 2 mm diameter sensor provided a signal-to-noise ratio larger than the 1 cm diameter sensor. The study did not proceed with size optimization, but recommended that this area should be investigated.

NASA tested PVDF film for use as a flow diagnostic tool (2). They investigated two sensor configurations, a rigidly mounted one and another mounted over an air filled cavity. Evaluation of the sensors included sensitivity and frequency response and data optimization. The results demonstrated that the rigidly mounted piezoelectric film was affected by structural responses; whereas, the cavity mounted sensor was influenced significantly less by the structure. Overall, the cavity mounted sensor exhibited a broader and more sensitive frequency response.

German researchers used piezoelectric film and multi-sensor piezoelectric arrays to measure forces in flow experiments (6). They developed three arrays for measuring dynamic pressure distributions. The arrays were shaped as strip, raster, and matrix arrays. The researchers conducted wind tunnel and free flight tests using the arrays and found that the array concept worked. Only basic data collection techniques were given; further development would be required to use the arrays on scale models.

Several university researchers developed a new charge readout technique for low-frequency pressure measurements with

piezoelectric film (7). This technique, called the Incremental Readout Algorithm (IRA), operates on a sample-and-reset principle that overcomes the charge decay problem of piezoelectric devices. The IRA allows low-frequency measurements with a high sensitivity and dynamic range. These measurement techniques removed the low-frequency limitations imposed by piezoelectric film pressure transducers.

#### Problem Statement

The purpose of this study was to develop a small and inexpensive pressure transducer from piezoelectric film. The transducer would be capable of measuring static and dynamic pressure. In addition, algorithms and electrical hardware were developed to measure and reduce the data collected from the transducer.

#### Assumptions

The following assumptions were made:

1. Pyroelectric effects are negligible compared to the piezoelectric response, since the operating temperatures are stable and below the non-linear temperature region of the piezoelectric film.
2. All surface stress effects are small and can be ignored because the film is rigidly attached to the model's surface.

### Scope

The scope of this study was to design, develop, and evaluate performance of a piezoelectric film pressure transducer. This process included developing digital circuits to collect and measure the transducer's response. Algorithms were developed to reduce the data to a practical (useable) format. A method was developed to apply the PVDF film to a body so that surface pressure could be measured. The research did not include film size and shape optimization, nor were different film adhesives addressed.

The study used commercially available components and did not develop any new items. Using existing resources helped keep the design simple and inexpensive. The PVDF film was modified, but its basic physical and electrical structure was not changed.

The project concluded when a pressure measurement was obtained with the piezoelectric transducers mounted on a body.

### Approach

The transducer development was divided into three phases which included the: 1) development of a charge amplifier circuit with a reset capability; 2) optimization of the charge amplifier to minimize DC offset and noise; and 3) performance evaluation of the transducer in a dynamic situation by comparing it to a known transducer. Each phase was subdivided into incremental steps, they are listed below:

1. Phase 1 - Development of a charge amplifier with reset capability.
  - o Develop the electronics required to discharge the piezoelectric film charge.
  - o Develop software to reduce the data.
  - o Refine the hardware, software and procedures to obtain accurate and repeatable data.
2. Phase 2 - Optimization of the charge amplifier circuit.
  - o Minimize charge leakage.
  - o Minimize DC offset and noise.
  - o Determine the upper and lower reset rate limits.
  - o Characterize the charge amplifier response.
3. Phase 3 - Development of a film application for pressure measurement.
  - o Determine a way to bond the PVDF film to a body.
  - o Test the film's capability to measure pressure.

#### Order of Presentation

Background information on piezoelectricity and piezoelectric materials are presented in Chapter II. The third chapter presents the details of the reset scheme, time history reconstruction technique, and testing. Chapter IV discusses test and evaluation results. The last chapter, Chapter V, summarizes the results and recommends areas of further research and development on the piezoelectric film pressure transducer.

## 11. Background

### History

A strange phenomenon was long known by the people in Ceylon and India. When a tourmaline crystal was thrown into a fire, it would attract the hot ashes and repel them when it cooled. In 1703, Dutch traders brought a "Ceylon Magnet" back from Ceylon to Europe (8:1). Linnaeus gave the scientific name *Lapis electricus* to this phenomenon in 1747 (8:1). In 1756 Aepinus investigated this effect and noted the electrical property of opposite polarities in the heated tourmaline crystal (8:1). Another investigator, Brewster, assigned the term "pyroelectricity" to this phenomenon after he had observed it in tourmaline and other crystals (8:1). The term "pyro-" comes from the Greek word meaning "fire", and the pyroelectric effect manifests the production of electricity in a material caused by the thermal stresses due to temperature changes.

Other investigators continued to observe the pyroelectric effect of crystals. But in 1880, the Curie brothers, Pierre and Jacques, discovered that when certain crystals were compressed in a particular direction, a charge accumulation results (8.2). The Curie brothers wrote of their discovery in a paper saying:

Those crystals having one or more axes whose ends are unlike, that is to say, hemihedral crystals with oblique faces, have the special physical property of giving rise to two electric poles of opposite signs at the extremities of these axes when they are subjected to a change in

temperature: this is the phenomenon known under the name of pyroelectricity. We have found a new method for the development of polar electricity in these same crystals, consisting in subjecting them to variations in pressure along their hemihedral axes. (8:2)

Following their initial discovery, the Curies observed the "polar electric" effect in other crystals such as : zinc blende, sodium chlorate, boracite, quartz, calamine, topaz, tartaric acid, cane sugar, and Rochelle salt (8:3). Immediately, a lot of interest was aroused in the scientific community. One of the interested parties, Hankel, proposed the name "piezoelectricity", since he thought the new discovery followed its own unique laws and was unrelated to pyroelectricity (8:3). From the Curies' discovery, arose both the name and field of piezoelectricity. Similar to the term "pyro-", "piezo-" means "to press" in the Greek language and the piezoelectric effect is caused by applying pressure to the material. In 1881, the converse of piezoelectricity was proposed by Lippman, and the Curies' verified this the same year (8:4).

Many others began to investigate the piezo- and pyro-electric phenomena. Among the most noted was Woldemar Voight, who based his theory on the thermodynamic principles of Lord Kelvin (8:5). In 1910, Voight published a work called *Lehrbuch der Kristallphysik*, which became a standard reference for piezoelectric researchers (8:5). His work identified 32 crystal classes that could display piezoelectric properties;

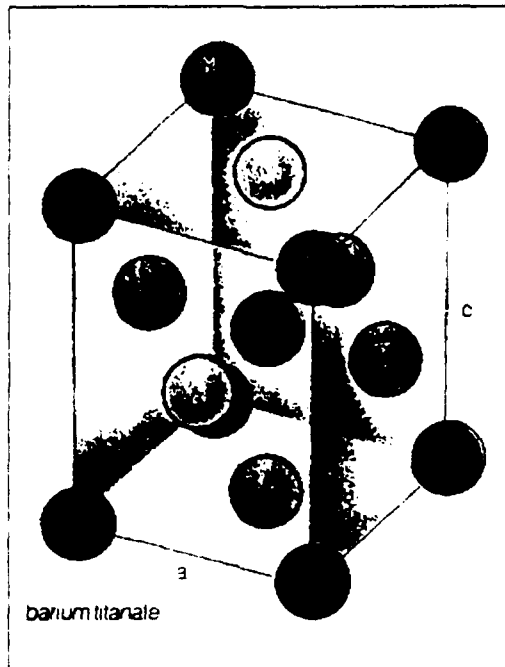


Figure 2-1. Barium Titanate: A Piezoelectric Crystal (9:1758).

and of the 18 piezoelectric coefficients, he showed which ones had nonzero values (8:5).

For the next three decades, piezoelectricity was confined to research, with no practical application. In France, at the beginning of World War I, a scientist by the name of Longevin developed a means to piezoelectrically exciting quartz plates. These plates could be used as high frequency emitters and receivers of sound waves in water. Longevin and others had developed an echo method, SONAR, which could locate objects underwater and map the contour of the ocean floor (8:5). Thus, Longevin became the father of ultrasonics, which is widely used today.

During World War I, research discovered many uses of piezoelectricity and the properties of crystals. Some of the



more useful purposes were; Rochelle salt crystals used for underwater signaling and quartz used for precision clocks (8:6). Researchers at MIT, in the late 1930's found that certain ceramics such as barium titanate (see Figure 2-1) and lead zirconate titanate (PZT) could be polarized to respond piezoelectrically (7:1). Researchers continued to investigate other piezoelectric materials such as ceramics, crystals, organic materials, human tissue, and bone (7:1).

In the late 1960's, a Japanese researcher, Kawai, found that a polarized polymer, polyvinylidene difluoride (PVDF), developed a much greater piezoelectric charge compared to other polymers (7:1, 1:328). This began the vast field of development of piezoelectric film.

#### Piezoelectricity

Before delving into a discussion of the fundamentals of piezoelectricity, two definitions by W.G. Cady are useful. Cady defines the piezo- and pyro- effects as follows:

Piezoelectricity is electric polarization produced by mechanical strain in certain crystals, the polarization being proportional to the amount of strain and changing sign with it. The reverse is also true; that is...an electrical polarization will induce a mechanical strain in piezoelectric crystals.

Pyroelectricity is electric polarization induced by thermal absorption in certain crystals, the polarization being proportional to the level of thermal change (8:4).

Piezoelectric Effect. The piezoelectric effect is only found in materials that have "ionic" bonds (atoms that are arranged in positive and negative pairs called dipoles)

(9:1757). When pressure is applied to the material, the dipoles are distorted or polarized. This behavior causes a separation about the center of inversion which creates an electric field (see Figure 2-2). The center of inversion, or geometric center gives rise to the property of piezoelectricity. If a crystalline material has perfect symmetry, no combination of uniform stresses will produce the distortion required for the piezoelectric effect. A common crystal with a perfectly symmetrical structure is sodium chloride (or salt), each positive charge is surrounded symmetrically by a negative charge. Barium titanate (see Figure 2-1) possesses an asymmetrically crystalline structure and is piezoelectric. It is one of the 20 (of the 32 overall) crystal classes that possess piezoelectric properties due to the asymmetries (9:1757).

Dipoles. The electric dipole helps explain why piezoelectricity occurs on a microscopic basis. An electric dipole consists of two point charges of equal magnitude, but different sign, which are spaced at a fixed distance (10:132).

Figure 2-3 shows two equal and opposite fundamental units of charge  $q$  spaced a distance  $d$  apart with a dipole strength of  $pq$  (10.132). The electrical potential  $\phi$  at an arbitrary point  $p$ , caused by  $+q$  and  $-q$  are given in equations 2-1 and 2-2.

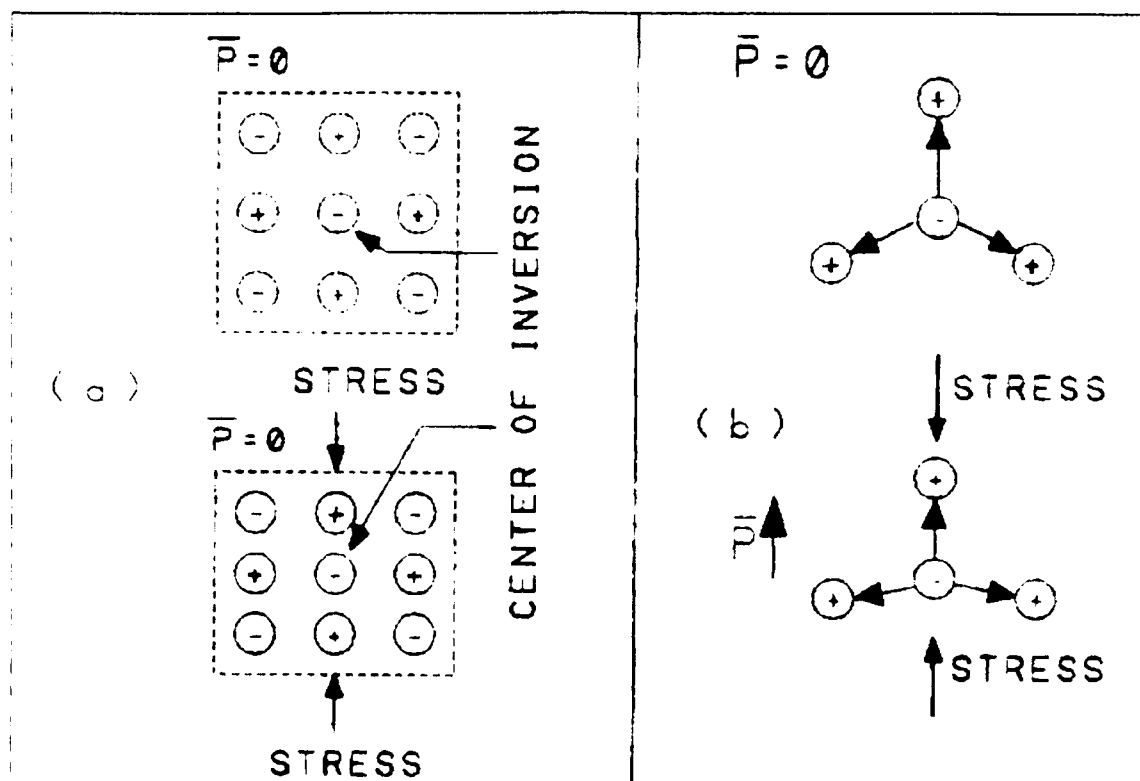


Figure 2-2. Concept of a Center of Inversion in a Crystalline Structure. (a) Crystal with a Center of Inversion, and (b) Crystal without a Center of Inversion (24:407).

$$V_1 = \frac{+q}{4\pi\epsilon_0 r_1} \quad (2-1)$$

$$V_2 = \frac{-q}{4\pi\epsilon_0 r_2} \quad (2-2)$$

Where  $\epsilon_0$  is the permittivity of vacuum. The total electric potential  $\phi$  at  $p$  is the superposition of the two potentials caused by the individual positive and negative charges. That is,

$$\phi = V_1 + V_2 = \frac{q}{4\pi\epsilon_0} \left( \frac{1}{r_2} - \frac{1}{r_1} \right). \quad (2-3)$$

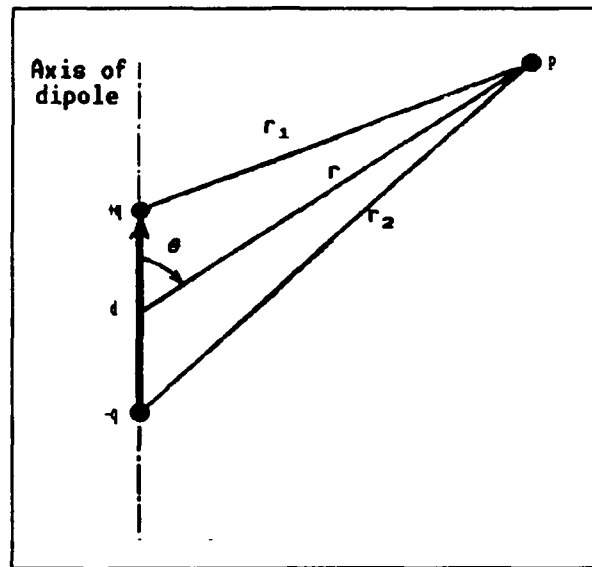


Figure 2-3. Simple Dipole (16).

If  $r$  is large compared to  $d$ , the distances from  $q$  to  $p$  can be simplified with the following approximations (10.133). That is,

$$r_1 = r + \left(\frac{d}{2}\right) \cos \theta \quad (2-4)$$

$$r_2 = r - \left(\frac{d}{2}\right) \cos \theta . \quad (2-5)$$

The total potential at point  $p$  becomes:

$$\phi = \frac{q}{4\pi\epsilon_0 r^2} \left( \frac{d \cos \theta}{1 - \left(\frac{d \cos \theta}{2r}\right)^2} \right) . \quad (2-6)$$

Since  $r$  was assumed to be much greater than  $d$ , the denominator can be approximated with the following form:

$$\phi = \frac{q d \cos \theta}{4\pi\epsilon_0 r^2} . \quad (2-7)$$

If  $qd$  is defined as the dipole moment  $P$  ( $P = qd$ ), the numerator of equation 2-7 can be written as a dot product; that is,  $qdcos\theta = P \cdot r$  (10.133).

The electric field  $E$  of the dipole is obtained from the relation  $E = -\nabla\phi$ . Thus, the general form of dipoles can be written in vector form as shown in equation 2-8. That is,

$$E = -\nabla\phi = -\nabla\left(\frac{P \cdot r}{4\pi\epsilon_0 r^3}\right). \quad (2-8)$$

To consider a simple example in a crystal, the electric field is expressed below in polar coordinates (16:36). That is,

$$E = \frac{qd}{2\pi\epsilon_0 r^3} \cos\theta \hat{r} + \frac{qd}{4\pi\epsilon_0 r^3} \sin\theta \hat{\theta}. \quad (2-9)$$

In an equilibrium or unstressed state (see Figure 2-4a), there are no deflections or electric fields. All dipoles are in the same plane, equidistant, and symmetrical about the negative charge,  $-q$ . The total electric field,  $E_{total}$ , is the sum of all contributions to the field (11:366). That is,

$$E_{total} = E_1 + E_2 + E_3. \quad (2-10)$$

Since the dipoles are symmetrical and equal in magnitude about  $-q$ , all the dipoles contribute equally and cancel their overall effect. Thus,

$$E_1 = E_2 = E_3 \text{ and } E_{total} = 0. \quad (2-11)$$

When a stress is applied, as shown in Figure 2-4b, the noncentral ions displace angularly about the center, creating

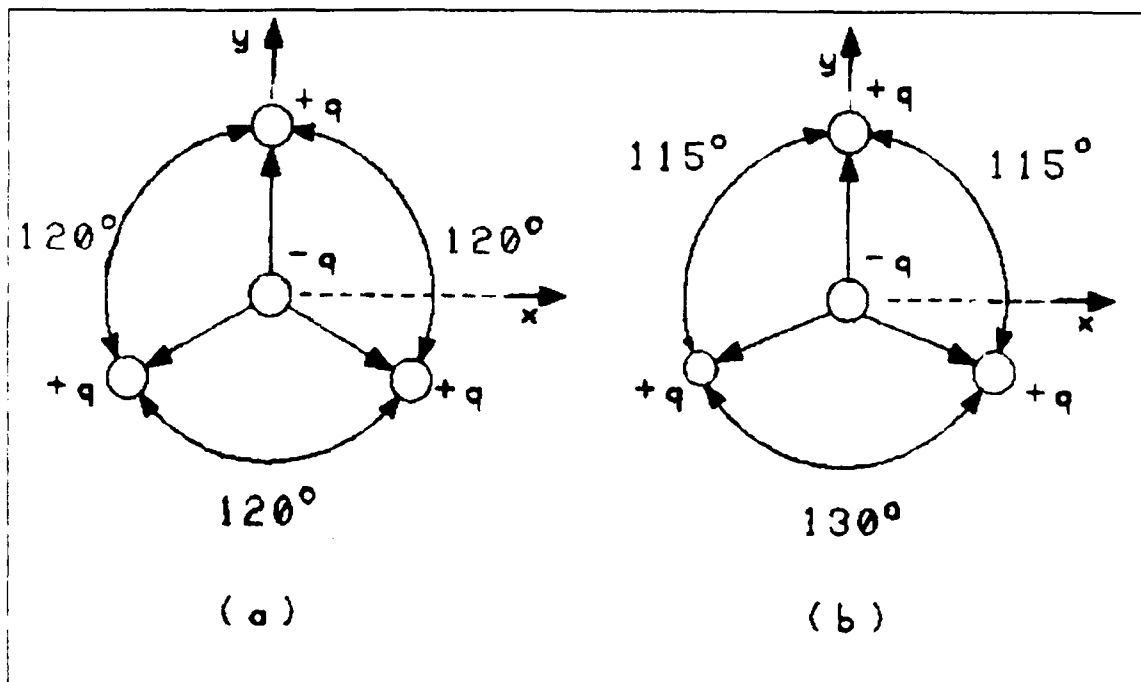


Figure 2-4. Example of (a) Unstressed and (b) Stressed Crystal with Angular Rotations.

an electric field. In this case, the individual contributions are unequal. That is,

$$E_1 \neq E_2 \neq E_3 . \quad (2-12)$$

The resulting expression for  $E_{total}$  is shown below. That is,

$$E = E_1 + E_2 + E_3 = \frac{qd}{4\pi\epsilon_0} (0.155) \theta \quad (2-13)$$

where  $d$  is the radial distance from  $-q$  to the positive charges, and  $r$  is the distance to an arbitrary observation point.

Though the microscopic perspective contributes an insight into the cause of the piezoelectric effect, it does not adequately describe the microscopic behavior of crystals. Cady states the limitations of this atomic theory. That is,

In spite of the fact that molecular or atomic theories of piezoelectricity began to appear very soon after the Curies' discovery, a satisfactory theoretical treatment of the phenomenon can hardly be said to have passed the initial stage. The resources of modern lattice dynamics are still unequal to the task of predicting anything better than a rough approach to the order of magnitude of the piezoelectric effect, even for the simplest structures. Incomplete though the story is, however, it offers much of interest on both the theoretical and the experimental side. (8:731)

### Piezoelectric Properties

The microscopic perspective of the piezoelectric effect helps to explain why a charge develops in a piezoelectric material, but it does not explain the macroscopic or the observable properties. Generally, a book would need to be written to completely describe all the properties and their applications; only a brief overview of selected ones will be given.

Piezoelectric materials generate a charge when they are deformed. This effect is reversible because if a charge is applied to the material, it will respond with a mechanical deformation (12:266). The electro-mechanical energy conversion principle is very useful, and it is the basis of many instruments that measure force, pressure, and acceleration (12:267).

Directionality. Piezoelectric materials display anisotropic behavior, because they respond differently, depending upon the material's orientation. The electrical and mechanical responses differ according to the axis that the

electric field or mechanical stress or strain is applied (5:9). In making any calculations, the material's directionality must be accounted for.

The sign convention used throughout this development is shown in Figure 2-5. The material's length  $l$ , corresponds to the 1-axis, 2 to the width  $w$ , and 3 to the thickness  $t$  (5:9). Double subscripts are used on numerical physical constants (presented in the following sections) to describe the occurring phenomenon (5:9; 12:267). The first subscript identifies the axis or direction of the electrical effect. The second subscript refers to the axis of the mechanical effect (12:267).

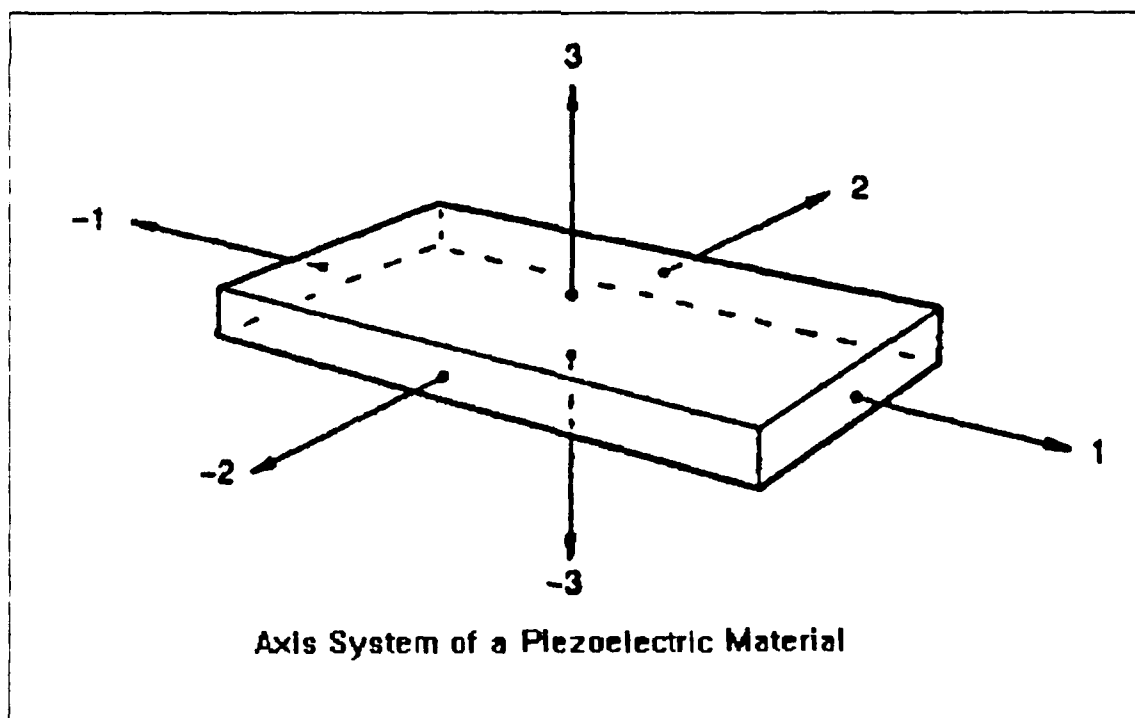


Figure 2-5. Axis System for a Piezoelectric Material (5:9).

Tensile forces or strains imply positive mechanical action, and compression is negative. Positive electrical



effects result in an increase in the charge polarization; negative electrical effects cause a decrease in the charge polarization (5:9).

Curie Temperature. The Curie temperature is the temperature above or below which the dipoles that compose electrets become randomly oriented (12:267). As a result, the material loses its piezoelectric property. If the material's temperature exceeds the Curie point, it will lose its piezoelectric effect; upon cooling, it returns to being piezoelectric only if it is poled again. Thus, the useful range of a piezoelectric material is below the Curie point (9:1758). The Curie point can also be changed in some materials by changing their chemical composition; this feature results in a more satisfactory Curie temperature (9:1758).

Capacitance. Typically, piezoelectric materials are inherently capacitive. In use, metal electrodes are deposited on two opposing faces of the material and wires are attached to access the developed charge. Piezoelectric materials are insulators and the electrodes become capacitor plates. Mechanical distortions result in a charge which in turn appears as a voltage between the electrodes. The resulting voltage follows the law for capacitors shown in equation 2-14.

$$E = \frac{Q}{C} \quad (2-14)$$

where E is the voltage, Q is the charge, and C is the capacitance.

Electromechanical Coupling Factor. The coupling factor  $k^2$  defines a piezoelectric material's ability to exchange electrical and mechanical energy, and the reverse (5:18). For example,  $k^2$ , would describe the electrical energy brought about by a mechanical strain divided by the input electrical energy (5:18). The following relations describe  $k^2$ :

$$k^2 = \frac{\text{mechanical energy converted to electrical energy}}{\text{input mechanical energy}} \quad (2-15a)$$

$$k^2 = \frac{\text{electrical energy converted to mechanical energy}}{\text{input electrical energy}} \quad (2-15b)$$

Mechanical Constants. There are three main types of mechanical constants for piezoelectric materials. They are the strain constant,  $d$ , the stress constant,  $g$ , and a related stress constant,  $e$ . The  $g$  constant gives the ratio of the electric field generated, under open circuit conditions, to the stress that is applied along a particular axis. The same constant,  $g$ , also gives the proportional amount of strain induced under stress free conditions, along an axis compared to the electrical charged applied per unit area of the electrode (5:17). Equations 2-16a and 2-16b show  $g$  in equation form, where  $D$  is the electrical displacement,  $E$  the electric field,  $X$  the stress, and  $x$  the strain.

$$g = \frac{\text{electrical field developed}}{\text{applied mechanical stress}} = \left( \frac{\partial E}{\partial X} \right)_D \quad (2-16a)$$

$$g = \frac{\text{strain developed}}{\text{applied charge density}} = \left( \frac{\partial x}{\partial D} \right)_X \quad (2-16b)$$

The strain constant,  $d$ , gives the change in the piezoelectric material dimensions, in all three axes, when electric field is applied to the material in a stress free state (5:17). Thus,  $d$  gives the proportionality constant of the stress free dimensional change relative to the field applied. Additionally,  $d$ , (see Figure 2-6) expresses the ratio of the short circuit charge per unit area of the electrode to the stress applied along a particular direction (5:17). These relationships are expressed in the following equations:

$$d = \frac{\text{electrical charge density developed}}{\text{applied mechanical stress}} = \left( \frac{\partial D}{\partial X} \right)_E \quad (2-17a)$$

$$d = \frac{\text{strain developed}}{\text{applied electrical field}} = \left( \frac{\partial x}{\partial E} \right)_X \quad (2-17b)$$

The constants can be calculated from both relationships provided the dielectric constant,  $\epsilon$ , of the material is known. That is,

$$C = \frac{ewl}{t} \quad (2-18)$$

where  $w$  is the width,  $t$  is the thickness,  $l$  is the length, and  $C$  is the capacitance. Finally,

$$g = \frac{\text{electrical field developed}}{\text{applied mechanical stress}} = \frac{e_0 wl}{tf} = \frac{e_0 C}{ef} = \frac{Q}{ef} = \frac{d}{e} \quad (2-19)$$

or

$$d = eg \quad (2-20)$$

where  $e$  ▲ electrical field developed  
 $f$  ▲ applied force  
 $Q$  ▲ charge developed(12:268).

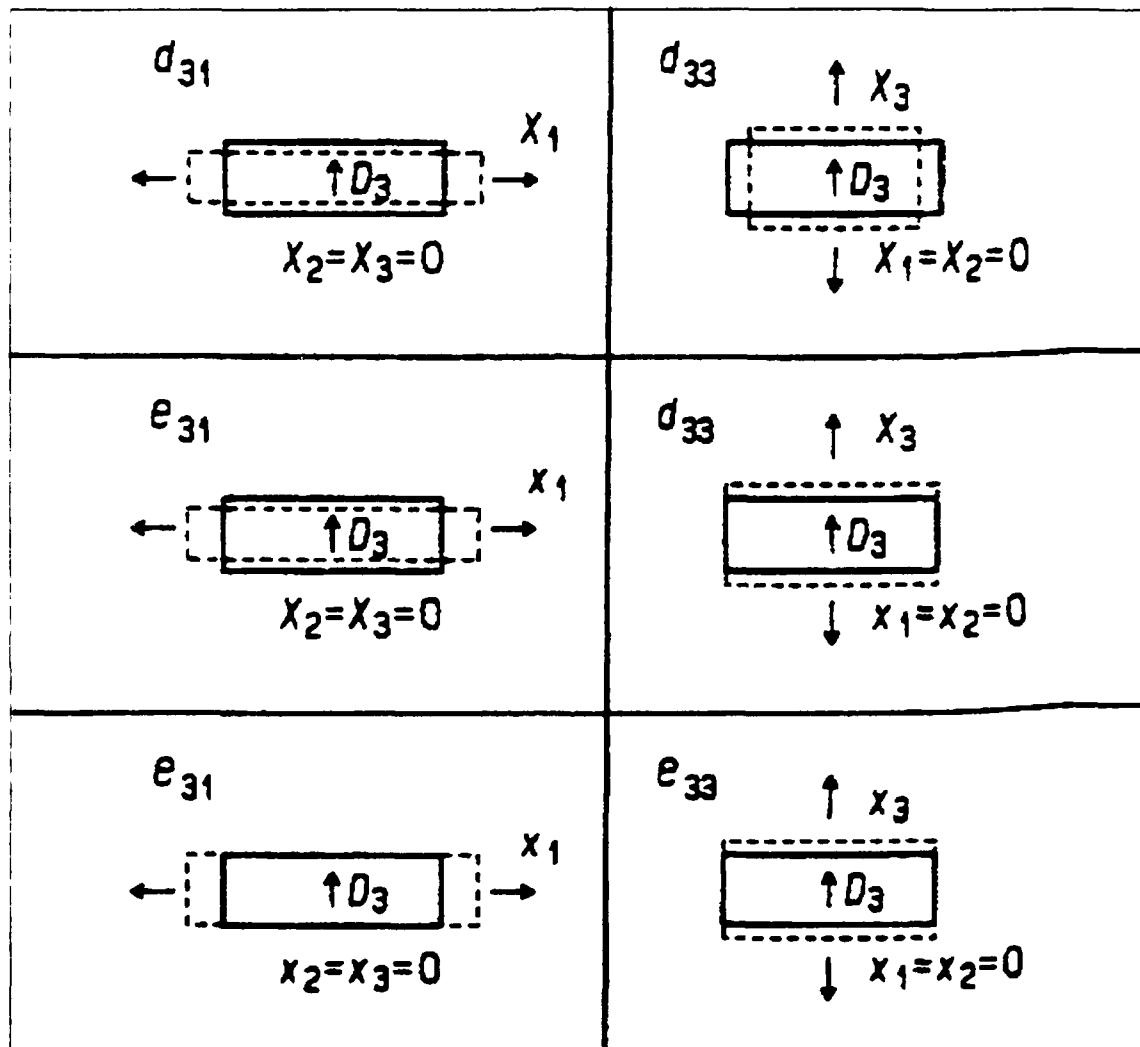


Figure 2-6. Types of Deformation, Defining Piezoelectric Constants  $d$  and  $e$  (22:378).

The other related stress constant,  $e$ , defines another relationship between the electric field and the stress and strain. Figure 2-6 gives the definition of  $e$  graphically, and the equations forms are shown below. That is,

$$e = \frac{\text{mechanical stress developed}}{\text{applied electrical field}} = \left( \frac{\partial X}{\partial E} \right)_x \quad (2-21a)$$

$$e = \frac{\text{electrical charge density developed}}{\text{applied strain}} = \left( \frac{\partial D}{\partial x} \right)_E \quad (2-21b)$$

Pyroelectric Constant. Some materials that are piezoelectric also exhibit pyroelectric behavior. Pyroelectric materials absorb thermal energy and expand, and the reverse. The dimensional changes result in charge being accumulated (5:19). The current that is developed is proportional to the temperature change rate. The pyroelectric constant  $p$  relates the charge developed ( $Q$ ) to the temperature change ( $\Delta T$ ) and the material's cross-sectional area ( $A$ ). This relationship is defined in equation form as:

$$Q = p \cdot \Delta T \cdot A. \quad (2-22)$$

The voltage ( $V$ ) due to the pyroelectric effect is proportional to the charge developed ( $Q$ ) divided by the material's capacitance ( $C$ ) (5:19). That is,

$$V = \frac{Q}{C} = \frac{p t (\Delta T) A}{\epsilon A} = \frac{p t (\Delta T)}{\epsilon}. \quad (2-23)$$

The variables represent the same quantities as defined in the previous examples.

#### Piezoelectric Materials

There are two main groups in which piezoelectric materials can be classified: natural (quartz, Rochelle salt) and

synthetic. The synthetic group can be further divided into crystals (lithium sulphur, ammonium dihydrogen phosphate) and polarized ferroelectrics. The polarized ferroelectrics are typically a ceramic, such as barium titanate, or an organic polymer like polyvinylidene fluoride (PVDF).

Rochelle Salt. Rochelle salt, (sodium potassium tartrate), which has a chemical formula of  $\text{NaKC}_4\text{H}_4\text{O}_6 \cdot 4\text{H}_2\text{O}$ , has an extremely high coupling factor,  $k$ , along its ferroelectric axis,  $\epsilon_1$  (17:17). The piezoelectric efficiency of Rochelle salt is only useful between its lower and upper Curie points ( $255^\circ$  to  $297^\circ$  K) (17:17). Outside these temperatures, the piezoelectric effect is greatly reduced. However, as pressure is applied to Rochelle salt, its upper and lower Curie points increase linearly (19:28).

Rochelle salt is environmentally sensitive, since it contains a significant amount of water (18:115). Mason, in his book on ultrasonics, discusses Rochelle salt's environmental limitations. He says that,

...if the humidity of the surrounding atmosphere is below 35 per cent at  $25^\circ$  C, the water vapor pressure of the crystal is greater than the vapor pressure of water surrounding atmosphere and the crystal will lose water and dehydrate...Above 85 per cent humidity, the crystal will absorb water from the atmosphere on its surface and will slowly dissolve if kept in such an atmosphere. (18:117)

Thus, the uses of Rochelle salt are very limited environmentally. It finds its primary use as a low frequency transducer (18:114).

Quartz. Quartz has a low efficiency of mechanical to electrical conversion (electromechanical coupling factor,  $k^2$ ). It also produces only a small charge for a given applied load (9:1758). Despite a low coupling factor, quartz has found use as an excellent oscillator due to its very stable resonant frequency (9:1758; 18:78).

Ceramics. A ceramic consists of a conglomeration of small crystals with randomly oriented axes, and no inherent piezoelectric properties. Ferroelectric ceramics must be artificially given the piezoelectric effect through 'poling' (12:267).

This process can be described as:

... the polarity needed to impart piezoelectric properties can be given to an originally isotropic polycrystalline ceramic, more or less permanently, by temporary application of a strong electric field. This process, called "poling", is analogous to the magnetizing of a permanent magnet. (15:1)

Typically 'poling' is done at high voltages (about 10 KV) while the material is heated above its Curie point, then allowed to cool. This procedure permanently orients the dipoles in the same direction, making it piezoelectric (12:267). Two of the more common piezoelectric ceramics are barium titanate (Figure 2-1) and lead zirconate titanate (PZT).

Organic polymers. Organic polymers as piezoelectric materials resulted from research by Kawai of Japan (21:975). He found that "the polarized homo polymer of vinylidene fluoride (PVDF) developed far greater piezoelectric activity

compared to any other synthetic or natural polymer" (5:1). PVDF and other polymers must first be poled before they exhibit piezoelectric behavior.

Poling. Polymers can be poled using two techniques: 1) application of a large DC electric field or 2) mechanical drawing. The electric field method is the same procedure that is used with ceramics (see Figure 2-7). The mechanical drawing reorients the polymer molecules so that its dipoles are uniaxial oriented, but not necessarily all pointing the same direction (22:326).

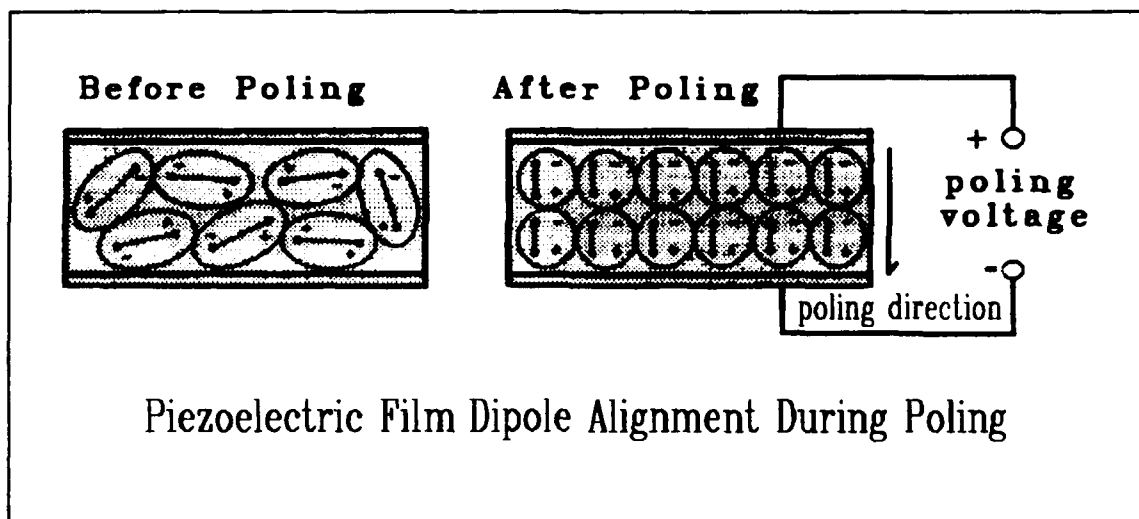


Figure 2-7. Piezoelectric Film Dipole Alignment During the Poling Process (5:5).

PVDF Fabrication. Of the many available polymers (such as vinylidene fluoride (VDF), vinylidene cyanide (VDCN), and polyvinylidene fluoride (PVDF)), the most popular one is PVDF. PVDF is a semi-crystalline polymer which has long chains of repeating units of  $\text{CH}_2\text{-CF}_2$  (5:5). In this (monomer) form, more than 90% of the  $\text{CH}_2\text{-CF}_2$  molecules are in a head-to-tail form, which accounts for its high dipole moment (5:5).



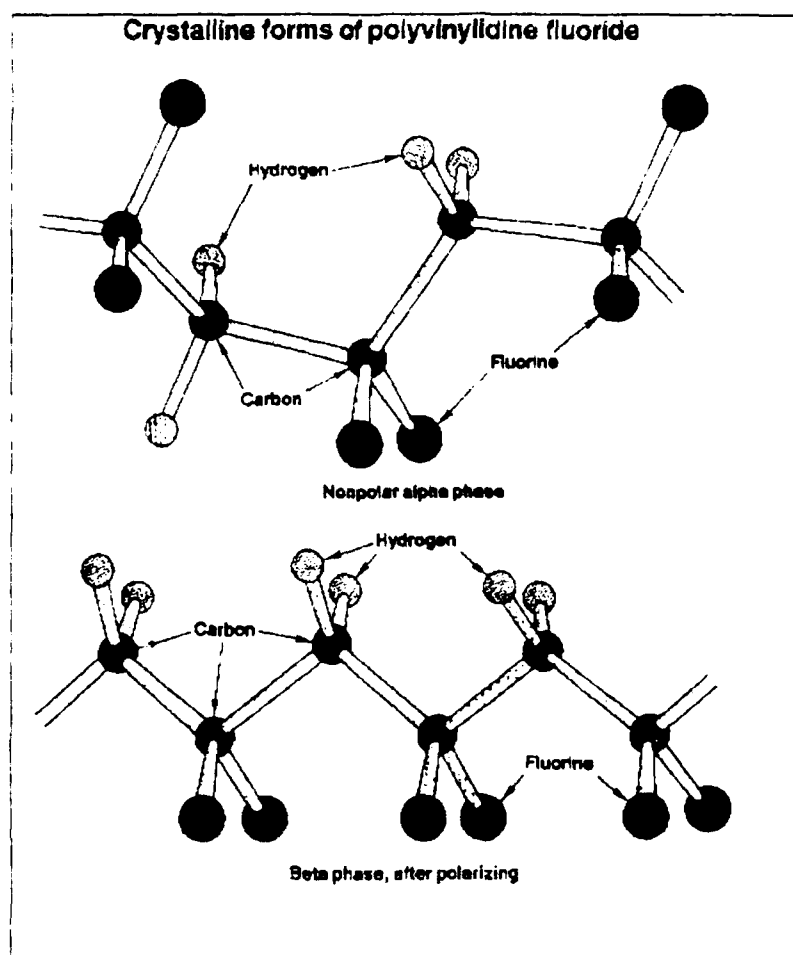


Figure 2-8. Crystalline Form of PVDF Before and After Poling (23-3).

There are three crystalline phases of PVDF: 1) alpha, 2) beta, and 3) gamma. The alpha-phase results after the polymer has cooled from the melt (see Figure 2-8); this phase is non-polar (5:5). To make PVDF piezoelectric, it first must be stretched. This stretching, at temperatures below the melting point, gives rise to the beta form which has carbon chains in parallel strips and planes with pairs of hydrogen and fluorine atoms randomly distributed about the carbon chain axis (23:3). Before poling (which gives the gamma-phase), both surfaces of the beta-phase film must be metallized (see Figure 2-9) to

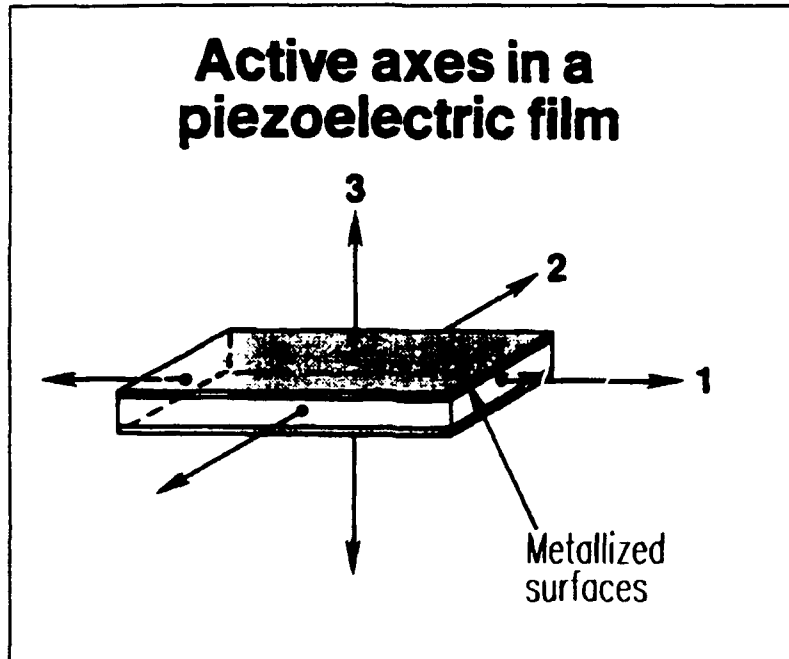


Figure 2-9. Metallized Film Surfaces for Poling and Film Axes.

create electrodes to aide in poling (23:3). In poling (see Figure 2-7), the hydrogen atoms rotate to a permanent position toward the high-potential side of the carbon atoms; and the fluorine atoms rotate to the low potential side of the carbon (see Figure 2-8) (23:3).

#### PVDF Pressure Transducers

A piezoelectric film pressure transducer has been developed and used in dynamic situations (3). It is inherently smaller and cheaper than traditional pressure transducers which use piezoelectric crystals or strain gage bridges. In general, it possesses the following advantages relative to conventional piezoelectric materials (5:9):

1. It has a broad frequency response (DC to 10 Mhz).
2. The film has a vast dynamic response ( $10^1$  to  $10^6$  psi) so it could detect almost any pressure.

3. The high electrical impedance of the film (greater than  $4 \times 10^{12}$  ohms) closely matches the impedance of CMOS devices, which reduces the electrical current leakage.
4. The film is thin and flexible so that it can be cut, formed, and bonded to complex or simple surface shapes.
5. The high mechanical strength of the film allows it to be used in extreme environments, such as shock transition zones.
6. Because of its high elastic compliance, it accurately responds to pressure.
7. The costs to fabricate and produce a film transducer are relatively low.

These characteristics of piezoelectric film make it a viable alternative for use as a pressure transducer.

In spite of its many desirable characteristics, piezoelectric film does possess some inherent disadvantages as a pressure transducer. Since piezoelectric film is capacitive, its response to a pressure decays, which make low frequency measurements difficult. Piezoelectric film is pyroelectric so it is sensitive to temperature changes. The low Curie point of the film limits its use to below  $100^{\circ}$  C. Any surface stresses induced by the surface the film was mounted to, would be transmitted to the film as well as external pressure stresses. Exposed electrodes are sensitive to electromagnetic radiation. This sensitivity would add error to a pressure measurement. Despite these limitations, most of the film's ill effects can be minimized or eliminated.

#### Summary

The piezoelectric effect has long been known, but not understood until recent times. This property occurs naturally

in some crystals, and it can be artificially induced in materials such as ceramics and polymers through 'poling'. Piezoelectric materials exhibit many properties, in the case of a pressure transducer, the ability to convert a force to an electrical signal makes piezoelectric transducers possible. Of the many piezoelectric materials, PVDF film has the potential to be very useful for pressure measurements. It would be small and relatively inexpensive compared to conventional piezoelectric transducers. Though PVDF does have limitations as a pressure sensor, most of these can be reduced or eliminated to make it a promising new type of transducer.

### III. Experimental Design, Development, and Evaluation

#### Procedures

To use piezoelectric film as a low-frequency and dynamic pressure transducer, several techniques must be developed (sampling-and-reset and time-history reconstruction). This task involves designing and developing an analog circuit to discharge the accumulated charge of the piezoelectric film. Also, a technique to identify reset pulses and to accurately reconstruct the data must be developed.

#### Reset Circuit Design

There are several aspects that must be considered in order to properly design a reset circuit. The equivalent electrical circuit of the film needs to be established to ensure an accurate interface. Since piezoelectric film manifests electrical capacitance and its charge decays, this property needs to be minimized. The reset circuit must have a response sufficiently broad to respond to the desired frequency range. Electrical components that are interfaced must have matched impedances to minimize charge leakage and sources of electrical noise.

Piezoelectric Film Equivalent Circuit. Piezoelectric film can be represented as a charge or current generator (as shown in Figure 3-1) with film capacitance,  $C_f$ , and film resistance,  $R_f$  (5:27). The piezoelectric film capacitance,  $C_f$ , is proportional to the electrode area and inversely proportional to the film's thickness (5:27). The charge generated

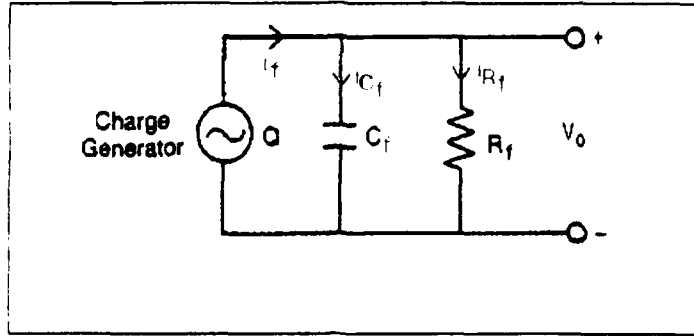


Figure 3-1. Equivalent Electrical Circuit for the Piezoelectric Film as a Charge Generator (5:27).

by the film is proportional to the applied force or induced displacement, and it can be expressed as:

$$Q = d_t * F = e_t * x_t \quad (3-1)$$

where  $d_t$  and  $e_t$  are piezoelectric constants,  $F$  is the force, and  $x_t$  is the deflection along the film's thickness (5:27; 12:269). In order to consider a more useful form, the charge generator can be converted to a current generator as illustrated in equation 3-2 and depicted in Figures 3-1 and

$$i_f = \frac{dQ}{dt} = e_t \left( \frac{dx_t}{dt} \right) \quad (3-2)$$

3-2. The current generated by the film is the sum of the currents flowing in  $C_f$  and  $R_f$ ; that is,

$$i_f = i_{C_f} + i_{R_f} \quad (3-3)$$

Since the output voltage ( $V_o$ ) is the ratio of the charge ( $Q$ ) to the film capacitance ( $C_f$ ), it can be written as:

$$V_o = \left( \int i_{C_f} dt \right) / C_f = \left( \int (i_f - i_{R_f}) dt \right) / C_f \quad (3-4)$$

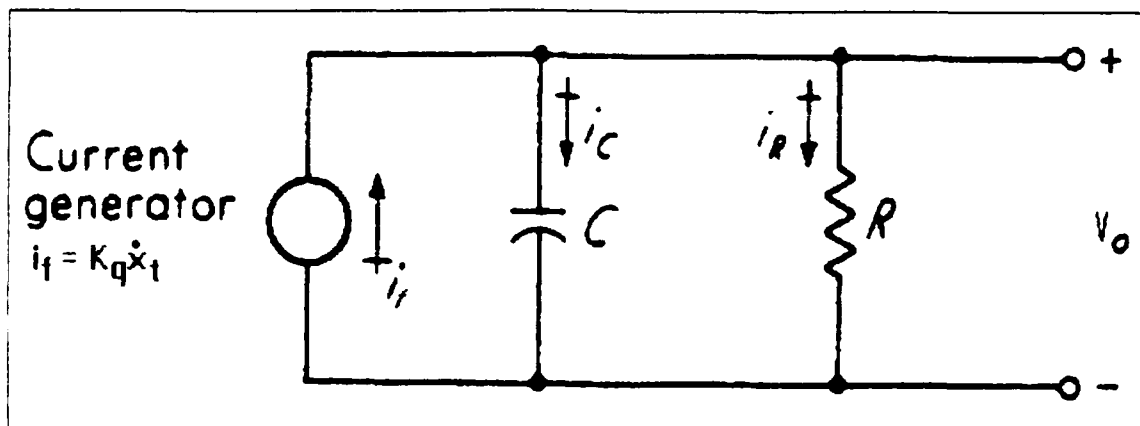


Figure 3-2. Equivalent Electrical Circuit for the Piezoelectric Film as a Current Generator (12:270).

The above equation can be solved for  $(i_f - i_R)$  by making substitutions for  $i_f$  and  $i_R$ . That is,

$$i_f - i_R = C \left( \frac{dV_o}{dt} \right) = e_t \left( \frac{dx_t}{dt} \right) - \frac{V_o}{R_t} \quad (3-5)$$

Rearranging terms and solving for the ratio of the output voltage to the displacement gives:

$$\frac{V_o}{x_t}(D) = \frac{K\tau D}{\tau D + 1} \quad (3-6)$$

where

$\tau$  ▲ time constant =  $R_t * C_t$  (sec)

$K$  ▲ sensitivity =  $e_t / C_t$  (V/cm)

$D$  ▲ derivative =  $d / dt$  (12:270).

Equation 3-6 can be rewritten to establish the time response of the piezoelectric film (12:270). That is,

$$(\tau D + 1)V_o = (\tau K D)x_t. \quad (3-7)$$

If an external force is suddenly applied and allowed to remain on a piece of PVDF film, it would cause the displacement "A"

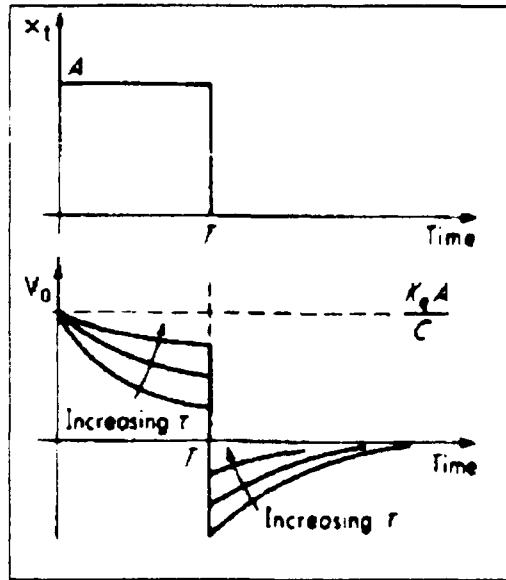


Figure 3-3. Charge Decay of a Piezoelectric Device (12:271).

and the voltage increase shown in Figure 3-3. Since "A" is constant for the time duration T, that is,  $0 < t < T$ , the right-hand side of equation 3-7 is zero. That is,

$$(\tau D + 1)V_0 = 0. \quad (3-8)$$

At  $t=0$ , when the force was applied, the charge instantaneously increased to  $e_t A$ , and it gives the following initial condition (12:271):

$$V_0 = \frac{e_t A}{C_f} \quad \text{at} \quad t=0^+. \quad (3-9)$$

Solving equation 3-8 with the initial condition gives the following result:

$$V_0 = (e_t A / C_f) \exp(-t/\tau_f) \quad \text{for} \quad 0 < t < T. \quad (3-10)$$

At  $t = T$ , the force is removed and  $x_t$  returns to its original value. This displacement behavior causes the same magnitude



of response voltage to be observed, but it is of opposite polarity. Thus,  $V_o$  decreases by  $e_t A/C_f$  at  $t = T$  (12:271). As a result at  $t = T'$ ,  $V_o$  is expressed as

$$V_o = \frac{-e_t A}{C_f} \left( \exp\left(-\frac{T}{\tau}\right) - 1 \right) \exp\left(-\frac{(t-T)}{\tau}\right) \text{ for } t > T. \quad (3-11)$$

This is the initial condition for  $t > T$ . When it is substituted into equation 3-8 and solved, the solution becomes

$$V_o = \frac{-e_t A}{C_f} \left( \exp\left(-\frac{T}{\tau}\right) - 1 \right) \quad (3-12)$$

which gives the solution for all time greater than  $T$ , the force release time (12:271). As the time constant  $\tau$  is increased, the response to  $x_t = A$  becomes more linear.

When the film is connected to a cable and some type of amplifier, this arrangement changes the response of the film. These effects must be accounted for in the reset circuit design. Figure 3-4 illustrates the typical equivalent circuit

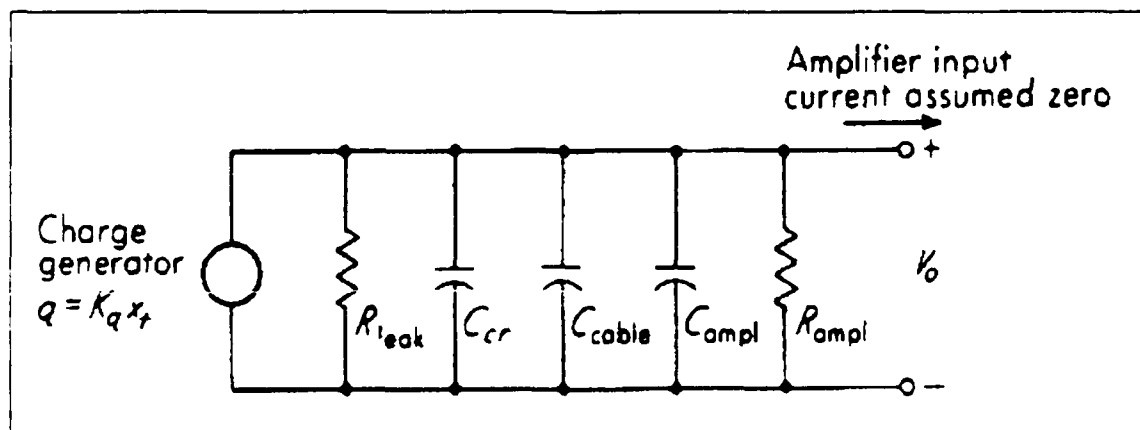


Figure 3-4. Equivalent Electrical Circuit for the Piezoelectric Film, Cable, and Amplifier (12:270).

for a piezoelectric film measuring circuit, cable, and amplifier circuit. These additional electrical impedance effects can be easily combined with the film's capacitance and resistance, as shown in equations 3-13 and 3-14. That is,

$$R = \frac{R_{amp} * R_f}{R_{amp} + R_f} \quad (3-13)$$

and

$$C = C_f + C_{cable} + C_{amp} \quad (3-14)$$

The cable resistance is neglected since it is small compared to the film or amplifier's resistance. Overall, these new values (R and C) need to be substituted into the equations for the film, to account for their cumulative effect.

Circuit Design. There are two fundamental types of analog circuits that could be used to measure the piezoelectric film's response. A voltage follower circuit, as shown in Figure 3-5, and a charge amplifier or integrator represented by Figure 3-6. Each circuit has distinct advantages and disadvantages.

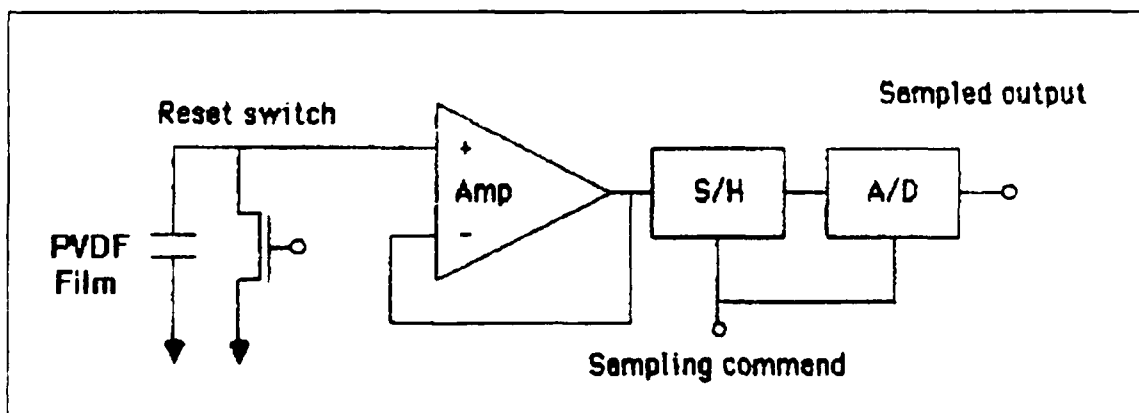


Figure 3-5. Voltage Follower Circuit (14:27).

The voltage follower circuit (Figure 3-5) is very simple and it can easily be modified to achieve different levels of gain. It is very sensitive to capacitive inputs, such as from the film or cable (14:105). A very high input impedance amplifier is needed to reduce charge leakage, which in turn, increases noise sensitivity. The rate of force application speed has an affect on the amplifier's output, since typical high impedance amplifiers have a slow slew rate (14:106).

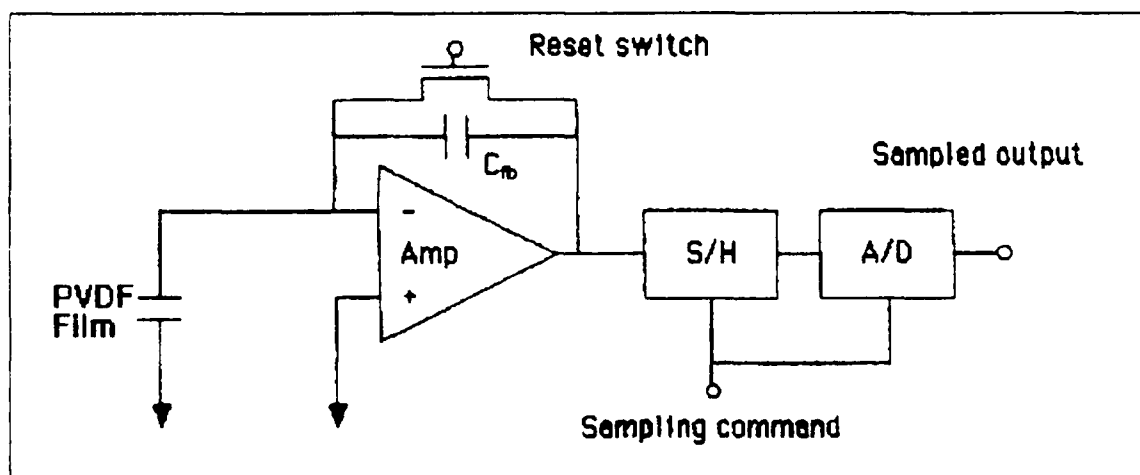


Figure 3-6. Charge Amplifier Circuit (14:25).

The charge amplifier circuit (Figure 3-6) is not influenced by the time constants of the piezoelectric film or the cable due to their capacitive nature. Since a charge amplifier is current driven with a zero input impedance, no voltage is generated across the film (5:30). Because the charge amplifier is immune to capacitance influences, looser tolerances can be used on film size and cable length (5:30, 12:718). Nor is the amplifier affected by variations of the film's dielectric constant due to temperature change (14:105).

In summary, the charge amplifier circuit possesses an abundance of desirable performance properties for capacitive type transducers. Thus, a charge amplifier is the circuit of choice.

#### Sampling and Reset Operation

The conventional charge amplifier would instantaneously indicate the force which is applied to its associated sensor. This behavior can cause problems if the input force is either a low frequency excitation or it has a large magnitude.

The charge amplifier cannot accurately read low frequencies from a piezoelectric sensor since a piezoelectric input decays with respect to time. The charge decay could be larger than the input force response. If the input force is highly dynamic, the input could saturate the amplifier's input, which would result in a saturated output (7).

The sampling and reset operational mode overcomes these limitations, and it is illustrated in Figure 3-7. The circuit implementation is shown with a charge amplifier in Figure 3-8. When the reset switch is open, the charge amplifier follows the input from the piezoelectric device, and the output is sampled as shown in Figure 3-7d. The input variations during the sampling period appear as an amplitude change of the sampled output (7:1). After sampling, the switch is closed to discharge the charge accumulation on the amplifier's capacitor. Again, after the switch opens, the amplifier follows the change of the input signal (7:2). This process practically eliminates amplifier saturation, which means that

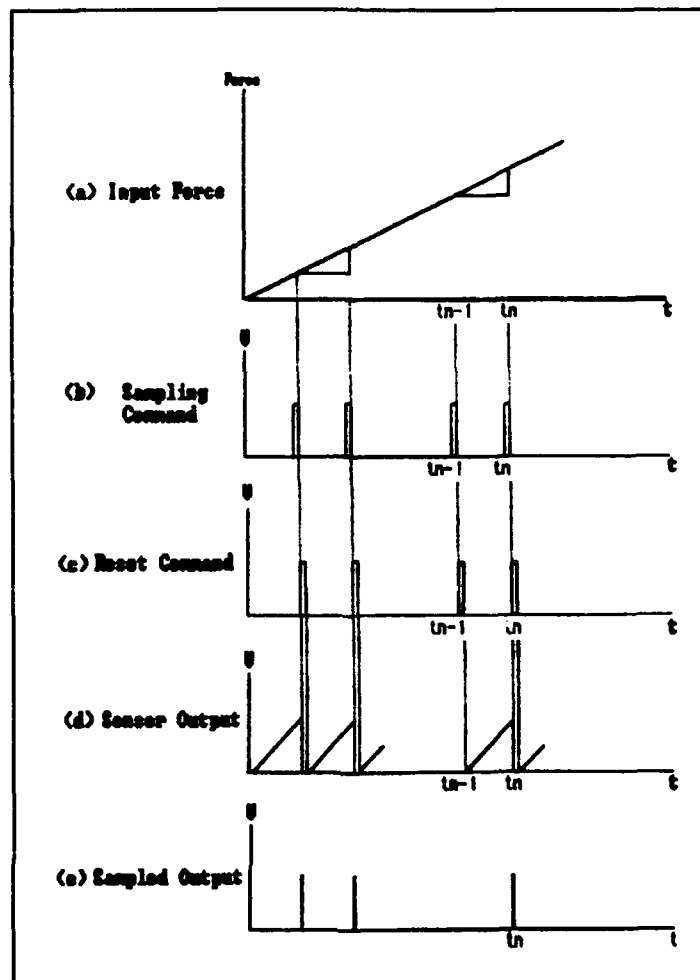


Figure 3-7. Sampling and Reset Operation (14:25).

the amplifier can operate with a broad and dynamic response. Low frequency measurements become possible since charge decay is minimized.

Reset Implementation. Figure 3-8 depicts the situation where the piezoelectric film is modelled as a capacitor  $C_f$ , which has an output proportional to an applied force (14:24). The reset switch could be mechanical or electrical, but in this development, it is electrical. It is characterized as having an  $R_{on}$  of about 400 ohms, and an  $R_{off}$  of  $1E15$  ohms, or virtually an open circuit.

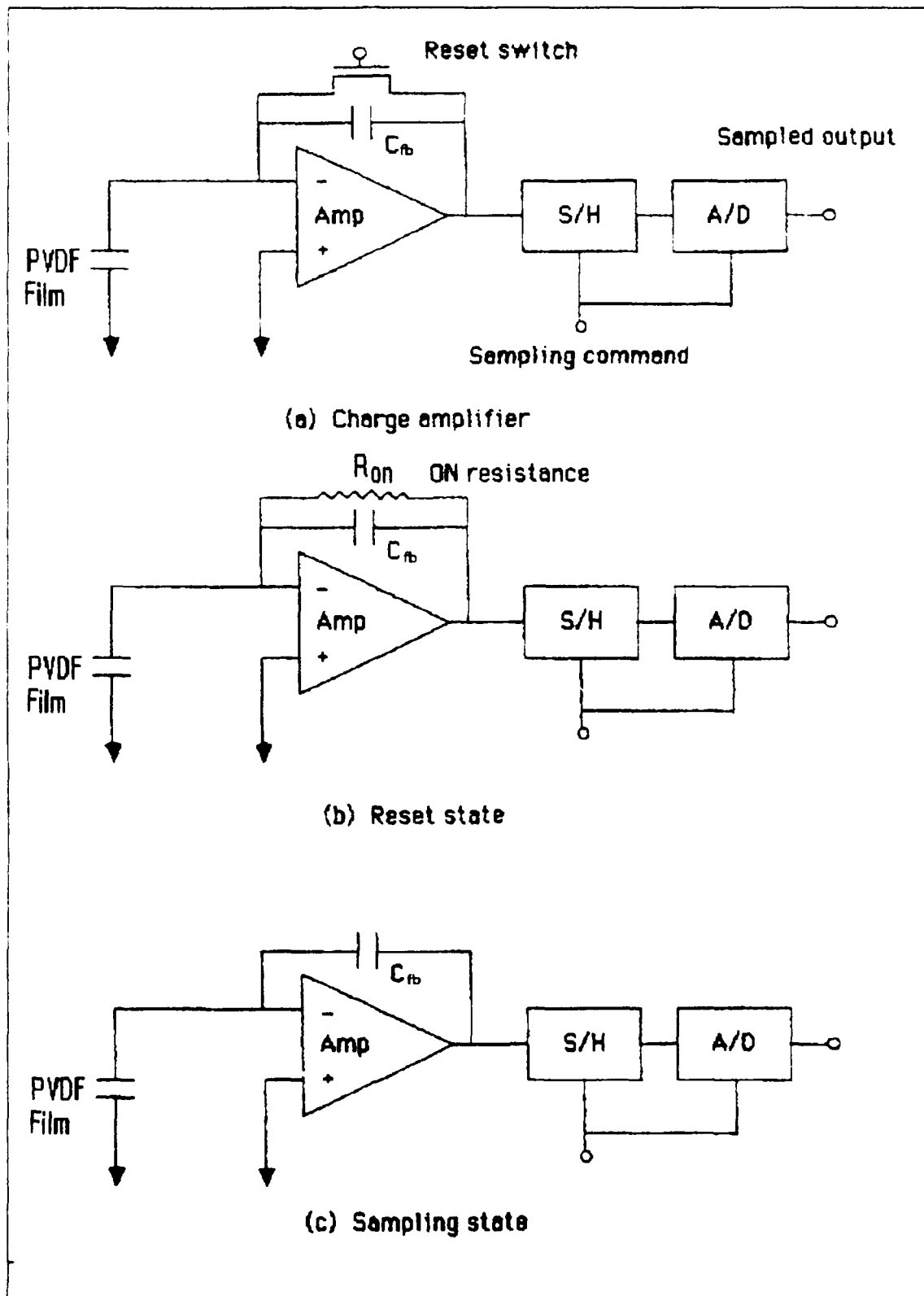


Figure 3-8. Charge Amplifier Reset and Sampling Scheme (14:26).

Reset State. When the reset switch is closed, it is modelled as  $R_{on}$  in Figure 3-8b. The closed switch causes the film's charge to be transferred to the feedback capacitor of the charge amplifier, and it is discharged through  $R_{on}$  in a short period of time called  $T_{reset}$  (14:24). Since the negative input terminal of an operational amplifier is at virtual ground level, the charge is effectively grounded through the reset technique (see Figure 3-7d) (13:178). During the reset period, the charge cannot be measured, even though the force may still be applied; thus, the reset command pulse width  $T_{reset}$  (see Figure 3-9) should be minimized (14:28). The minimum reset time is a function of the time constant of the reset circuit  $\tau_{reset}$  (14:28). That is,

$$T_{reset} > \tau_{reset} = R_{on} * C_{fb} . \quad (3-15)$$

Typically, the reset pulse width should be established for 3 to 5 time constants ( $\tau_{reset}$ ) so that most of the charge can be dissipated. If  $T_{reset} = 3 * \tau_{reset}$ , 95% of the charge will be dissipated, and if  $T_{reset} = 5 * \tau_{reset}$ , it will dissipate 99.3% of the charge (15:9).

Sampling State. As the reset pulse ends (goes low) and the switch in Figure 3-8c opens, the amplifier follows the input signal, as illustrated in Figure 3-7d (14:29). The signal flows predominantly through the capacitor, since  $R_{off}$  is like an open circuit. Now, the amplifier's output signal can be sampled by the A/D converter. The sampling period lasts for the time duration  $(t_s - t_{n-1})$ . Next, the reset pulse goes

## Sampling and Reset Pulse Terminology

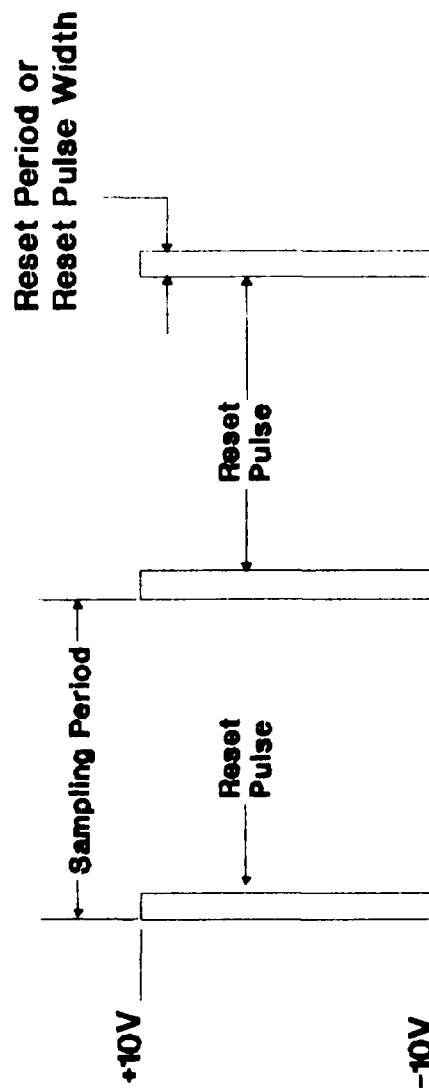


Figure 3-9. Sampling and Reset Pulse Terminology.



high, and the reset process repeats. To get the actual time history, the sampled outputs must be integrated to recreate the equivalent output history.

#### Reset Circuit Characteristics

Offset Calibration. The reset scheme eliminates the need to do a zero offset calibration for the measurement. Each reset cycle clears the accumulated charge due to any initial conditions (14:31). However, the operational amplifier must be adjusted for zero offset, but this situation is independent of the PVDF film.

Sensitivity and Dynamic Range. The conventional charge amplifier is limited by sensitivity and dynamic range (14:31). However, the product of the two is a constant. That is,

$$\text{Sensitivity} \times \text{Dynamic Range} = \text{Constant} . \quad (3-16)$$

The constant is determined by the saturation limits of the charge amplifier; it is typically  $\pm 15\text{V}$ . Thus, the sensitivity can be increased by a decrease in the dynamic range, and vice versa (14:31).

The reset scheme minimizes this interdependence, since a higher reset frequency allows less of an input amplitude increase before it is reset. Thus, the interdependency is reduced.

The limit of the sensitivity associated with the reset scheme is bounded by the saturation voltage of the charge amplifier ( $V_{sat}$ ). This relationship is expressed below by the saturation voltage limit. That is,

$$|S_p| \left( \frac{dF}{dt} \right) \Delta T = |S_p| \left( \frac{dF}{dt} \right) \left( \frac{1}{f} \right) < |V_{sat}| \quad (3-17)$$

or

$$|S_{p_{max}}| = |V_{sat}| / \left( \frac{dF}{dt} \right) \left( \frac{1}{f} \right) \quad (3-18)$$

where  $S_p \triangleq (d_i \cdot X_i \cdot t) / \epsilon =$  film sensitivity (V/lb<sub>f</sub>)

$t \triangleq$  film thickness (μm)

$\epsilon \triangleq$  film dielectric constant (F/m)

$dF/dt \triangleq$  force application speed (lb<sub>f</sub>/sec)

$f \triangleq$  reset command rate (Hz)

$V_{sat} \triangleq$  charge amplifier saturation voltage (V).

As a result, a higher reset rate or slower force application speed increases the sensitivity (14:32,33).

Low Frequency Response. As mentioned previously, piezoelectric film cannot measure static forces since its charge decays with time. With the reset process, the developed charge is sampled and discharged before the charge decay process manifests a significant effect. Thus, the reset rate must be sufficiently short for the amplifier to operate in the "linear" portion of the charge curve. For practical purposes, this is limited to about one-fifth of the circuit time constant (15:14). Thus, a larger circuit time constant permits a slower reset rate.

To better understand the effect of the reset frequency on minimizing the charge decay, a linear input force application process can be examined. The applied force causes a charge to be developed on the film that is proportional to the force

application rate. This situation can be represented as follows:

$$c = \frac{dQ_c(t)}{dt} = \text{Charge Development Rate} \left( \frac{\text{Coul}}{\text{sec}} \right) \quad (3-19)$$

where  $c = C_f * S_f * dF/dt$

$dF/dt$  = force application rate.

Since the PVDF film's output voltage is the developed charge divided by the film capacitance, the film's residual charge can be found by multiplying equation 3-10 by  $C_f$  to get:

$$Q(t) = Q_o \exp\left(\frac{-t}{\tau}\right) \quad (3-20)$$

where  $Q_o = e_i * A$  = an initial charge.

But while the charge is accumulating, it is also decaying by an amount,  $Q_d$ . Multiplying equation 3-11 by  $C_f$  gives an expression for  $Q_d$ .

$$Q_d(t) = Q_o \left( 1 - \exp\left(\frac{-t}{\tau}\right) \right) \quad (3-21)$$

The difference between the charging and discharging rates is shown below. That is,

$$\frac{dQ(t)}{dt} = \frac{dQ_c(t)}{dt} - \frac{dQ_d(t)}{dt} \quad (3-22)$$

Solving equation 3-22 yields the observable charge at an instant of time  $t$ . That is, when  $t = T$ , the charge is:

$$Q(T) = \tau c \left( 1 - \exp\left(-\frac{t}{\tau}\right) \right) . \quad (3-23)$$

If  $\tau$  were infinite, the output would be linear; and the observed charge would be equal to the developed charge (14:36). Since  $\tau$  is indeed finite, at best, the observed charge will be  $\tau * c$ .

With the reset scheme, the time  $T$  becomes  $\Delta T$ , the time between reset cycles. The accumulated charge for each sampling period becomes:

$$Q(\Delta T) = \tau c \left( 1 - \exp\left(-\frac{\Delta T}{\tau}\right) \right) . \quad (3-24)$$

The complete charge time history at time  $T$  is given by the summation of the sampled outputs (14:38). That is,

$$\begin{aligned} Q(T) &= \sum (\tau c) (1 - \exp(\Delta T/\tau)) \\ &= \left( \frac{T}{\Delta T} \right) \tau c (1 - \exp(-\Delta T/\tau)) . \\ &= \tau c T f (1 - \exp(-1/\tau f)) \end{aligned} \quad (3-25)$$

If equation 3-24 is divided by  $cT$ , the result is the ratio of the observed charge to the developed charge. By letting this ratio define an error function, called  $Q_e$  (14:38), then

$$Q_e = \frac{Q(T)}{cT} = \tau f \left( 1 - \exp\left(-\frac{1}{\tau f}\right) \right) . \quad (3-26)$$

As the product  $\tau * f$  is increased, the charge error decreases. When  $\tau * f$  is 100, the charge error is less than one percent ( $Q_e = 0.9950$ ), and each decade improvement of  $\tau * f$  decreases the charge error by a similar amount (14:40). Table 3-1 shows the charge error for several  $\tau * f$  products.

Table 3-1. Charge Error for Various  $\tau \cdot f$  Products (14:40).

$\tau \cdot f$	$Q_e$ (%)
0.01	1.00
0.1	10.00
1	63.21
3	85.04
5	90.63
10	95.16
100	99.50
1000	99.95
10000	99.995

This behavior shows that  $Q_e$  is minimized by a large  $\tau \cdot f$  product. In this case, a shorter reset rate is required for a larger  $\tau$ , or as  $\tau$  decreases,  $f$  must increase to maintain the same level of accuracy (14:39).

Reset Rate Limits. The maximum reset rate is determined by the minimum detectable signal of the charge amplifier or the minimum resolution of the A/D device. For a particular A/D device, the minimum level is defined by the resolution of the Least Significant Bit (LSB). From equation 3-16, the minimum detectable voltage is

$$|V_{\min}| = |S_p| |dF/dt| (1/f) \quad (3-16)$$

or

$$f_{\text{reset}_{\max}} = |S_p| \left( \frac{df}{dt} \right) / |V_{\min}| \quad (3-27)$$

Hence, the upper reset rate can be increased by: 1) increasing the sensitivity; 2) lowering the minimum detectable signal; or 3) increasing the force application rate (14:48).

The charge decay time constant ( $\tau_{\text{circuit}}$ ) and charge development rate can also determine the upper reset frequency. From equation 3-23

$$Q(\Delta T) = \tau C \left( 1 - \exp\left(\frac{-1}{\tau f}\right) \right) = |Q_{\text{min}}| . \quad (3-23)$$

When  $Q(\Delta T) = |Q_{\text{min}}| = |V_{\text{min}}| * C$ , the maximum reset rate can be obtained from equation 3-28 (14:48). That is,

$$f_{\text{reset}_{\text{max}}} = \left( \frac{1}{\tau} \right) \frac{1}{\ln[1 - (|V_{\text{min}}| C_{\text{circuit}} / \tau C)]^{-1}} . \quad (3-28)$$

The lower reset frequency is likewise determined by the charge amplifier limits. In this case, the voltage saturation level ( $V_{\text{sat}}$ ) sets this lower bound. Equation 3-16 can be used to determine the saturation voltage. That is,

$$|V_{\text{sat}}| > |S_p| |dF/dt| (1/f) . \quad (3-16)$$

Solving for  $f$  yields the following:

$$f_{\text{reset}_{\text{min}}} = \left| \frac{S_p}{V_{\text{sat}}} \right| \left| \frac{dF}{dt} \right| . \quad (3-29)$$

The circuit time constant and charge development rate can also determine the lower reset rate. Similar to the development for  $f_{\text{reset}_{\text{min}}}$ , the lower rate can be determined by equation 3-30 (14:49). That is,

$$f_{\text{reset}_{\text{min}}} = \left( \frac{1}{f} \right) \frac{1}{\ln[1 - (C_{\text{circuit}} |V_{\text{sat}}| / \tau_{\text{circuit}} C)]^{-1}} . \quad (3-30)$$

### Circuit Implementation

Two of the primary purposes of the charge amplifier with reset are to minimize charge leakage, and then to discharge the accumulated film charge during the reset period. Ideally, the input impedance of the operational amplifier would be infinite and would draw no current or have a zero input bias current. Similarly, the reset switch would have a zero  $R_{on}$  resistance and infinite  $R_{off}$  resistance. Since neither of these conditions are possible, a circuit that comes close to satisfying these conditions will suffice. If the simple resetting charge amplifier in Figure 3-6 were to be used with a FET reset switch, the drain-to-source current leakage would cause a small current to flow into the summing junction when the switch is off. This situation would dissipate the charge on the film and increase the measurement error (13:223). The charge amplifier circuit, with reset configuration shown in Figure 3-11, minimizes the current leakage and has a low  $R_{on}$  resistance. Even with an ultra-low bias current operational amplifier and a low leakage feedback or integrating capacitor, the summing junction current leakage can be the dominant error source (13:224). The reset part of the circuit uses two n-channel, enhancement-mode MOSFETs ( $Q_1$  and  $Q_2$ ) as the reset switch. Both MOSFETs are switched simultaneously.  $Q_1$  is switched with gate voltages of zero and plus ten volts. This situation eliminates gate and source-to-drain current leakage during the sampling period when the switches are off (zero gate voltage) and the reset command pulse is low (13:224).

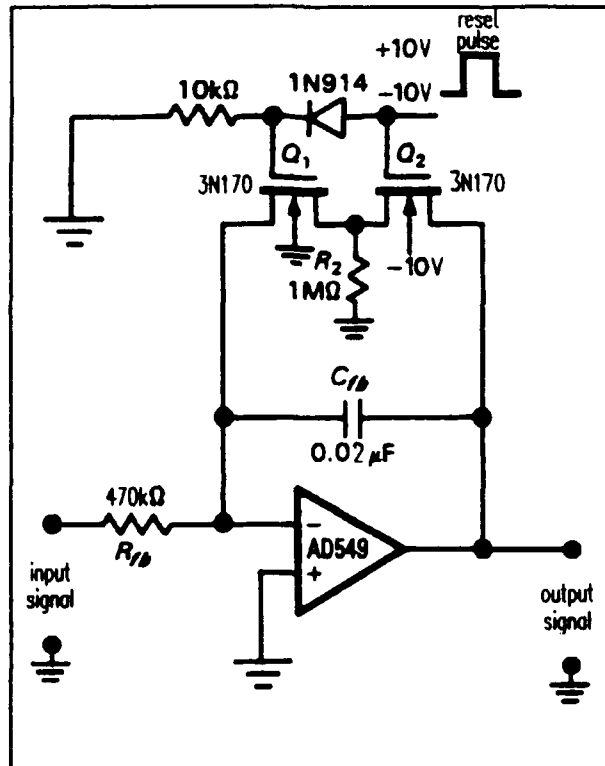


Figure 3-10. Charge Amplifier with a Low-Leakage Reset Switch (13:224).

When the reset pulse command is high, the MOSFET switches turn-on, and the capacitor is discharged with the effective resistance  $R_{on}$ . The  $R_{on}$  resistance is the sum of  $R_{on}$  for  $Q_1$  and  $Q_2$  ( $R_{on} = 200\Omega + 200\Omega = 400\Omega$ ). When the reset command goes low again and the MOSFETs are off, the small leakage current through  $Q_1$  passes through  $R_2$  to ground with a negligible voltage drop (13:224). The summing junction has no current leakage since the source, drain, and substrate of  $Q_1$ , are all at the same voltage level. Thus, current leakage during the off cycle is minimized through the reset switch.



Component Selection. With the proper selecting components, the current leakage can be reduced. Typical operational amplifiers have an input impedance greater than 2 M $\Omega$  and an associated input bias current which is typically several hundred nanoamps in magnitude. The large impedance mismatch between the film ( $R_f > 4.2E12 \Omega$ ) and the operational amplifier, along with the relatively large input current, would dissipate charge from the film. An ultra-low bias current JFET operational amplifier, such as the OPA128 which is typically called an electrometer operational amplifier, has an input impedance of  $1E15$  ohms and an input bias current as low as  $60E-15$  amps (60 femtoamps) (25:2-64). This type of operational amplifier has an input impedance greater than the film's impedance, and this greatly reduces current leakage as compared to the "typical" operational amplifier.

The integrating or feedback capacitor can contribute to current leakage. Standard film capacitors have an insulation resistance (IR) (resistance to a DC current flow under steady state conditions) on the order of 50,000 to 100,000 M $\Omega$ - $\mu$ F. A high quality teflon or polystyrene capacitor has an IR greater than 1,000,000 M $\Omega$ - $\mu$ F. Assuming a 0.02  $\mu$ F feedback capacitor is used, the capacitor's leakage resistance is on the order of 5E7 M $\Omega$  ( $5E13$  ohms) (14:224).

If components such as these are used, the circuit leakage currents (not including the reset switch) at the summing junction, under a worse case of 10V full scale, are less than 1 picoamp (14:224). A common switching MOSFET, such as the

3N170, has a maximum specified leakage current of 10 nanoamps. As a result, the MOSFET switch contributes up to 10,000 times as much leakage current as does the capacitor and operational amplifier combined (14:224). Thus, the overall circuit design is very important in order to minimize the MOSFET's source leakage current. Properly selected components can further reduce this current leakage to a tolerable level.

#### Design Calculations

Before some of the component values can be established, the expected film properties and output response must be known. These values are based upon the anticipated PVDF pressure transducer's operating environment and equipment limitations. Some of the equipment limitations are imposed locally, and not by the commercial availability of better equipment.

The equipment limitations include: 1) 32,000 Hz sampling rate limit for the A/D board; 2) 12-bit resolution of the A/D board; 3) memory limitation of 4096 sampled points; and 4) maximum reset pulse amplitude of  $\pm 10V$ . These limitations will be discussed as they are encountered in the following discussion.

The design was based on the following operational limits: 1) a pressure range of 0-2 pounds per square inch; and 2) a frequency band from DC to 16,000 Hz. The pressure response is typical for commercially available dynamic pressure transducers. It is not imposed by the film, but it does affect the choice of secondary gain and A/D device selection.

The frequency band width is imposed by the available A/D board, and this limit could easily be improved with a faster sampling board. However, with these constraints, the film properties can be calculated.

Film Calculations. The film size was selected to be 1 square centimeter. This feature was not based upon any optimized size, but rather, it was influenced by the ease of handling, fabrication, and a standard unit of length. The voltage output for the film under a pressure field is proportional to its thickness and is independent of its area (5:21). Thus, smaller film areas would produce the same output voltage, but a smaller amount of accumulated charge, which is proportional to the film's area (5:21).

Film Capacitance ( $C_f$ ) and Sensitivity ( $S_p$ ). The film sensitivity ( $S_p$ ) indicates the output voltage per unit of applied force. Since the prospective piezoelectric film transducer will measure pressure, its output needs to have the units of volts per square centimeter. Equation 3-31 establishes the relationship between film sensitivity, film constants, and film dimensions. That is,

$$S_p = \frac{d_t X_3 t}{e} \quad (mv/psi) . \quad (3-31)$$

Film capacitance is also an important parameter involved in many calculations and it is found from the following expression. That is,

$$C = \epsilon A / t . \quad (3-32)$$

In both equations,  $t$  is the film's thickness,  $\epsilon$  is the film's dielectric constant ( $106\text{E-}12$  (Farads/meter)),  $X_i$  is the applied pressure,  $A$  is the electrode area ( $1\text{ cm}^2$ ), and  $d_i$  is the piezoelectric strain constant ( $-22\text{E-}12$  ( $\text{C}/\text{cm}^2$ )/( $\text{N}/\text{m}^2$ )). The values for  $C_i$  and  $S_i$  for three film thickness are shown in Table 3-2.

Table 3-2. Film Capacitance and Sensitivity.

Film Thickness ( $\mu\text{m}$ )	$C_i$ (pF)	$S_i$ (mv/psi)
28	378.6	40.10
52	203.8	74.40
110	96.40	157.4

Reset Rate Limit Calculation. The upper and lower reset rates were calculated from the equations given in the Reset Rate Limits section. Before this calculation can be accomplished, several other constants must be found. The minimum detectable voltage is determined by the LSB resolution of the A/D board which is  $5\text{V}/4095 = 1.22\text{ mv}$ . The force application rate is limited by the maximum sampling rate of 32,000 Hz. Since 10 samples per reset period are used to accurately reconstruct the time history, the highest force application rate would correspond to 2 psi in one-half of a sampling cycle.

$$\frac{dF_{\max}}{dt} = 2 \text{ psi} * \frac{32,000 \text{ Hz}}{10} * 0.5 = 12,800 \frac{\text{psi}}{\text{sec}} \quad (3-33)$$

To find the reset limits imposed by the circuit's time constant and charge development rate, these constants ( $\tau_{\text{circuit}}$  and  $c$ ) need to be calculated. From equations 3-13 and 3-14,  $\tau_{\text{circuit}}$  can be calculated based upon the values for an OPA128 type operational amplifier,  $R_f$  and  $C_f$  for each film thickness, and a  $C_{\text{cable}}$  of 50 pF. For 28  $\mu\text{m}$  film  $\tau_{\text{circuit}}$  is 1,798 seconds, which is  $4.2 \times 10^{12}$  ohms times 429 pF. The value for  $c$  (charge development rate) is determined from the following equation:

$$c = C_f * S_p * \frac{dF_{\max}}{dt} \quad (3-34)$$

Table 3-3 summarizes the results for  $c$  and  $\tau_{\text{circuit}}$  as a function of film thickness.

Table 3-3. Circuit Time Constant and Charge Development Rate.

Film Thickness ( $\mu\text{m}$ )	$C_f$ (pF)	$\tau_{\text{circuit}}$ (s)	$c$ (nC/s)	$R_f$ ( $\Omega$ )
28	379	1798	194.6	4.2E12
52	204	1971	194.3	7.8E12
110	96.4	2398	193.4	16.5E12

Now that all the required parameter values have been calculated  $f_{\text{out}}$  and  $f_{\text{in}}$  can be calculated. These values are shown in Table 3-4 for each film thickness.

Table 3-4. Reset Rate Limits.

Film Thickness	$f_{min}$ (Hz)		$f_{max}$ (kHz)	
	$V_{sat}$	$\tau_{circuit}$	$V_{min}$	$\tau_{circuit}$
28 $\mu m$	51.2	51.2	159.0	420
52 $\mu m$	94.7	95.4	159.2	780
110 $\mu m$	201.0	205.8	158.8	1.65

The minimum reset rate in each case is determined by the operational amplifier saturation voltage, not the circuit constants. The theoretical upper limit is set by the minimum detectable voltage of the A/D board; but in fact, the highest reset rate is imposed by (1/10 of 32,000 Hz or 3200 Hz) the A/D board. Thus, the actual reset rate can range from 51 Hz to 3200 Hz depending upon the film thickness.

An initial reset rate of 500 Hz is selected so that the charge error will be less than 0.12%. This condition will allow up to 0.82 seconds (4096 samples) of the sampled data to be recorded. Although this time duration is not long, it is adequate for initial testing. In an actual application, more memory would be required to support a longer test run or a higher sampling rate.

Reset Pulse Width. The reset pulse, which is determined by the time constant of the reset switch and feedback capacitor, can be calculated using equation 3-14. Using a pair of 3N170 MOSFETs with  $R_{on} = 200$  ohms each, and a 0.02  $\mu F$  feedback capacitor,  $\tau_{reset}$  becomes:

$$\tau_{reset} = 0.02 \mu f * 2 * 200 \Omega = 8 \mu sec . \quad (3-35)$$

Assuming  $T_{reset} = 5 * \tau_{reset}$  so that over 99% of the charge is dissipated,  $T_{reset}$  is 40  $\mu s$ . This value gives a starting point for circuit testing.

#### Time History Reconstruction

The piezoelectric film's output is reset periodically to eliminate any charge decay error. Each reset period is composed of ten data points. To get the entire history, the sampling periods have to be integrated and the error, induced by the DC offset and rise rate, must be removed.

This procedure involves locating the beginning of each reset period and adding that point to the last point of the prior reset period sample. The process of locating each initial portion of a collected sample can be difficult for low-level signals. There are many ways to do this, but two of the simpler methods are: 1) to synchronize the reset pulse and digital sampling; and 2) to make the reset pulse sufficiently wide so that at least one sample data point is taken during the reset pulse width, giving a saturated signal.

The second method was chosen because it was simpler and since the purpose of this thesis was to demonstrate a concept rather than accomplish a complete sensor development. The pulse width was selected to be 100  $\mu s$ , as opposed to a minimum of approximately 40  $\mu s$  needed to discharge the feedback capacitor.

Once the sample interval's beginning and end are established, the first point of the new reset period is erroneous and cannot be used as data. Thus, a simple straight line interpolation is made between the previous end point and the second data point measured with respect to the beginning of the data record. In equation form, the value for the "bridge" point can be found as follows:

$$x_n = \frac{x_{n-1} + (x_{n-1} + x_{n+1})}{2} \quad (3-35)$$

where  $x_n$  is the "bridge" point,  $x_{n-1}$  the end point, and  $x_{n+1}$ , the second point at the beginning of the record.

DC offset and rise rate errors are removed next. The DC offset is a function of the amplitude of a sampled data point and it is independent of time and location. The amplitude is scaled by a constant to remove this error. The rise-rate error, due to the feedback capacitor charging, is time dependent. It is zero for the first sample, and it is a linear function of time for the remaining samples. Once the rise slope is known, the error can be subtracted from each sample value based upon the length of time it occurs relative to the first data point in the record.

#### Circuit Layout

The output from the charge amplifier has level gain below 1 Hz and has a calculated 3 dB point of 17 Hz. This feature implies that low frequencies will pass relatively unaffected, but that high frequencies will be significantly attenuated. The film's output for a 2 psi load will, at best, be 0.3 V,



based upon a 110  $\mu\text{m}$  thick film. Thus, the charge amplifier's output signal will require amplification in order to obtain adequate resolution with the A/D board.

An instrumentation amplifier with a programmable gain provides accurate gains of 1, 10, 100, and 1000, and it can be used to amplify the charge amplifier's output. An Analog Device AD524BD instrumentation amplifier was selected to satisfy this requirement. Figure 3-11 shows the arrangement of the charge amplifier with the instrumentation amplifier.

A Qua Tech A/D board in a Zenith Z-248 computer was used to sample and record the data. The circuit block diagram in Figure 3-12 shows the general arrangement used for testing and development.

#### PVDF Transducer

One centimeter square pieces of film were cut from bulk pieces of PVDF film using an X-acto knife. The bulk film sheet was placed on a large piece of glass to minimize damage to the electrode metal which could short circuit the film and make it unusable. The film was tested for electrical continuity to ensure that all the cuts were clean. Next, shielded two-wire leads were attached to the film using highly-conductive silver paint. A layer of adhesive tape was used to protect the film from corrosion and to reinforce the lead attachments. After the transducer was finished, it was bonded to a cylinder with an adhesive spray and covered with another layer of adhesive tape to prevent debonding. Throughout the process, the film was not touched, but handled

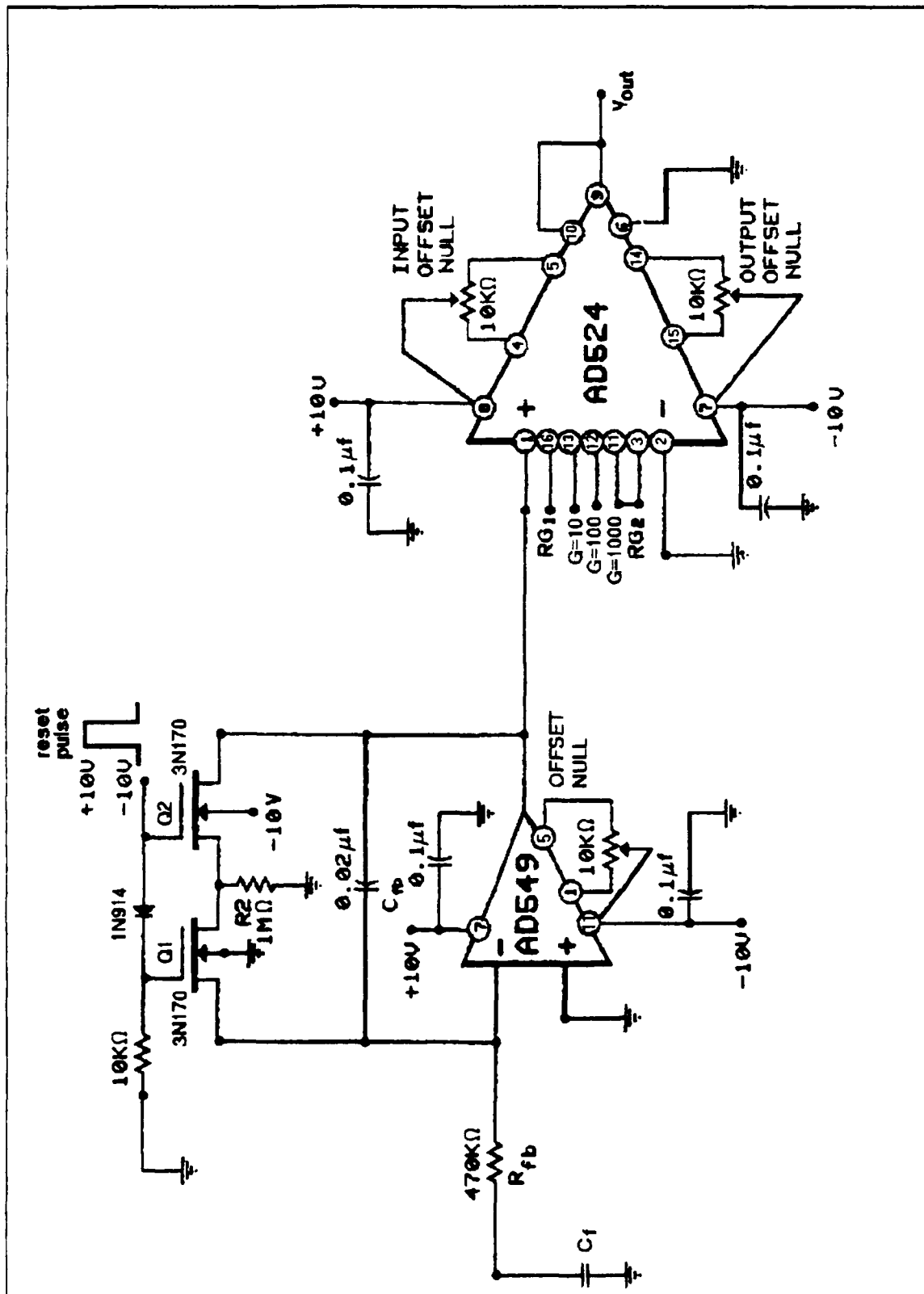


Figure 3-11. Charge Amplifier with Instrumentation Amplifier Gain Set to 1000.

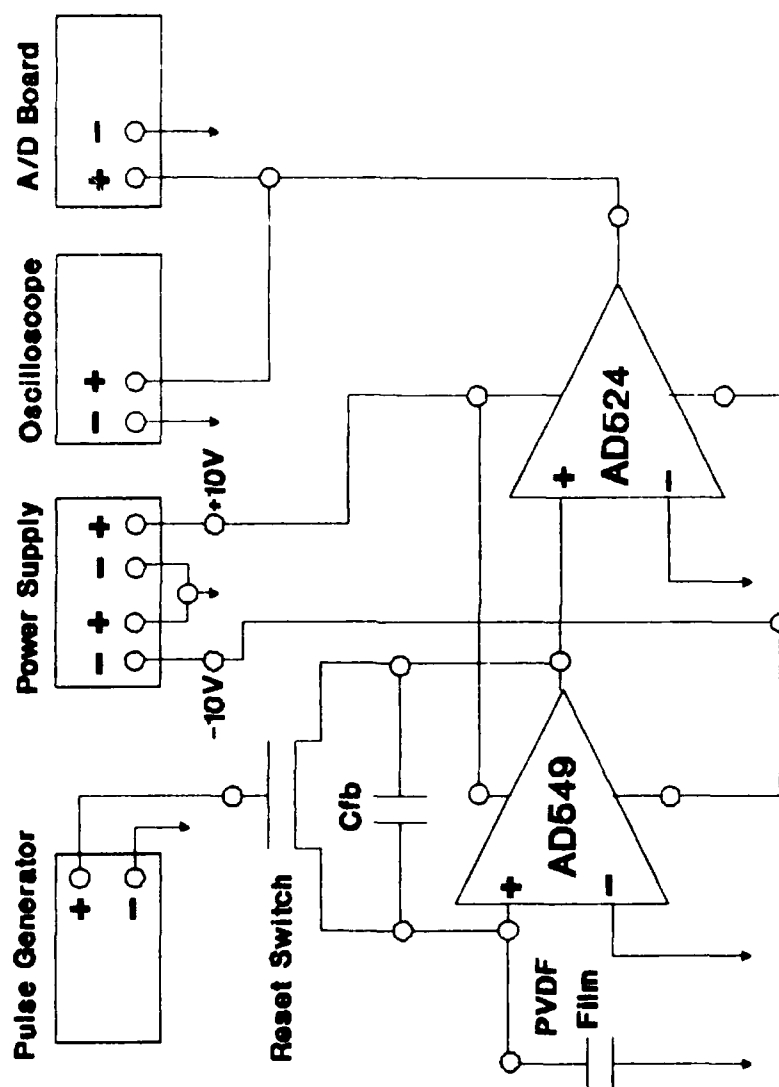


Figure 3-12. General Circuit Arrangement Used for System Testing.

with tweezers to avoid fingerprints which can corrode the electrode metallization (5:49).

#### Test and Evaluation

The final design area involved the development of a procedure for testing the circuit and film transducer. Each procedure represented a small step, so that the insight gained would contribute to the next.

Film Characterization. The film was characterized to determine its time constant and sensitivity  $S_f$ . That is,

- 1) The film transducer was placed between two pads that matched the electrode area and did not contact the lead attachment area.
- 2) The upper pad had a weight placed on it to act as an inertial mass to avoid transients.
- 3) A weight of known mass was placed on the inertial mass. It was quickly removed by hand to create an output proportional to the mass. As the mass was removed, the output voltage would rise, and the film's sensitivity could be found from the magnitude of the response and the time constant from the charge decay.
- 4) The film's output was fed into a simple voltage follower shown in Figure 3-13. The same operational amplifier used in this circuit was also used in the charge amplifier network so that the input impedances would be the same to ensure similar response characteristics.

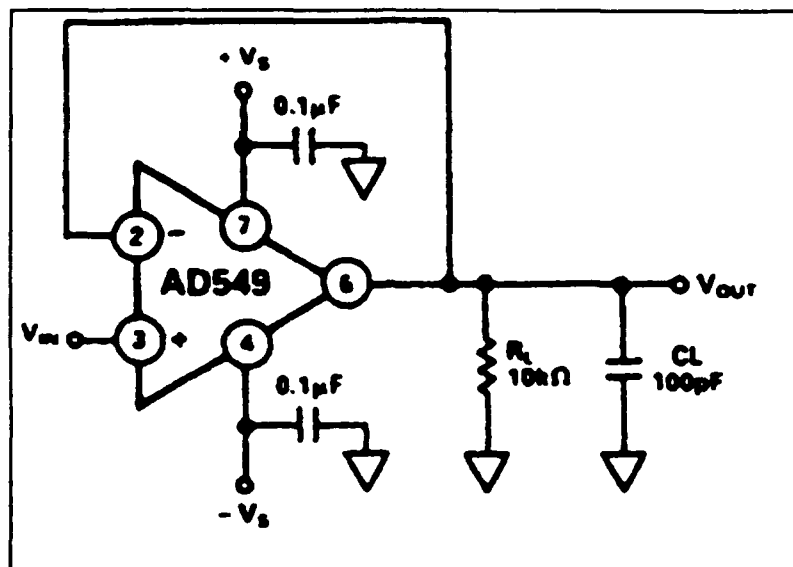


Figure 3-13. Unity Gain Voltage Follower (25:2-67).

- 5) The film's output was recorded on a digitizing oscilloscope (Tektronx 2430A) set in its single-trigger mode. Sample responses were recorded through the GPIB bus for subsequent graphing and analysis.
- 6) This procedure was repeated 27 times with three different weights (50, 100, 205 gm) for each thickness of film. This effort facilitated calculating a statistical average for each weight and film combination.

Circuit Characterization. There are four required parts to characterize the charge amplifier circuit: 1) rise rate minimization; 2) frequency response; 3) reset pulse minimization; and 4) DC offset characterization. The reset pulse width and DC offset testing are interrelated, but they were tested individually.

Frequency Response. The charge amplifier's frequency response was tested with the reset pulse command disabled so that complete signals could be measured. That is,

- 1) A signal generator (Tektronix FG502) was connected to the input of the charge amplifier.
- 2) The output was not amplified but fed directly into a digitizing oscilloscope (Tektronix 2430A).
- 3) A sine wave of known frequency and amplitude (measured on the oscilloscope) was connected to the charge amplifier's input, and the circuit output was measured.
- 4) The frequency was swept from 0.1 Hz to 1 MHz. The results were recorded and plotted in Figure 4-2 to produce the frequency response curve for a resistive input.

Rise Rate Characterization. The circuit rise rate defines the linear charge rate of the feedback capacitor. It varies with different  $C_f$  and  $R_f$  values. The rise rate creates a linear offset error which starts after the first element in the data record. It can be subtracted during the reconstruction process once it is known. That is,

- 1) The charge amplifier and reset inputs were disconnected.
- 2) A digitizing oscilloscope (Tektronix 2430A) was connected to the amplifier's output.
- 3) The voltage supply was established at  $\pm 10V$  DC.
- 4) The feedback capacitor was shorted across its terminals to discharge it.

- 5) The output was recorded on the oscilloscope in units of volts per second.
- 6) The feedback resistor and capacitor were varied to see the effect on rise rate by repeating steps 4 and 5. The feedback time constant ( $R_f * C_f$ ) target was 0.01 seconds.

Pulse Width Minimization. The ideal pulse width would be very short, and it would completely discharge the feedback capacitor. In practice, its limit is determined by the reset switch resistance and feedback capacitance. As the reset time is reduced, the capacitor does not fully discharge, and a DC offset results. If the reset time is increased beyond 5 time constants, no benefits are gained since the capacitor is over 99% discharged. That is,

- 1) The input of the charge amplifier with the reset switch was connected to a signal generator (Tektronix FG502), and a pulse generator (Wave Tek 278) was connected to the reset circuit.
- 2) The charge amplifier's output was connected to a digitizing oscilloscope (Tektronix 2430A).
- 3) The pulse amplitude was set to  $\pm 10$  V. A 50 Hz,  $\pm 1$  V square wave was connected to the input of the amplifier.
- 4) The pulse width was varied, and the amplifier's output was recorded on the oscilloscope.
- 5) The output was triggered on the reset pulse, and the offset was measured and recorded.

DC Offset Characterization. The DC offset values results from the charge decay of the feedback capacitor and charge injection from the gate to the sampling mode through the gate to channel capacitance (14:100). It causes a DC shift in the output which results in an error in the reconstructed time history. If the DC shift can be characterized, it can be removed.

This test used the same procedure as the pulse width test with two exceptions:

- 1) The pulse width was kept constant at five time constants (40  $\mu$ s); and
- 2) The square wave amplitude was varied from 7 mv peak-to-peak to 1.75 V peak-to-peak. After the data was collected, a statistical average of the maximum and minimum values for the sampling period was collected. The values were plotted to obtain the DC offset characterization.

Secondary Gain Characterization. The secondary gain provides the amplification needed to obtain adequate resolution on the A/D board. It should be linear at all gains below 32,000 Hz to ensure accurate results.

- 1) The secondary amplifier (AD524BD) input was zeroed by grounding the inputs and setting the gain to 1000. The 10 kohm resistance offset nulling potentiometer was adjusted so that the output was zero on the oscilloscope.



- 2) The AD524BD's output was zeroed using the same procedure described in step 1, but the gain was set to one, and the output potentiometer was adjusted to zero at the output.
- 3) A signal generator (Tektronix FG502) was connected to the inputs. The frequency was swept from 1 to 10 MHz with a sine wave of constant amplitude. The gain was varied from 1, 10, 100, to 1000, and the frequency sweep was repeated each time.
- 4) The output and input were monitored on a dual trace oscilloscope. The data were recorded and reduced.

#### Time History Reconstruction Test

In order for the piezoelectric film transducer to be useful, an accurate time history had to be reconstructed. This test would determine if the process would work. That is,

- 1) The charge amplifier and reset circuit was configured with a 500 Hz reset pulse that was 40  $\mu$ s wide.
- 2) The input was connected to the signal generator (Tektronix FG502) producing a 50 Hz sine wave with a known amplitude.
- 3) The output of the signal generator and charge amplifier were recorded on the Qua Tech A/D board at a rate of 5000 samples per second.
- 4) The data were post-processed to remove the DC offset, rise rate error, and to integrate the samples. The results were plotted with the original input, the "chopped" output, and the reconstructed output.

### System Testing

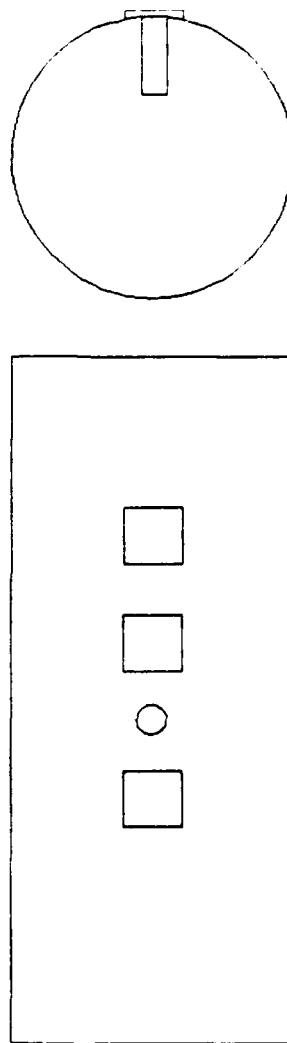
This test would determine if a piezoelectric film pressure transducer is a viable option for measuring pressure frequencies ranging from DC to 2,500 Hz. The film response was compared to the output of a calibrated dynamic pressure transducer (Endevco 8510-B). Each film thickness was tested as a separate run due to the 2 channel limit of the A/D board. That is,

- 1) The three piezoelectric traducers were mounted along the side of a dynamic pressure gage as shown in Figure 3-14. It was assumed that the lateral distance from the "reference" gage would not create a significant pressure difference in a large volume flow field.
- 2) The output of the reference gage was connected to its signal conditioner.
- 3) The charge amplifier was driven with a 500 Hz reset rate with a 100  $\mu$ s pulse width.
- 4) The outputs of the transducers were zeroed, and a nominal condition was recorded on the A/D board at 5000 samples a second. This would facilitate an additional offset to be removed from the test data.
- 5) The cylinder with the gages was placed in a flow field and the flow around the cylinder was measured with a pitot tube. This measurement established the relative magnitude of the flow field. Figure 3-15 shows the cylinder and flow field arrangement.

# Gage Mounting On Cylinder

Top View

Side View



□ PVDF Gage

○ Endevco Gage

Figure 3-14. General Arrangement of the Pressure Transducers Mounted on the Cylinder.

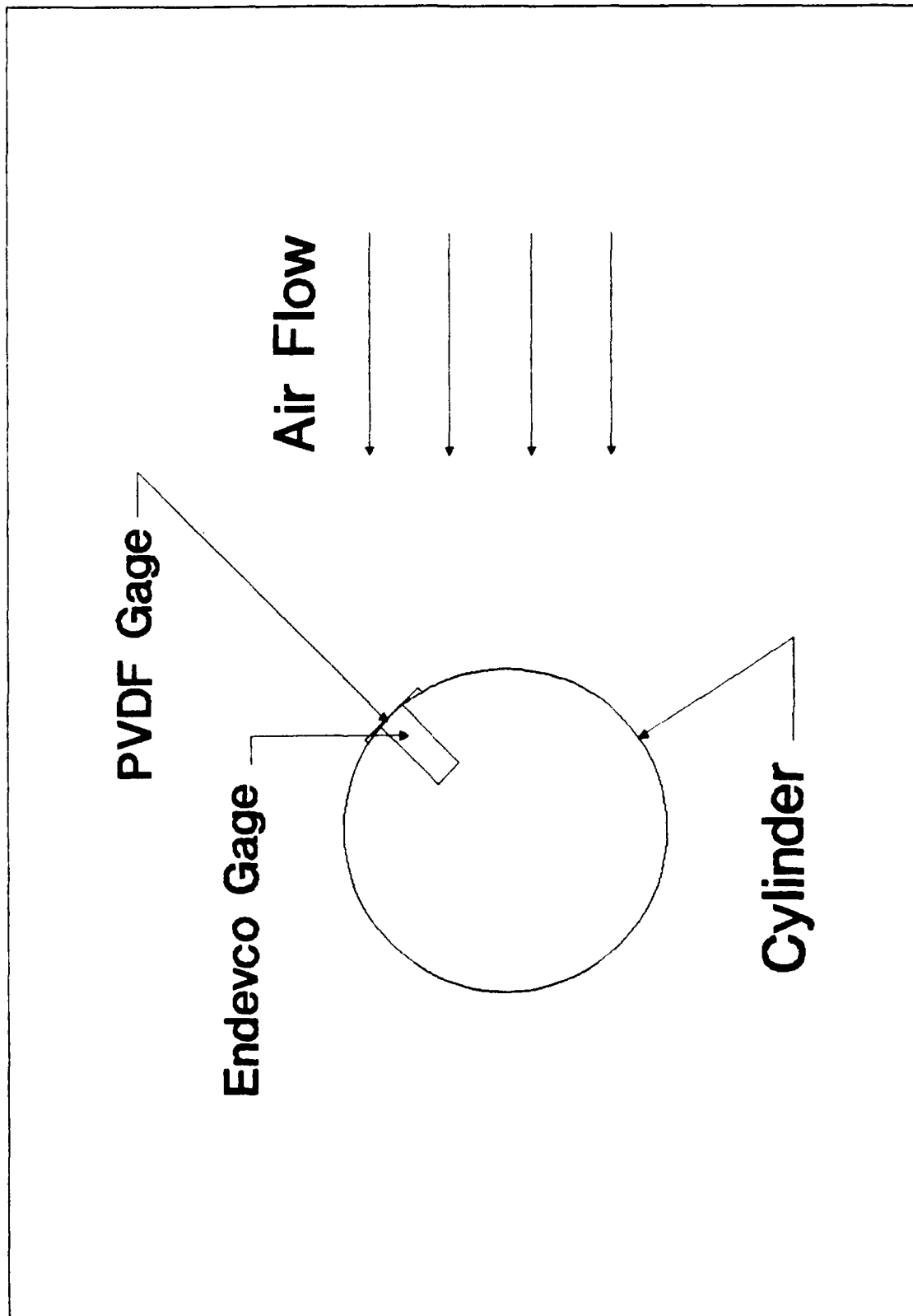


Figure 3-15. Cylinder with Pressure Transducers in the Flow Field.

- 6) A test run was initiated by blocking the flow with a solid aperture. The data acquisition process was initiated and the plate was removed. This condition created a "no-flow" and a "ramp" pressure distribution on the transducers. The "no-flow" condition is important since a nominal condition must be known in order to have an accurate starting point for the time history reconstruction process.
- 7) The data from the "reference" gage was scaled with its calibration data. The piezoelectric gage data was reconstructed with the same process used in the reconstruction test.
- 8) The results for each gage were put on the same plot and analyzed.

#### Summary

This chapter presented additional material required to design and understand the charge amplifier reset circuit. Design calculations were presented to determine an initial point for the performance testing and development. Finally, the test procedure was presented to verify and improve the transducer's design.

#### IV. Experimental Data and Analysis

##### Introduction

The presentation of this section parallels the order of the tests. The results, conclusions, and additional insights gained from testing are discussed.

##### Film Characterization

The results from the sensitivity tests are presented in Table 4-1. The PVDF film's response in all cases was within 7% of the theoretical values. The relatively large standard deviations can be attributed to the experimental test variations. If the weight was not removed at the same speed or perfectly vertical, a slight deviation from the ideal value was noted. The standard deviation was found from the following relationship:

$$\sigma = \sqrt{\frac{\sum X^2}{n} - \bar{X}^2}$$

Each measurement was repeated 27 times to establish a simple average.

The measured charge decay rate, or film time constant was significantly different compared to the calculated result. The theoretical value was on the order of 30 minutes; whereas, the actual values were on the order of 1.5 seconds. Also, the longest decay should have been associated with the 28  $\mu\text{m}$  thick film, but the observed decay was longest for the 110  $\mu\text{m}$  thick

Table 4-1. PVDF Film Sensitivity.

Film-Property	50 gm	100 gm	206 gm
28 $\mu\text{m-S}$ , Theory	28.5 mv	57.0 mv	117.0 mv
28 $\mu\text{m-S}$ , Measured	30.4 mv	59.3 mv	122.3 mv
28 $\mu\text{m-Variance}$	5.9 mv	8.5 mv	17.3 mv
52 $\mu\text{m-S}$ , Theory	52.9 mv	105.6 mv	217.0 mv
52 $\mu\text{m-S}$ , Measured	51.3 mv	107.0 mv	212.5 mv
52 $\mu\text{m-Variance}$	6.9 mv	10.9 mv	17.6 mv
110 $\mu\text{m-S}$ , Theory	116.6 mv	223.4 mv	458.4 mv
110 $\mu\text{m-S}$ , Measured	119.4 mv	220.0 mv	463.0 mv
110 $\mu\text{m-Variance}$	12.8 mv	18.5 mv	27.5 mv

film. Figure 4-1 shows a sample charge decay plot for the 110  $\mu\text{m}$  film.

The difference between the observed and theoretical charge decay times can be attributed to non-ideal components and the small amount of charge generated. Anytime an electrical interface with a finite impedance is connected to a capacitor, it will sink the storage charge, thus increasing the charge decay rate associated with of the capacitor. One method of more accurately measuring the charge decay rate would be to use a higher input impedance instrument such as an electrometer (which was not available).

The PVDF film characterization also revealed the polarity of the film. This would allow the transducers to be constructed so that a compressive force creates a positive

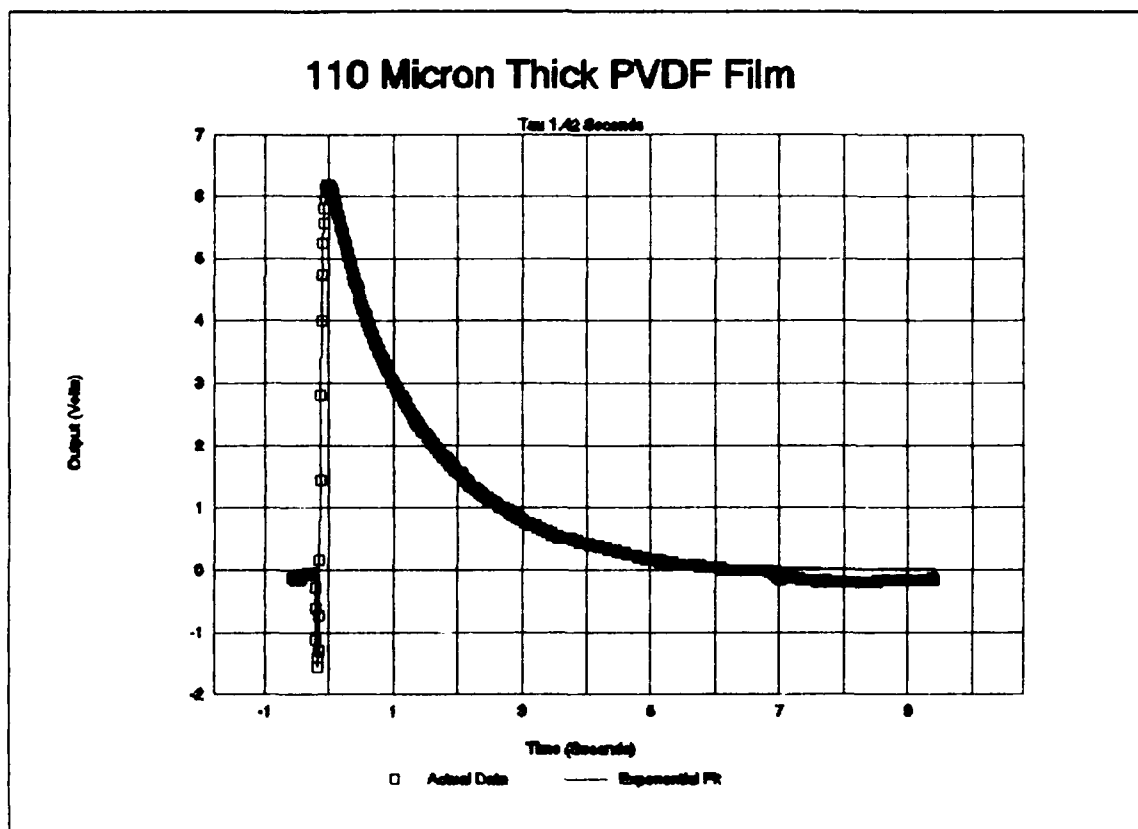


Figure 4-1. Charge Decay of the 110  $\mu\text{m}$  Thick PVDF Film.

voltage deflection. This is the convention commonly used by the "reference" pressure transducer.

#### Circuit Characterization

This set of tests included the evaluation of the charge amplifier frequency response, rise rate characteristics, pulse-width minimization, and DC-offset characteristics.

Frequency Response. The gain of the charge amplifier was plotted in dB [ $20 \cdot \log_{10}(V_{out}/V_{in})$ ] as a function of frequency in Figure 4-2. The calculated 3 dB point was 17 Hz, and the measured result occurred at 32.5 Hz. The gain decreased monotonically as the frequency increased. The linear least-squares line reveals that the relationship between gain and



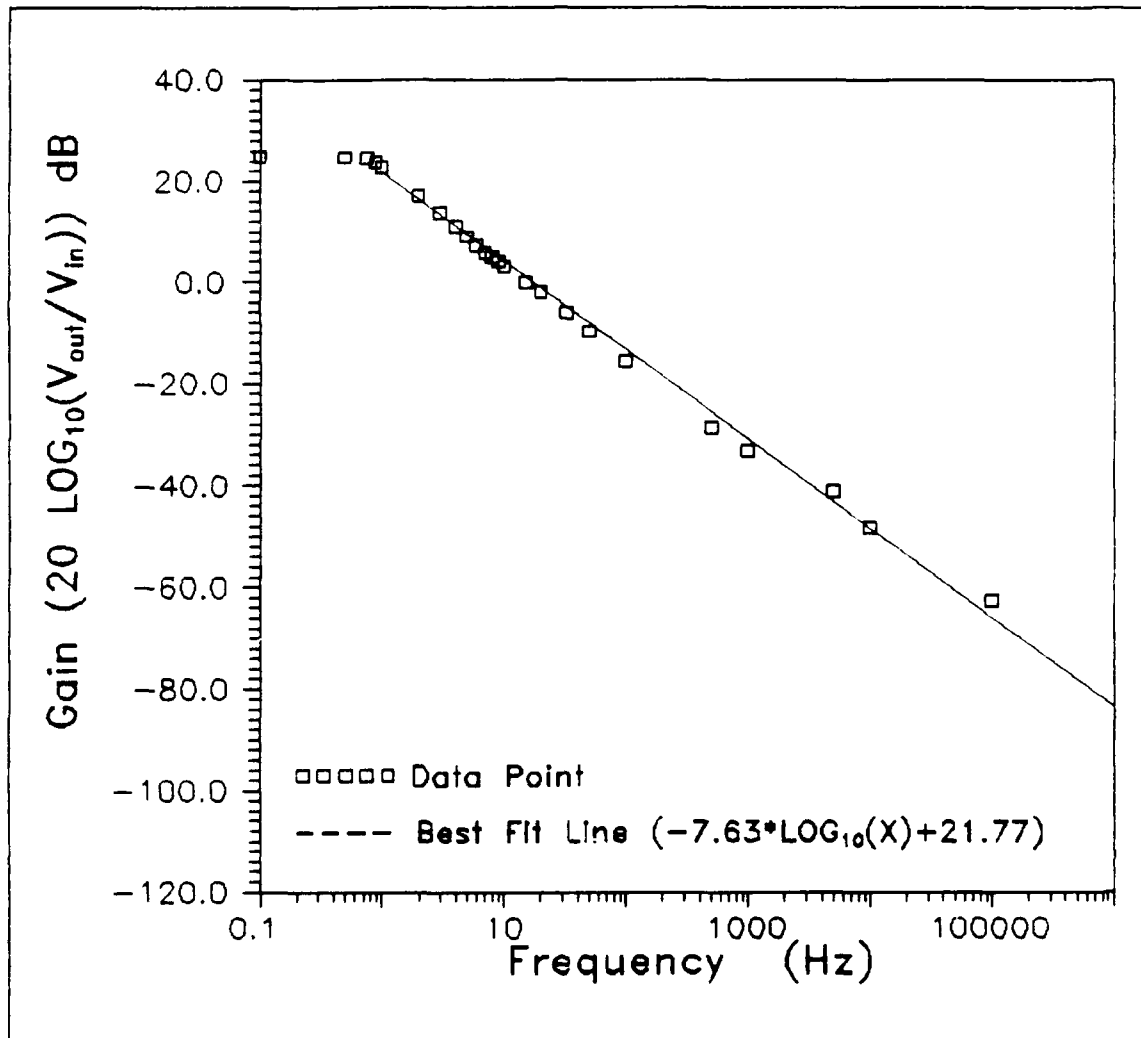


Figure 4-2. Frequency Response of the Charge Amplifier Circuit.

frequency is:

$$\text{Gain} = 21.77 - 7.63 * \log(\text{Frequency}) \quad (4-1)$$

The behavior of the linear response establishes excellent agreement between the theory and the experimental results. The rapid fall-off feature at low frequencies affords the circuit its integration properties for resistive inputs.

Rise Rate Characteristics. The rise rate measurements revealed that, as the size of  $C_{fb}$  was decreased, the charging rate increased. These results are summarized in Table 4-2. Using a larger  $R_{fb}$  increased the rise rate slightly. Different combinations of R and C with the same RC product resulted in different rise rates. In each case,  $C_{fb}$  was the dominant parameter. To keep the RC product at approximately 0.01 (1/s) and to minimize rise rate error,  $C_{fb}$  was set at 0.02  $\mu\text{F}$ . Consequently,  $R_{fb}$  was established at 470,000 ohms to improve gain, since gain is proportional to  $1/RC$ .

Table 4-2. Rise Rates for the Circuit's Various RC Combinations.

$C_{fb}$ ( $\mu\text{F}$ )	$R_{fb}$ (k $\Omega$ )	Rise Rate (V/S)	RC (1/s)
0.002	10	0.46	2E-5
0.002	100	0.53	2E-4
0.002	1000	0.55	2E-3
0.01	10	0.112	1E-4
0.01	1000	0.120	1E-2
0.02	10	0.052	2E-4
0.02	470	0.057	9.4E-3
0.02	1000	0.062	2E-2

Pulse Width Minimization. The pulse-width variations investigated were found to increase the DC offset when it was set to less than 5 time constants. In fact, if the pulse time constant was measured, it was found to be within 1  $\mu\text{s}$  of the calculated value. Figure 4-3 shows a reset pulse with the associated switching noise and feedback capacitor charge

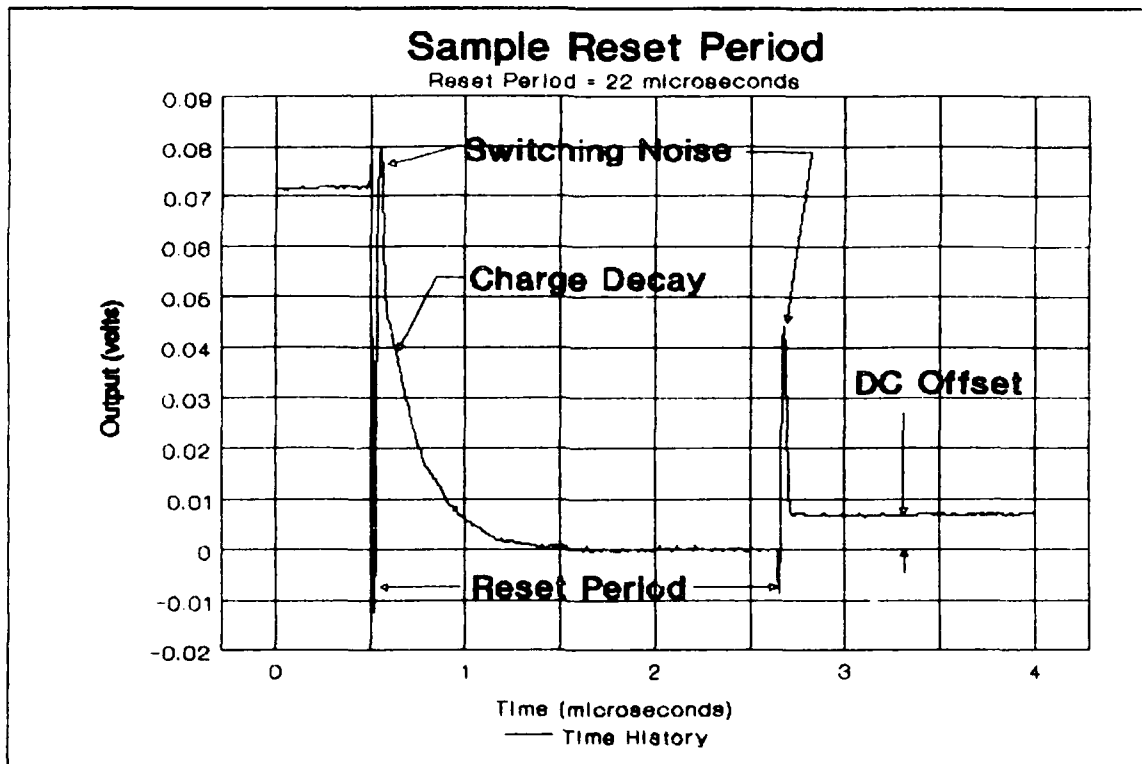


Figure 4-3. Sample Reset Period with Switching Noise and Feedback Capacitor Decay.

decay. As the pulse-width was increased to be larger than 5 time constants, there was no additional decrease in the DC offset. As a result, the reset pulse-width was selected to be equal to 5 time constants.

DC Offset Characteristics. The magnitude of the last reset period sample relative to the first reset period sample (DC offset) was found to vary linearly with magnitude. This means that the DC offset could easily be removed during the time history data reconstruction process. Figure 4-4 shows a data sample used to determine a DC offset point. The complete results are plotted in Figure 4-5. The linear least-squares line has the equation:

$$Y = 0.04904x + 6.58E-4$$

(4-2)

Secondary Gain. The AD524BD instrumentation amplifier is designed to give precise gains of 1, 10, 100, and 1000. The test results agreed precisely with the specification values throughout the entire operational frequency range; Table 4-3 shows the cutoff frequency for each level of gain.

Table 4-3. Measured and Specified Bandwidth for AD524BD Instrumentation Amplifier.

Gain	Measured -3 dB Point	Specified -3 dB Point
1	376 kHz	1 MHz
10	430 kHz	400 kHz
100	309 kHz	150 kHz
1000	43 kHz	25 kHz

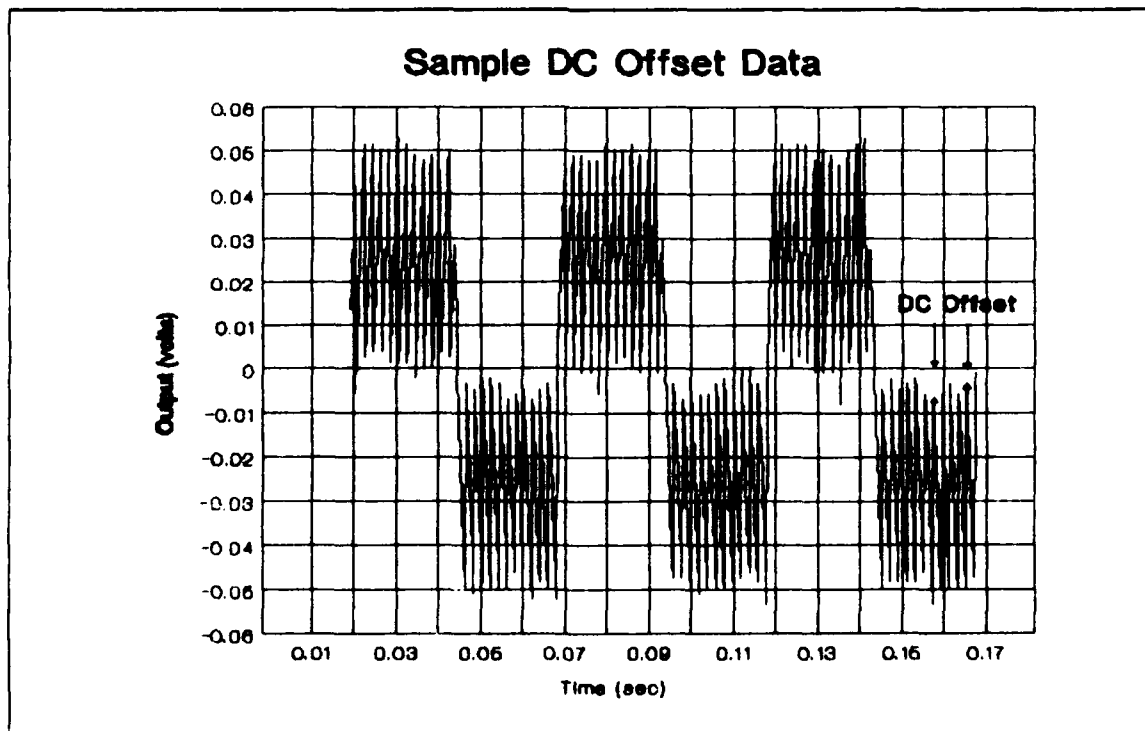


Figure 4-4. Sample DC Offset Data.

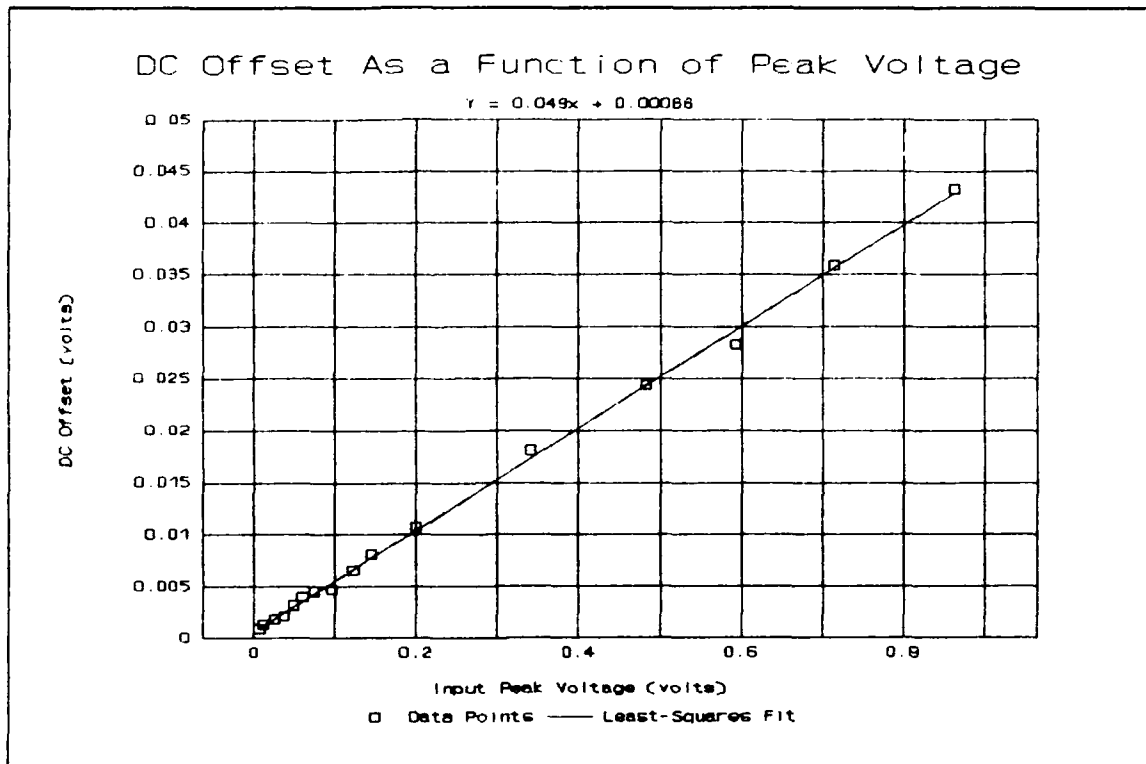


Figure 4-5. DC Offset as a Function of Input Voltage.

#### Time History Reconstruction Process

With the DC offset characterized, the "chopped" time history could be reconstructed. Figure 4-6 shows a plot of a "chopped" sine wave, the reconstructed sine wave, and the input sine wave. The original chopped sine wave had a nonzero mean. To facilitate the reconstruction process, the mean was adjusted to zero by subtracting the operational amplifier's induced offset from all data points (not the DC offset value). The nonzero mean was caused by an imprecise trim adjustment of the charge amplifier.

In this simple case, the reset points were located using a saturated condition metric; that is, by counting 10 points to the next reset period, or by an obvious mismatch in

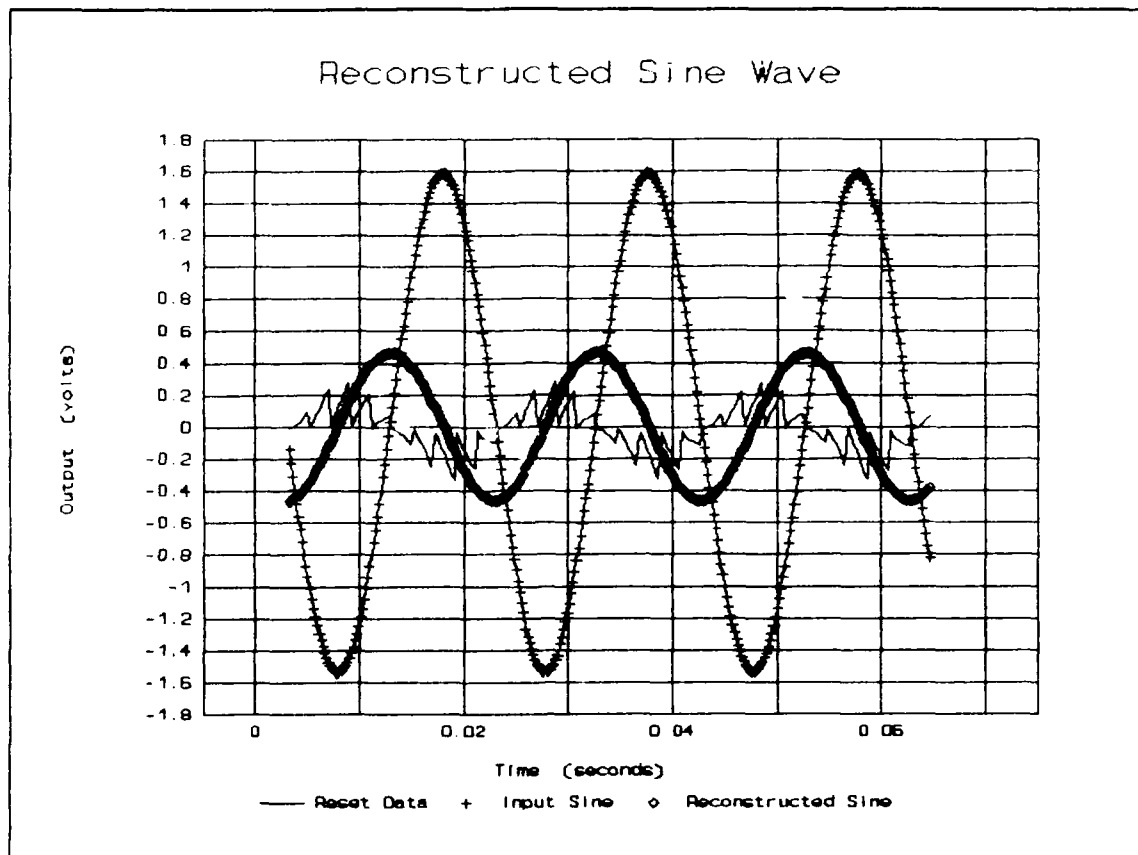


Figure 4-6. Reconstructed Sine Wave Showing the Sampled Data and Input Sine Wave.

amplitude. When the samples were integrated, the "bridge" points showed the slight mismatch. Various other methods were used to try to make the transition smoother. In some cases the "bridge" was smooth, but at other points, the "bridge" was worse. Therefore, the point averaging method appeared to be the most effective procedure.

The DC offset reductions significantly decreased a steadily increasing amplitude. However, the amplitude still was not level. It still manifested an amplitude rise due to the circuit's rise rate. The DC offset adjusting factor was increased and decreased to see if it would correct the

amplitude rise. This consideration contributed no improvements, so a linear least-squares line was fitted through the peak amplitude points, and the circuit's rise rate slope was determined. The slope (-1.172673 volts per second) was subtracted from each point as a function of its time shift relative to the first recorded point. This data processing procedure made the amplitude consistent.

The reconstructed sine wave was phase shifted by nearly 90 degrees relative to the input signal. Since the signal was 50 Hz, it was attenuated by 10 dB, as predicted by Figure 4-2. This demonstration shows that the reconstruction technique was accurate for the test case with a known input.

#### System Testing

The laboratory instrumentation sampling rate of 5000 Hz limits the frequency content analysis to 2500 Hz due to the Nyquist sampling theorem. With this limitation, the data were digitally filtered with an 8-pole, 0.01 dB ripple, low-pass Chebyshev filter to prevent aliasing in the frequency domain. The filter not only reduce aliasing, but also alternates the 20 kHz signal that was present in all the data when viewed on the oscilloscope. The source of the 20 kHz signal source could not be found, so it was filtered.

There was also a 60 Hz noise signal in all of the measured data due to a ground loop. The ground loop occurred between the pulse generator and the circuit ground. Whenever the pulse generator was completely disconnected, the 60 Hz signal

disappeared. In some cases, the 60 Hz noise was as large as 40 mv RMS. Various grounding techniques were implemented, but none contributed an improvement. Consequently, the dynamic pressure transducer data was filtered with a 60 Hz 4-pole, -40 dB stopband filter before any analysis or data processing was accomplished. The sampled data was filtered after reconstruction, but before additional processing was implemented.

Frequency Content. Power spectral density plots were calculated for both the PVDF film data and the pressure gage data to determine their frequency content. This behavior indicates that the PVDF film was responding dynamically and similar to the commercial pressure gage. The frequency resolution was on the order of 20 Hz, so accurate low frequency analysis was not possible from the PSDs. Consequently, the low frequency magnitude response was determined from the time history.

Comparing the two PSDs shows that the film's frequency response matched the gage response above 200 Hz. Below 200 Hz, the film PSD shows that the response is 40 dB greater than the relative magnitude of the gage PSD. Figures 4-7 and 4-8 illustrate the two representative PSDs for the 110  $\mu$ m thick film. Between 200 and 1000 Hz, the peaks of the PVDF film's PSD occur close to the same frequencies as those of the gage. At 700 Hz, the

film response is smaller relative to the gage, and it is 20 dB less compared to the other peaks on the film's PSD.



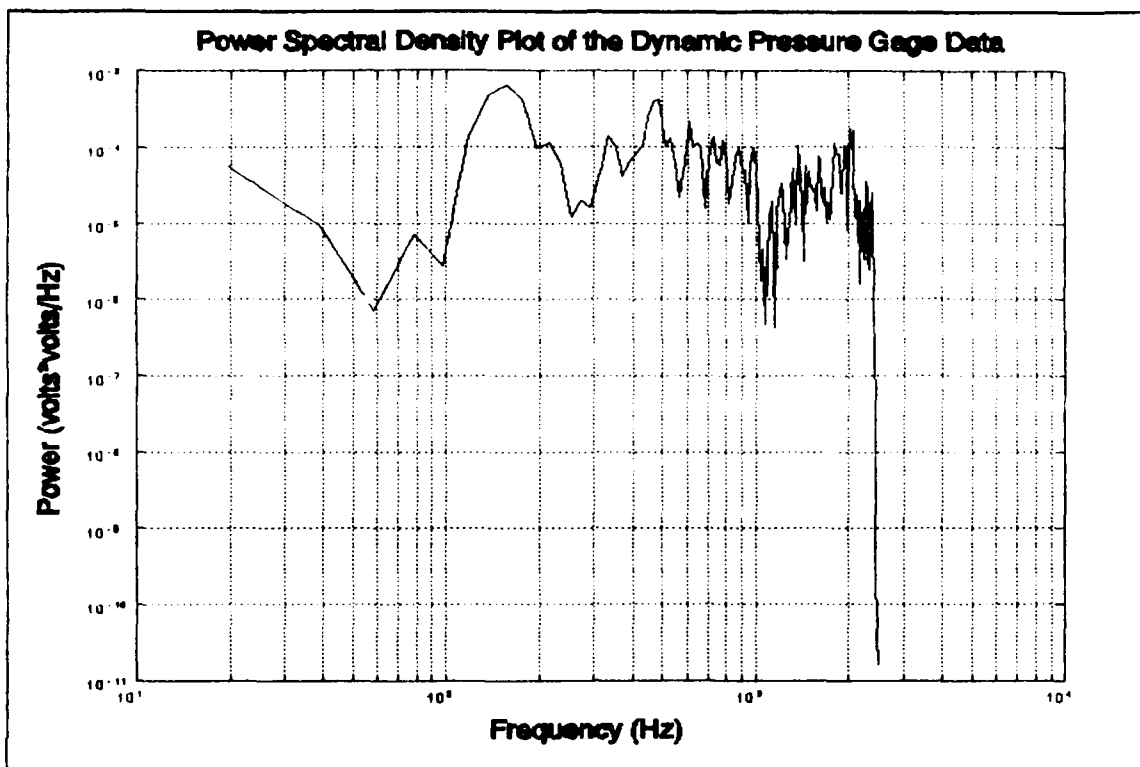


Figure 4-7. PSD of Dynamic Pressure Gage Time History Data.

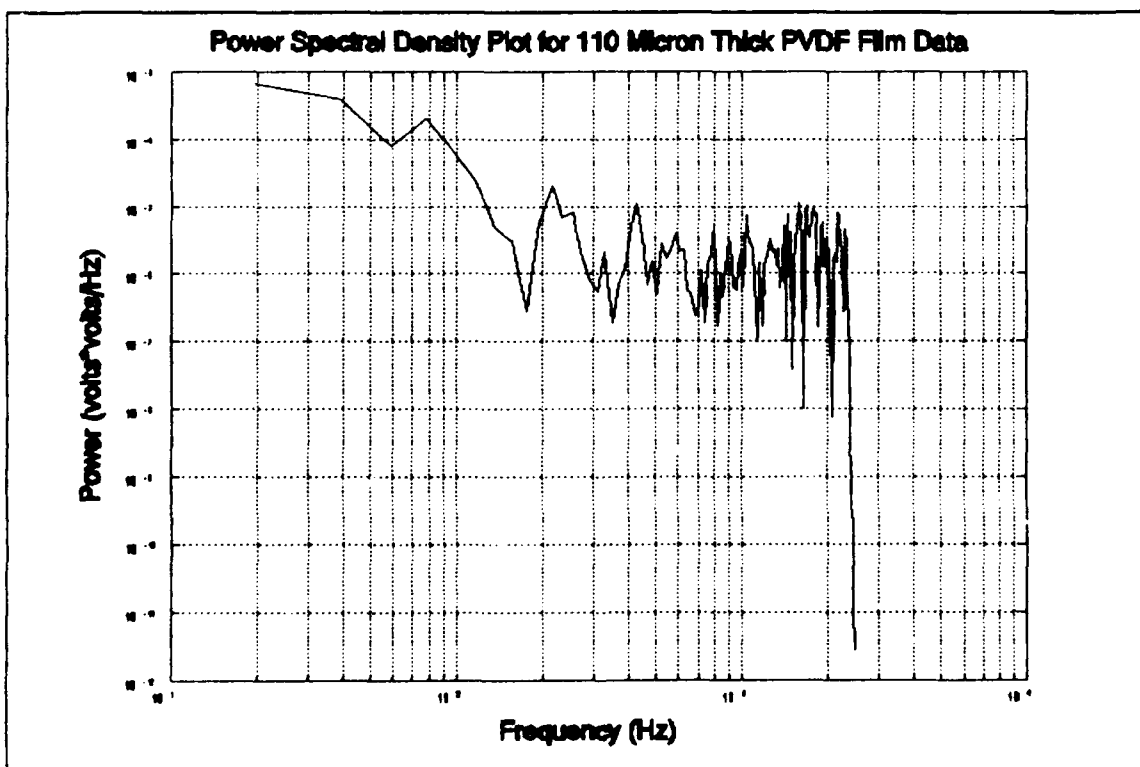


Figure 4-8. PSD of PVDF Film Time History Data.

Between 1000 and 2500 Hz, the responses are not nearly as similar. The gage response decreases by more than 20 dB after 1000 Hz, and then it increases 40 dB and peaks at 2060 Hz, and then decreases after this. The film shows a strong response up to 1160 Hz, and then it has a 20 dB decrease out to 1200 Hz. Above 1200 Hz, the PVDF film's response increases by 20 dB and peaks at 2200 Hz. Both responses decrease by more than 20 dB after 2500 Hz due to filtering.

Below 200 Hz the two responses differ considerably. The PVDF film's response shows a dominant low frequency component at 2 Hz that diminishes as the frequency increases to 180 Hz. The gage frequency response decreases steadily from 2 to 60 Hz, the stopband's center frequency, and it increases by almost 60 dB and peaks at 160 Hz. The magnitude of the peak on the gage response is the significant difference between the film and gage. The PVDF's film response manifests a stronger low frequency response, and the gage indicates a large response centered at 160 Hz.

Time History. The time histories of the film and gage show similar trends. These are shown in Figures 4-9 and 4-10. Overall, the gage shows a much greater dynamic response, but the low frequency and DC trends of both gages are very similar. On a point-by-point basis, the film's response appears to be time shifted by approximately 5 ms. This time shift is attributed to be the cause of the phase shift observed in the charge amplifier's output.

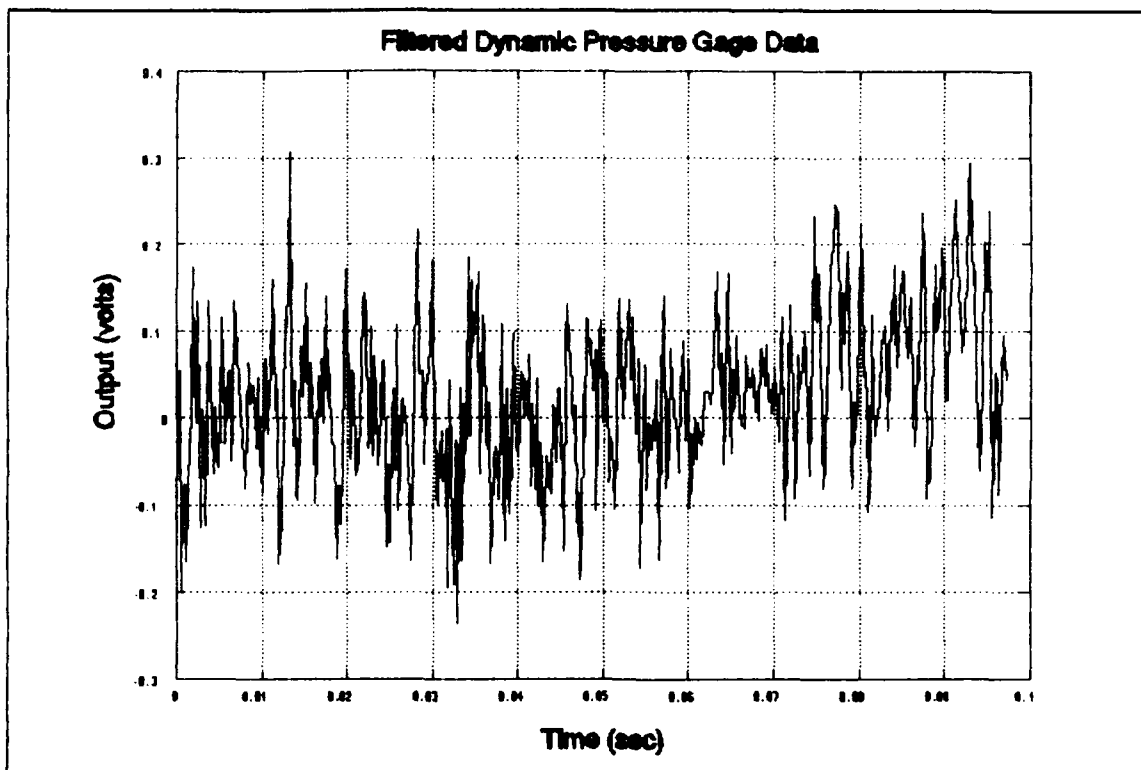


Figure 4-9. Filtered Data for the Dynamic Pressure Gage.

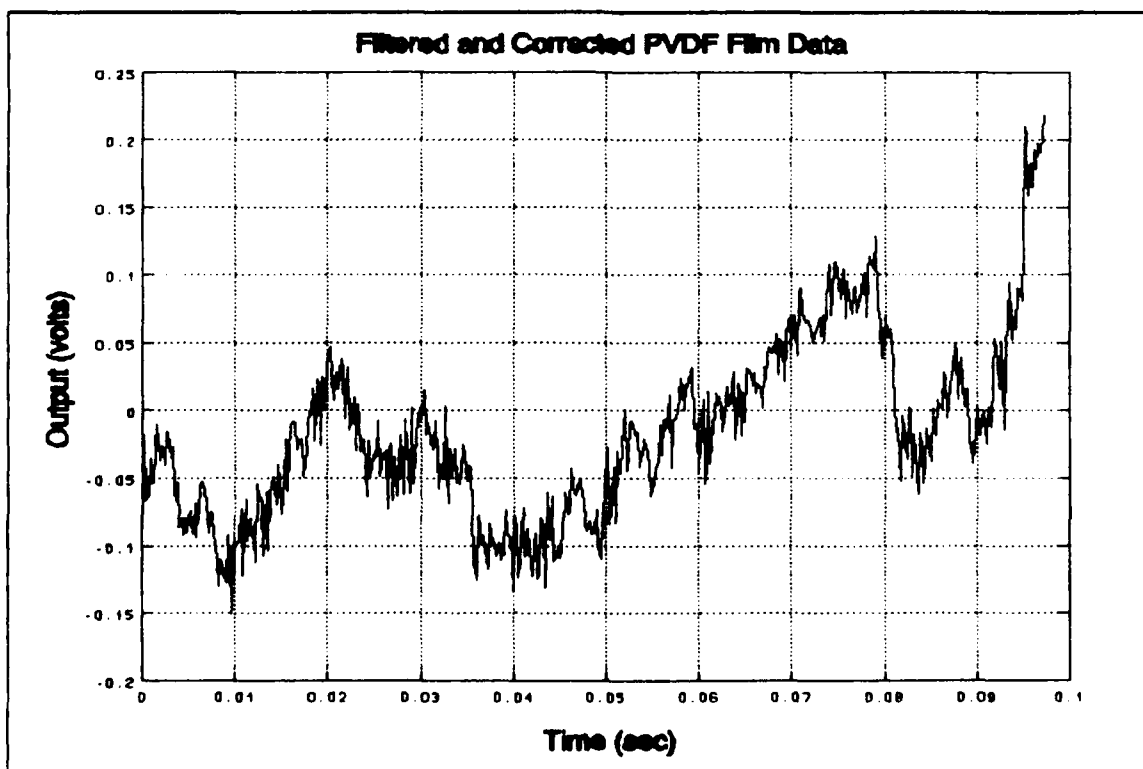


Figure 4-10. Filtered and Corrected PVDF Film Gage Data.

Figures 4-11 and 4-12 show the time histories for 52 thick film. The PVDF film's response clearly shows the pressure rise due to the unblocking of the air flow. This indicates that the PVDF film transducer can detect low frequency pressure fluxuations. The dynamic pressure gage does not show a similar step response because it does not give an integrated output.

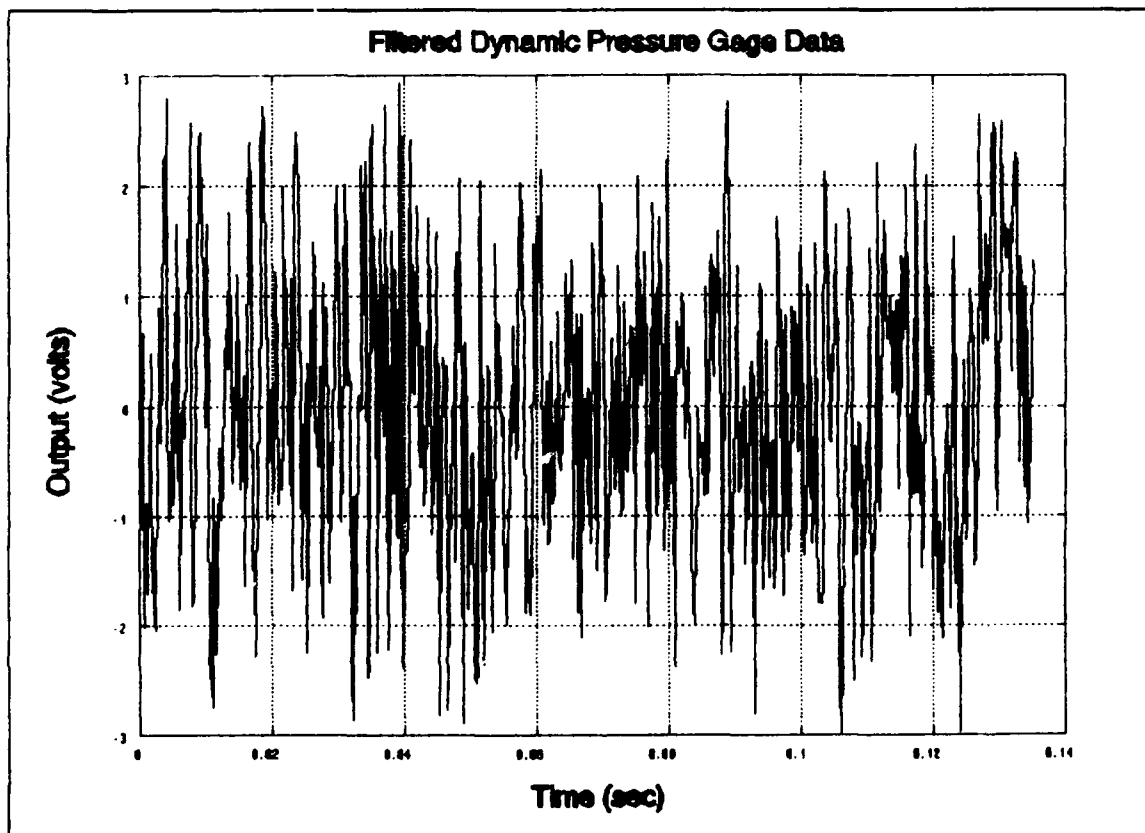


Figure 4-11. Filtered Dynamic Pressure Gage Data.

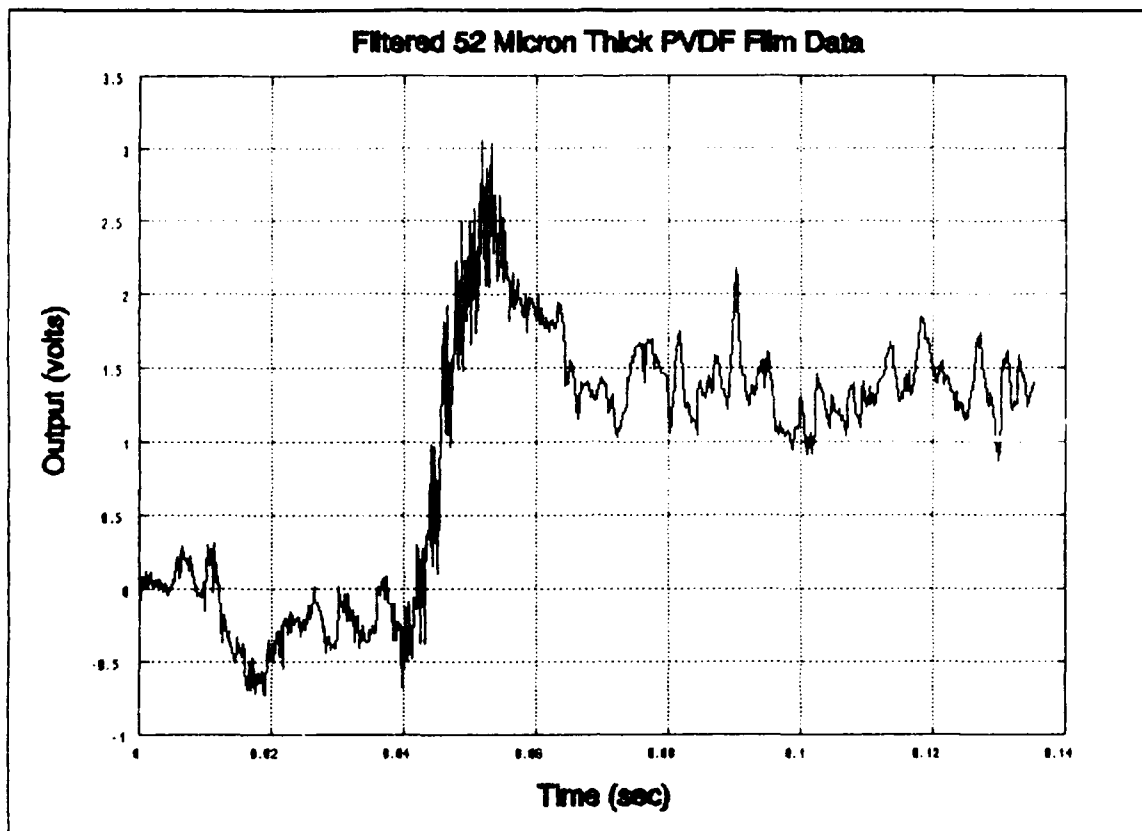


Figure 4-12. Filtered and Corrected 52 Micron Thick PVDF Film Gage Data.

#### Observations

Several areas were not evaluated such as pyroelectric effects, electromagnetic interference, and external vibrational effects. In the PVDF film's response tests, if a warm hand was brought near any film sample, it would produce several hundred millivolts, which is as large as the response to a pressure. Thus, the pyroelectric effect requires additional investigation. The effect of electromagnetic radiation was not apparent in any testing. However, external vibration sources can be a significant problem with the piezoelectric film. If something was dropped on the test bench, the PVDF film, but not the commercial gage, would show

a response. It would also respond to any stresses or vibrations in the model or surface it was mounted on. The next section will address some possible improvements for these problems.

#### Conclusion

All of the performance tests proved to be beneficial and facilitated the design process and the choice of components. The time history reconstruction test proved that an accurate response picture can be obtained from the sampled data. This process facilitated collecting a pressure history of the film and its reconstruction to determine if the PVDF pressure transducer was a viable concept. The initial data analysis shows agreement between the film and gage responses.

## V. Conclusions and Recommendations

### Conclusions

The purpose of this investigation was to design and evaluate the performance of a piezoelectric film pressure transducer to measure frequencies from DC to over 32 kHz. To do this, a reset and sampling technique was implemented with an analog circuit design. A process had to be developed and verified to reconstruct the sampled segments of data into a complete record. Next, the circuit and reconstruction process was used to determine if piezoelectric film could be applied to a body to function as a pressure transducer.

This investigation was successful concerning the design and performance evaluation of the analog reset circuit and sampled data reconstruction process for a known input. The piezoelectric film gage appears to have potential as a pressure gage, but additional development is required before it could be used in a practical application. The film agreed with the dynamic pressure gage at frequencies below 1000 Hz. The dynamic response of the piezoelectric film was limited compared to the dynamic pressure gage at frequencies above 1000 Hz.

### Recommendations

The following recommendations are presented to improve the design and development of the piezoelectric film pressure transducer.

- 1) The charge amplifier circuit needs to be better isolated from the 60 Hz grounding loop. By making a differential amplifier with several operational amplifiers, the film and amplifier would not be connected to the same ground as the operating instrumentation. This feature would facilitate avoiding ground loops and minimize the effect of 60 Hz noise.
- 2) With a more sophisticated A/D device, the reset command pulse and data sampling process could be synchronized. This would eliminate ambiguity in identifying the start of each sampling period. As a result, the first data point of each sample could be used and this feature would improve accuracy. In addition, the data reduction process would be simpler and faster.
- 3) The effects of vibration and heat on the piezoelectric film need to be investigated. In a more advanced test configuration, a "reference" gage that was isolated from the pressure field, could be used. The signal of the reference gage could be subtracted from the pressure gage, thus nulling any pyro, vibration, or strain effects.
- 4) A method must be developed to identify the sensor's initial condition on a long data run. Possibly, a slow sampling and reset rate could be used until the system stabilized, then the rate increased to get the desired data.
- 5) All of the components used in this investigation were the best available. One of the original intents was to use inexpensive commonly available components. Repeating a



standard test with inexpensive components would determine the effect these parts have concerning charge leakage and accuracy. As a result, if there was no degradation in performance, these parts could be used.

- 6) Since the film is flexible and compliant, it can be attached to almost any surface with an adhesive, for example, an area on a aerodynamic body covered with a single piece of film with an etched array of piezoelectric gages on it. This arrangement would facilitate the creation of a pressure map. This particular area needs to be fully exploited and developed to capture the potential of piezoelectric film as a pressure transducer.

## Appendix A: Materials and Equipment

Table A-1. Materials

Kynar PVDF film (28  $\mu\text{m}$ , 52  $\mu\text{m}$ , and 110  $\mu\text{m}$ ),  
Pennwalt Corporation,  
Valley Forge PA  
AD549JH operational Amplifier,  
Analog Devices,  
Norwood MA  
AD524BD Instrumentation Amplifier,  
Analog Devices,  
Norwood MA  
0.02  $\mu\text{F}$  Teflon Capacitor (J11B203KSW),  
Component Research Company,  
Santa Monica CA  
3N170 Transistors  
1 M $\Omega$  Resistor  
470 k $\Omega$  Resistor  
10k  $\Omega$  Resistor  
0.1  $\mu\text{F}$  Ceramic Capacitors  
10 k $\Omega$  Potentiometer  
1N914 Diode  
Conductive Silver Paint  
Spray Adhesive  
2" Polyester Tape  
Twin Lead Shielded Cable  
18 Gauge Solid Copper Wire  
BNC Test Leads

Table A-2. Equipment

Tektronix 2430A Digital Oscilloscope,  
Tektronix, Beaverton OR  
Tektronix FG502 Function Generator,  
Tektronix, Beaverton OR  
Tektronix DM501A Multimeter,  
Tektronix, Beaverton OR  
Power Ten 3103-A-2000 DC Power Supply,  
Power Ten, Sunnyvale CA  
Wavetek 278 Function Generator,  
Wavetek San Diego,  
San Diego CA  
Zenith 248 Data Collection Computer (With IEEE-488 Interface),  
Zenith Data Systems,  
Glenview IL  
Qua Tech 12 Bit A/D converter System (In Z-248),  
Qua Tech, Akron OH

Endevco 8510-B Pressure Transducer,  
Endevco,  
San Juan Capistrano CA  
Endevco 4225 and 4423 Signal Conditioners,  
Endevco,  
San Juan Capistrano CA  
Weights (3)  
Protoboard  
X-acto knife  
Tweezers  
Glass Cutting Surface  
2" Acrylic Tubing (cylinder)  
100 psi Regulated Air Supply

## Appendix B: Recommended Materials

Table B-1. Recommended Operational Amplifiers.

Analog Devices AD549  
Burr - Brown OPA128  
PMI OP-80

Table B-2. Recommended Transistors.

3N169  
3N170  
3N171  
Motorola 2N7000  
Motorola VN2222LL

## Appendix C: Data Collection and Analysis Programs

### Oscilloscope with IEEE-488 Interface Data Collection Program

```
' Declarations for Quick BASIC 4.0/4.5 applications.

' NOTE : include this file only if you are using Quick BASIC
'        Version 4.0 or higher.

' Common GPIB status variables

COMMON SHARED /NISTATBLK/ IBSTA%, IBERR%, IBCNT%

' GPIB Subroutine Declarations

DECLARE SUB IBBNA (BD%, BDNAME$)
DECLARE SUB IBCAC (BD%, V%)
DECLARE SUB IBCLR (BD%)
DECLARE SUB IBCMD (BD%, CMD$)
DECLARE SUB IBCMDA (BD%, CMD$)
DECLARE SUB IBDMA (BD%, V%)
DECLARE SUB IBEOS (BD%, V%)
DECLARE SUB IBEOT (BD%, V%)
DECLARE SUB IBFIND (BDNAME$, BD%)
DECLARE SUB IBGTS (BD%, V%)
DECLARE SUB IBIST (BD%, V%)
DECLARE SUB IBLOC (BD%)
DECLARE SUB IBONL (BD%, V%)
DECLARE SUB IBPAD (BD%, V%)
DECLARE SUB IBPCT (BD%)
DECLARE SUB IBPPC (BD%, V%)
DECLARE SUB IBRD (BD%, RD$)
DECLARE SUB IBRDA (BD%, RD$)
DECLARE SUB IBRDF (BD%, FLNAME$)
DECLARE SUB IBRDI (BD%, IARR%(), CNT%)
DECLARE SUB IBRDIA (BD%, IARR%(), CNT%)
DECLARE SUB IBRPP (BD%, PPR%)
DECLARE SUB IBRSC (BD%, V%)
DECLARE SUB IBRSP (BD%, SPR%)
DECLARE SUB IBRSV (BD%, V%)
DECLARE SUB IBSAD (BD%, V%)
DECLARE SUB IBSIC (BD%)
DECLARE SUB IBSRE (BD%, V%)
DECLARE SUB IBSTOP (BD%)
DECLARE SUB IBTMO (BD%, V%)
DECLARE SUB IBTRAP (MASK%, MODE%)
DECLARE SUB IBTRG (BD%)
DECLARE SUB IBWAIT (BD%, MASK%)
DECLARE SUB IBWRT (BD%, WRT$)
DECLARE SUB IBWRTA (BD%, WRT$)
```

```

DECLARE SUB IBWRTF (BD%, FLNAME$)
DECLARE SUB IBWRTI (BD%, IARR%(), CNT%)
DECLARE SUB IBWRTIA (BD%, IARR%(), CNT%)

```

#### GPIB Function Declarations

```

DECLARE FUNCTION ILBNA% (BD%, BDNAME$)
DECLARE FUNCTION ILCAC% (BD%, V%)
DECLARE FUNCTION ILCLR% (BD%)
DECLARE FUNCTION ILCMD% (BD%, CMD$, CNT%)
DECLARE FUNCTION ILCMDA% (BD%, CMD$, CNT%)
DECLARE FUNCTION ILDMA% (BD%, V%)
DECLARE FUNCTION ILEOS% (BD%, V%)
DECLARE FUNCTION ILEOT% (BD%, V%)
DECLARE FUNCTION ILFIND% (BDNAME$)
DECLARE FUNCTION ILGTS% (BD%, V%)
DECLARE FUNCTION ILIST% (BD%, V%)
DECLARE FUNCTION ILLOC% (BD%)
DECLARE FUNCTION ILONL% (BD%, V%)
DECLARE FUNCTION ILPAD% (BD%, V%)
DECLARE FUNCTION ILPCT% (BD%)
DECLARE FUNCTION ILPPC% (BD%, V%)
DECLARE FUNCTION ILRD% (BD%, RD$, CNT%)
DECLARE FUNCTION ILRDA% (BD%, RD$, CNT%)
DECLARE FUNCTION ILRDF% (BD%, FLNAME$)
DECLARE FUNCTION ILRDI% (BD%, IARR%(), CNT%)
DECLARE FUNCTION ILRDIA% (BD%, IARR%(), CNT%)
DECLARE FUNCTION ILRPP% (BD%, PPR%)
DECLARE FUNCTION ILRSC% (BD%, V%)
DECLARE FUNCTION ILRSP% (BD%, SPR%)
DECLARE FUNCTION ILRSV% (BD%, V%)
DECLARE FUNCTION ILSAD% (BD%, V%)
DECLARE FUNCTION ILSIC% (BD%)
DECLARE FUNCTION ILSRE% (BD%, V%)
DECLARE FUNCTION ILSTOP% (BD%)
DECLARE FUNCTION ILTMO% (BD%, V%)
DECLARE FUNCTION ILTRAP% (MASK%, MODE%)
DECLARE FUNCTION ILTRG% (BD%)
DECLARE FUNCTION ILWAIT% (BD%, MASK%)
DECLARE FUNCTION ILWRT% (BD%, WRT$, CNT%)
DECLARE FUNCTION ILWRTA% (BD%, WRT$, CNT%)
DECLARE FUNCTION ILWRTF% (BD%, FLNAME$)
DECLARE FUNCTION ILWRTI% (BD%, IARR%(), CNT%)
DECLARE FUNCTION ILWRTIA% (BD%, IARR%(), CNT%)
INPUT "NAME DATA FILE FOR DATA STORAGE:XXXXX NO EXTENSION";
  NA$
NA$ = "D:" + NA$ + ".DAT"
OPEN NA$ FOR OUTPUT AS #1

UDNAME$ = "DEV1"

CALL IBFIND(UDNAME$, DEV1%)
WRT$ = "CLE"

```

```

JU$ = SPACE$(50)
CALL IBWRT(DEV1%, WRT$)
CALL IBRD(DEV1%, JU$)
    WRT$ = "CH1?VOL"
    CALL IBWRT(DEV1%, WRT$)
    VO$ = SPACE$(100)
    CALL IBRD(DEV1%, VO$)
    VO! = VAL(VO$)
    VO! = VO! * .04
    PRINT VO!
    WRT$ = "HOR?BSE"
    CALL IBWRT(DEV1%, WRT$)
    ho$ = SPACE$(100)
    CALL IBRD(DEV1%, ho$)
    ho = VAL(ho$)
    ho = (ho * 20) / 1024
    PRINT ho
WRT$ = "PAT OFF"
CALL IBWRT(DEV1%, WRT$)
INPUT; "PRESS ENTER TO COLLECT WAVEFORM "; XXX$ 'WRT$=" WA?"
WRT$ = "CURV?"
CALL IBWRT(DEV1%, WRT$)
RD$ = SPACE$(5100)

CALL IBRD(DEV1%, RD$)

HO1 = 0
WRT$ = "LOC OFF"
CALL IBWRT(DEV1%, WRT$)
    Z = 0
    K = 0
    txtlength = LEN(RD$)
    p = 0
    FOR I = 1 TO txtlength
        C$ = MID$(RD$, I, 1)

        IF C$ = "," THEN
            Z = VAL(D$): D$ = "": C$ = "": PRINT #1, USING
            1"###.####^" ; HO1;
            PRINT #1, Z * VO!: HO1 = HO1 + ho
            p = p + 1
        END IF
        D$ = D$ + C$
        K = K + 1
    NEXT I
PRINT p, K
CLOSE

```

This program was written in Microsoft Quick Basic version 4.5.

Qua Tech A/D Board Data Collection Program

```
10 CLS
20 COLOR ,1
30 PRINT "THE QUATECH BOARD IS A 12 BIT A/D CONVERTER"
40 PRINT
50 PRINT "IT IS SETUP FOR + AND - 2.5 VOLTS INPUT MAX"
60 PRINT
70 PRINT "THE SAMPLE RATE AND NUMBER OF DATA POINTS"
80 PRINT
90 PRINT "ARE USER SELECTABLE"
100 PRINT
110 INPUT "PRESS RETURN TO CONTINUE      ",CCC$
120 COLOR ,0
130 CLS
140 CLS
150 COLOR ,1
1 *****
170 'THE FIRST TEN LINES OF THE PROGRAM ARE FOR LINKING THE
    BASIC *
180 'CALL COMMANDS TO THE QUATECH MACHINE LANGUAGE

1 *****
200 ADC.SETUP=&H3:SETCTM=&H6
210 SETC0=&H9
220 INADC12.B=&HC:SEGADDR=&HF:INADC12.BB=&H12
230 SETMD1=&H15:SETMD2=&H18:SETC1=&H1B:SETC2=&H1E
240 RSETC1=&H21:RSETC2=&H24:READC1=&H27:READC2=&H2A
250 DEF SEG=0
260 CSEG2=PEEK(&H3CA)+256*PEEK(&H3CB)
270 DEF SEG=CSEG2
280 GOSUB 330          'QUATECH BOARD SETUP
290 GOSUB 860          'DATA FILE SETUP
300 GOSUB 1010         'AQUIRE DATA
310 '
320 END
330 *****
340 ' THIS IS THE SUBPROGRAM THAT SETS UP THE QUATECH *
350 ' BOARD FOR SAMPLE RATE AND NUMBER OF DATA POINTS.*
360 *****
370 '
380 '
390 DIM ARRAY%(9000)
400 DIM VOLT!(9000)
410 ADDRESS%=&H300
420 N%=2
430 CALL ADC.SETUP(ADDRESS%,N%)
440 '
450 PRINT "CHOSE A SAMPLE RATE BETWEEN 200 HZ - 32000 HZ"
460 PRINT
```



```

470 INPUT " INPUT SAMPLE RATE IN Hz:  ",HZ%
480 C0% = 5000000!/HZ%          ' SETS SAMPLE RATE
490 CALL SETCO (C0%)
500 PRINT
510 PRINT
520 PRINT
530 '
540 PRINT "CHOSE THE NUMBER OF DATA POINTS BETWEEN 65-8191"
550 PRINT
560 '
570 INPUT "ENTER NUMBER OF DATA POINTS:  ", LENGTH%
580 COLOR ,0
590 CLS
600 COLOR ,1
610 '
620 '
630 PRINT "SAMPLE RATE:  " HZ%
640 '
650 PRINT
660 PRINT
670 PRINT
680 '
690 PRINT "NUMBER OF DATA POINTS:  " LENGTH%
700 '
710 PRINT
720 PRINT
730 PRINT
740 TM = (1/HZ%)*LENGTH%
750 PRINT TM " SEC  TOTAL DATA ACQUISITION TIME"
760 PRINT
770 PRINT
780 PRINT
790 INPUT "ARE THE SAMPLE RATE AND NUMBER OF POINTS CORRECT:
      Y/N  ";T$
800 IF T$= "N" OR T$ = "n" THEN 470
810 '
820 '
830 COLOR ,0
840 COLOR ,1
850 RETURN
860 '*****
870 'THIS SUBPROGRAM WILL SETUP YOUR DATA FILE.          *
880 '*****
890 COLOR ,0
900 CLS
910 COLOR ,1
920 '
930 INPUT "NAME DATA FILE FOR DATA STORAGE: XXXXX NO
      EXTENSION, 5 CHR OR LESS  ";NA$
940 '
950 NAT$= "D:" + NA$ + "T" + ".DAT"
960 'NA$ = "D:" + NA$ + "F" + ".DAT"
970 '

```

```

980 'OPEN NA$ FOR OUTPUT AS #1
990 OPEN NAT$ FOR OUTPUT AS #2
1000 RETURN
1010 '*****
1020 ' THIS SUBPROGRAM IS TO ACQUIRE DATA AND CHANGE IT *
1030 ' TO A VOLTAGE. *
1040 '*****
1050 '
1060 COLOR ,0
1070 CLS
1080 COLOR ,1
1090 INPUT "PRESS RETURN TO ACQUIRE DATA. ",B$
1100 '
1110 COLOR ,0
1120 CLS
1130 COLOR ,1
1140 PRINT "ACQUIRING DATA !!!!!!!!!!"
1150 TM = (1/HZ%)*LENGTH%
1155 PRINT
1160 PRINT TM " SEC TOTAL DATA ACQUISITION TIME"
1170 '
1180 CALL INADC12.B(LENGTH%,ARRAY%(1)) 'STORE INTO ARRAY
1184 PRINT
1185 PRINT "DATA HAS BEEN ACQUIRED AND IS BEING STORED."
1190 T!=0
1200 TT=0
1210 FOR I = 1 TO (LENGTH%*2) STEP 2
1220 T!= 1/HZ% * TT
1230 VOLT!(I)= -(ARRAY%(I)+.5)* (5/4095)+ 2.5
1235 VOLT!(I+1)= -(ARRAY%(I+1)+.5)* (5/4095)+ 2.5
1240 'PRINT#1,USING"##.####"; VOLT!(I)
1250 PRINT#2,USING"##.###^ ^ ^ "; T!;
1260 PRINT#2,USING"##.### "; VOLT!(I);
1265 PRINT#2,USING"##.###"; VOLT!(I+1)
1270 TT=TT+1
1280 NEXT I
1290 COLOR ,0
1300 CLS
1310 COLOR ,1
1320 RETURN

```

This program was written in Microsoft GW-Basic version 3.1.

## MATLAB PSD and Digital Filtering Program

```
echo on
clc
%   This program filters data through a Chebyshev lowpass
%   and stopband filter. Then the PSD is plotted after each
%   filtering.

pause % Strike any key to continue.
clc

n=length(y);
plot(y(1:n)), title('Input Data'), pause
clc

N = 4; % Filter order
stopband = [.0225 .0255]; % Stopband specification
[Bb,Ab] = butter(4, stopband,'stop');
stopband = [.023 .025]; % Stopband specification
ripple = 40; % Allowable attenuation in decibels
[Bc,Ac] = cheby2(N, ripple, stopband,'stop');

N = 8; % Filter order
passband = [.95]; % Lowpass specification
[Bb1,Ab1] = butter(N, passband);

ripple = .01; % Allowable ripple, in decibels
[Bc1,Ac1] = cheby1(N, ripple, passband);

%   Let's filter the data with the Chebyshev stopband filter
%   and plot the PSD.

Y = filtfilt(Bc,Ac,y);

P = spectrum(Y,1024);

specplot(P,5000), grid, pause
clc

%   Let's filter the data again with the Chebyshev lowpass
%   filter and plot the resulting PSD.

Z = filtfilt(Bc1,Ac1,Y);

Q = spectrum(Z,1024);

specplot(Q,5000), grid, pause
clc
```

This program was written using MATLAB version 3.5f.

Sample LOTUS 123 Cell Formulas for Reducing Reset Data

A2: 0.0008  
B2: 0.564  
C2: -2.501  
D2: (A1-\$A\$1)  
E2: (@IF(@ABS(C2)>2,@TRUE,@FALSE)=1)  
F2: (@IF(E2=1,0,0.951\*C2))  
G2: (F2)  
H2: (G2-12.492\*D2)  
A3: 0.001  
B3: 0.612  
C3: 0.153  
D3: (A2-\$A\$1)  
E3: (@IF(@ABS(C3)>2,@TRUE,@FALSE)=1)  
F3: (@IF(E3=1,0,0.951\*C3))  
G3: (F3)  
H3: (G3-12.492\*D3)  
A4: 0.0012  
B4: -0.23  
C4: 0.171  
D4: (A3-\$A\$1)  
E4: (@IF(@ABS(C4)>2,@TRUE,@FALSE)=1)  
F4: (@IF(E4=1,0,0.951\*C4))  
G4: (F4)  
H4: (G4-12.492\*D4)  
A5: 0.0014  
B5: -2.121  
C5: 0.079  
D5: (A4-\$A\$1)  
E5: (@IF(@ABS(C5)>2,@TRUE,@FALSE)=1)  
F5: (@IF(E5=1,0,0.951\*C5))  
G5: (F5)  
H5: (G5-12.492\*D5)  
A6: 0.0016  
B6: -0.882  
C6: 0.211  
D6: (A5-\$A\$1)  
E6: (@IF(@ABS(C6)>2,@TRUE,@FALSE)=1)  
F6: (@IF(E6=1,0,0.951\*C6))  
G6: (F6)  
H6: (G6-12.492\*D6)  
A7: 0.0018  
B7: -1.86  
C7: 0.079  
D7: (A6-\$A\$1)  
E7: (@IF(@ABS(C7)>2,@TRUE,@FALSE)=1)  
F7: (@IF(E7=1,0,0.951\*C7))  
G7: (F7)  
H7: (G7-12.492\*D7)

A8: 0.002  
 B8: -0.464  
 C8: 0.087  
 D8: (A7-\$A\$1)  
 E8: (@IF(@ABS(C8)>2,@TRUE,@FALSE)=1)  
 F8: (@IF(E8=1,0,0.951\*C8))  
 G8: @IF(E8=0,(F8+\$G\$7),((\$G\$7+G7+F9)/2))  
 H8: (G8-12.492\*D8)  
 A9: 0.0022  
 B9: 0.294  
 C9: 0.105  
 D9: (A8-\$A\$1)  
 E9: (@IF(@ABS(C9)>2,@TRUE,@FALSE)=1)  
 F9: (@IF(E9=1,0,0.951\*C9))  
 G9: @IF(E9=0,(F9+\$G\$7),((\$G\$7+G8+F10)/2))  
 H9: (G9-12.492\*D9)  
 A10: 0.0024  
 B10: -0.674  
 C10: 0.122  
 D10: (A9-\$A\$1)  
 E10: (@IF(@ABS(C10)>2,@TRUE,@FALSE)=1)  
 F10: (@IF(E10=1,0,0.951\*C10))  
 G10: @IF(E10=0,(F10+\$G\$7),((\$G\$7+G9+F11)/2))  
 H10: (G10-12.492\*D10)  
 A11: 0.0026  
 B11: -1.724  
 C11: 0.018  
 D11: (A10-\$A\$1)  
 E11: (@IF(@ABS(C11)>2,@TRUE,@FALSE)=1)  
 F11: (@IF(E11=1,0,0.951\*C11))  
 G11: @IF(E11=0,(F11+\$G\$7),((\$G\$7+G10+F12)/2))  
 H11: (G11-12.492\*D11)  
 A12: 0.0028  
 B12: -1.895  
 C12: -2.501  
 D12: (A11-\$A\$1)  
 E12: (@IF(@ABS(C12)>2,@TRUE,@FALSE)=1)  
 F12: (@IF(E12=1,0,0.951\*C12))  
 G12: @IF(E12=0,(F12+\$G\$11),((\$G\$11+G11+F13)/2))  
 H12: (G12-12.492\*D12)  
 A13: 0.003  
 B13: -2.303  
 C13: 0.029  
 D13: (A12-\$A\$1)  
 E13: (@IF(@ABS(C13)>2,@TRUE,@FALSE)=1)  
 F13: (@IF(E13=1,0,0.951\*C13))  
 G13: @IF(E13=0,(F13+\$G\$11),((\$G\$11+G12+F14)/2))  
 H13: (G13-12.492\*D13)  
 A14: 0.0032  
 B14: -0.326  
 C14: 0.017  
 D14: (A13-\$A\$1)  
 E14: (@IF(@ABS(C14)>2,@TRUE,@FALSE)=1)

F14: (@IF(E14=1,0,0.951\*C14))  
 G14: @IF(E14=0,(F14+\$G\$11),((\$G\$11+G13+F15)/2))  
 H14: (G14-12.492\*D14)  
 A15: 0.0034  
 B15: -0.248  
 C15: 0.033  
 D15: (A14-\$A\$1)  
 E15: (@IF(@ABS(C15)>2,@TRUE,@FALSE)=1)  
 F15: (@IF(E15=1,0,0.951\*C15))  
 G15: @IF(E15=0,(F15+\$G\$11),((\$G\$11+G14+F16)/2))  
 H15: (G15-12.492\*D15)  
 A16: 0.0036  
 B16: 0.913  
 C16: -0.023  
 D16: (A15-\$A\$1)  
 E16: (@IF(@ABS(C16)>2,@TRUE,@FALSE)=1)  
 F16: (@IF(E16=1,0,0.951\*C16))  
 G16: @IF(E16=0,(F16+\$G\$11),((\$G\$11+G15+F17)/2))  
 H16: (G16-12.492\*D16)  
 A17: 0.0038  
 B17: -0.614  
 C17: 0.021  
 D17: (A16-\$A\$1)  
 E17: (@IF(@ABS(C17)>2,@TRUE,@FALSE)=1)  
 F17: (@IF(E17=1,0,0.951\*C17))  
 G17: @IF(E17=0,(F17+\$G\$11),((\$G\$11+G16+F18)/2))  
 H17: (G17-12.492\*D17)  
 A18: 0.004  
 B18: 0.371  
 C18: 0.009  
 D18: (A17-\$A\$1)  
 E18: (@IF(@ABS(C18)>2,@TRUE,@FALSE)=1)  
 F18: (@IF(E18=1,0,0.951\*C18))  
 G18: @IF(E18=0,(F18+\$G\$11),((\$G\$11+G17+F19)/2))  
 H18: (G18-12.492\*D18)  
 A19: 0.0042  
 B19: 1.943  
 C19: -0.07  
 D19: (A18-\$A\$1)  
 E19: (@IF(@ABS(C19)>2,@TRUE,@FALSE)=1)  
 F19: (@IF(E19=1,0,0.951\*C19))  
 G19: @IF(E19=0,(F19+\$G\$11),((\$G\$11+G18+F20)/2))  
 H19: (G19-12.492\*D19)  
 A20: 0.0044  
 B20: 1.748  
 C20: 0.011  
 D20: (A19-\$A\$1)  
 E20: (@IF(@ABS(C20)>2,@TRUE,@FALSE)=1)  
 F20: (@IF(E20=1,0,0.951\*C20))  
 G20: @IF(E20=0,(F20+\$G\$11),((\$G\$11+G19+F21)/2))  
 H20: (G20-12.492\*D20)

A21: 0.0046  
 B21: 2.499  
 C21: -0.029  
 D21: (A20-\$A\$1)  
 E21: (@IF(@ABS(C21)>2,@TRUE,@FALSE)=1)  
 F21: (@IF(E21=1,0,0.951\*C21))  
 G21: @IF(E21=0,(F21+\$G\$11),((\$G\$11+G20+F22)/2))  
 H21: (G21-12.492\*D21)  
 A22: 0.0048  
 B22: 0.245  
 C22: -2.501  
 D22: (A21-\$A\$1)  
 E22: (@IF(@ABS(C22)>2,@TRUE,@FALSE)=1)  
 F22: (@IF(E22=1,0,0.951\*C22))  
 G22: @IF(E22=0,(F22+\$G\$21),((\$G\$21+G21+F23)/2))  
 H22: (G22-12.492\*D22)  
 A23: 0.005  
 B23: -1.339  
 C23: -0.076  
 D23: (A22-\$A\$1)  
 E23: (@IF(@ABS(C23)>2,@TRUE,@FALSE)=1)  
 F23: (@IF(E23=1,0,0.951\*C23))  
 G23: @IF(E23=0,(F23+\$G\$21),((\$G\$21+G22+F24)/2))  
 H23: (G23-12.492\*D23)

Appendix D: Sample Cost Data

Table D-1. PVDF Film Transducer Cost

<u>Material</u>	<u>Cost</u>
PVDF Film	\$ 0.20 cm <sup>2</sup>
AD549 Operational Amplifier	\$ 17.00 each
3N170 Transistor	\$ 3.00 each
Twin Lead Shielded Cable	\$ 0.20 ft
AD525 Instrumentation Amplifier	\$ 25.00 each
8 Channel Multiplexing Chip	<u>\$ 0.42 each</u>
Approximate cost for eight transducers:	\$ 60.00

Table D-2. Dynamic Pressure Transducer Cost

<u>Material</u>	<u>Cost</u>
Endevco 8510-B Pressure Transducer	\$ 350.00 each
Signal Conditioner	<u>\$ 350.00 each</u>
Approximate cost for eight transducers:	\$5600.00



## Appendix E: Digital Filter Data

### MATLAB Filter Demonstration Program

```
echo on
clc
% This example shows the use of the FFT function for
% spectral analysis. A common use of FFT's is to find the
% frequency components of a signal buried in a noisy time
% domain signal.

pause % Strike any key to continue.
clc
% First we need to create some data. Consider data sampled
% at 5000 Hz. We start by forming a time axis for our
% data, running from t=0 until t=.41 in steps of 0.2
% millisecond:

t = 0:.0002:.4096;

pause % Strike any key to continue.

% Next we can form a signal containing 60 Hz:

x = sin(2*pi*60*t);

pause % Strike any key to continue.

% and add some random noise with a standard deviation of 2
% to produce a noisy signal y:

rand('normal')
y = x + 2*rand(t);

pause % Strike any key to continue.
x=[];t=[];
clc
% Let's take a look at our noisy signal y by plotting it.

pause % Strike any key for plot.

plot(y(1:1024)), title('Noisy time domain signal'), pause
clc
% Clearly, it is difficult to identify the frequency
% components from looking at the original signal; that's
% why spectral analysis is so popular.
% Finding the discrete Fourier transform of the noisy
% signal y is easy. We just take the fast-Fourier transform
% (FFT); using the Spectrum Function:
```

```

P = spectrum(y,1024);

pause % Strike any key to continue.

%   The power spectral density, a measurement of the energy
%   at various frequencies, is found with:

%   P=spectrum(y,1024)

pause % Strike any key to continue.

clc
%   To plot the power spectral density, we must first form a
%   frequency axis:

f = 5000/2048*(0:1024);

%   which we do for the first 1024 points. (The remainder of
%   the 1024 points are symmetric.) We can now plot the
%   power spectral density:

pause % Strike any key for plot.

specplot(P,5000), pause
clc
%   Let's zoom in and plot only up to 600 Hz:

pause % Strike any key for plot.

plot(f(1:128),P(1:128,1)), title('Power spectral density'), ...
xlabel('Frequency (Hz)'), pause

rand('uniform')
clc

%   This example demonstrates the use of the BUTTER and
%   CHEBY2 functions to design stopband filters. A sampling
%   rate of 5000 Hz is assumed.

%   We start by specifying the desired frequency response,
%   point-wise, with 1.0 corresponding to half the sample
%   rate:

f = [0 .0236 .0236 .0244 .0244 1];
H = [1 1 0 0 1 1];

pause % Strike any key to continue.

clc
%   Next we plot the desired frequency response to make sure
%   it is what we want. To plot the frequency response, we
%   can scale the normalized frequency axis:

```

```

fs = 5000;           % sampling rate
fhz = f*fs/2;

%   Now we are ready to plot.

pause % Strike any key for plot.

plot(fhz,H), title('Desired Frequency Response'),...
xlabel('Frequency (Hz)'), ylabel('Magnitude'), pause
clc
%   If the desired frequency response did not look right,
%   we would go back and change H. However, in this case
%   everything looks OK so we perform the design:

format compact

n = 1024;

ff = fs/(2*n) * (0:n-1);
%   Now let's design Butterworth and Chebyshev stopband
%   filters
%   with the same stopband (defined between 0.0 and 1.0).

N = 4;               % filter order
stopband = [.0225 .0255]; % Stopband specification
[Bb,Ab] = butter(4, stopband,'stop');
stopband = [.023 .025]; % Stopband specification
ripple = 40;         % Allowable attenuation in decibels
[Bc,Ac] = cheby2(N, ripple, stopband,'stop');

%   Now find the frequency responses:

hb = freqz(Bb,Ab,n);
hc = freqz(Bc,Ac,n);
hm = [abs(hb)];
hn = [abs(hc)];

pause % Strike any key for plot.

plot(ff,hm), title('Butterworth filter'), ..
xlabel('Frequency (Hz)'), ylabel('Magnitude'), grid, pause
clc
%   Often it is useful to look at the frequency response on
%   logarithmic (dB) scales.

pause % Strike any key for plot.

plot(ff(15:35),20*log10(hm(15:35,:))),...
title('Butterworth filter'), ..
xlabel('Frequency (Hz)'), ylabel('Magnitude in dB'),grid,
pause
clc
plot(ff,hn), title('Chebyshev filters'), ..

```

```

xlabel('Frequency (Hz)'), ylabel('Magnitude'), grid, pause
clc
%   Often it is useful to look at the frequency response on
%   logarithmic (dB) scales.

pause % Strike any key for plot.

plot(ff(15:35),20*log10(hn(15:35,:))),...
title('Chebyshev filters'), ..
xlabel('Frequency (Hz)'), ylabel('Magnitude in dB'),grid,
pause
clc
%   This example demonstrates the use of the BUTTER and
%   CHEBY1 functions to design low-pass filters. A sampling
%   rate of 5000 Hz is assumed.

%   We start by specifying the desired frequency response,
%   point-wise, with 1.0 corresponding to half the sample
%   rate:

f = [0 .95 .95 1];
H = [1 1 0 0];

clc
%   Next we plot the desired frequency response to make sure
%   it is what we want. To plot the frequency response, we
%   can scale the normalized frequency axis:
%   Now we are ready to plot.

fhx = f*fs/2
pause % Strike any key for plot.

plot(fhx,H), title('Desired Frequency Response'),..
xlabel('Frequency (Hz)'), ylabel('Magnitude'), grid, pause
clc
%   If the desired frequency response did not look right,
%   we would go back and change H. However, in this case
%   everything looks OK so we perform the design:

format compact
clc

%   Now let's design Butterworth and Chebyshev low-pass
%   filters with the same band (defined between 0.0 and 1.0).

N = 8; % Filter order
passband = [.95]; % Low-pass specification
[Bb1,Ab1] = butter(N, passband);

ripple = .01; % Allowable ripple, in decibels
[Bc1,Ac1] = cheby1(N, ripple, passband);

```

```

%    Now find the frequency responses:

hb1 = freqz(Bb1,Ab1,n);
hc1 = freqz(Bc1,Ac1,n);
h1 = [abs(hb1) abs(hc1)];

pause % Strike any key for plot.

plot(ff,h1), title('Butterworth and Chebyshev filters'), ..
xlabel('Frequency (Hz)'), ylabel('Magnitude'),pause
clc
%    Often it is useful to look at the frequency response on
%    logarithmic (dB) scales.

pause % Strike any key for plot.

plot(ff(2:n),20*log10(h1(2:n,:))),..
title('Butterworth and Chebyshev filters'), ..
xlabel('Frequency (Hz)'), ylabel('Magnitude in dB'), grid,
pause
clc

%    Let's filter the data with the Chebyshev stopband filter
%    and plot the PSD.

Y = filtfilt(Bc,Ac,y);

P = spectrum(Y,1024);

specplot(P,5000), grid, pause
clc

%    Let's filter the data again with Chebyshev low-pass
%    filter and plot the resulting PSD.

Z = filtfilt(Bc1,Ac1,Y);

Q = spectrum(Z,1024);

specplot(Q,5000), grid, pause
clc

```

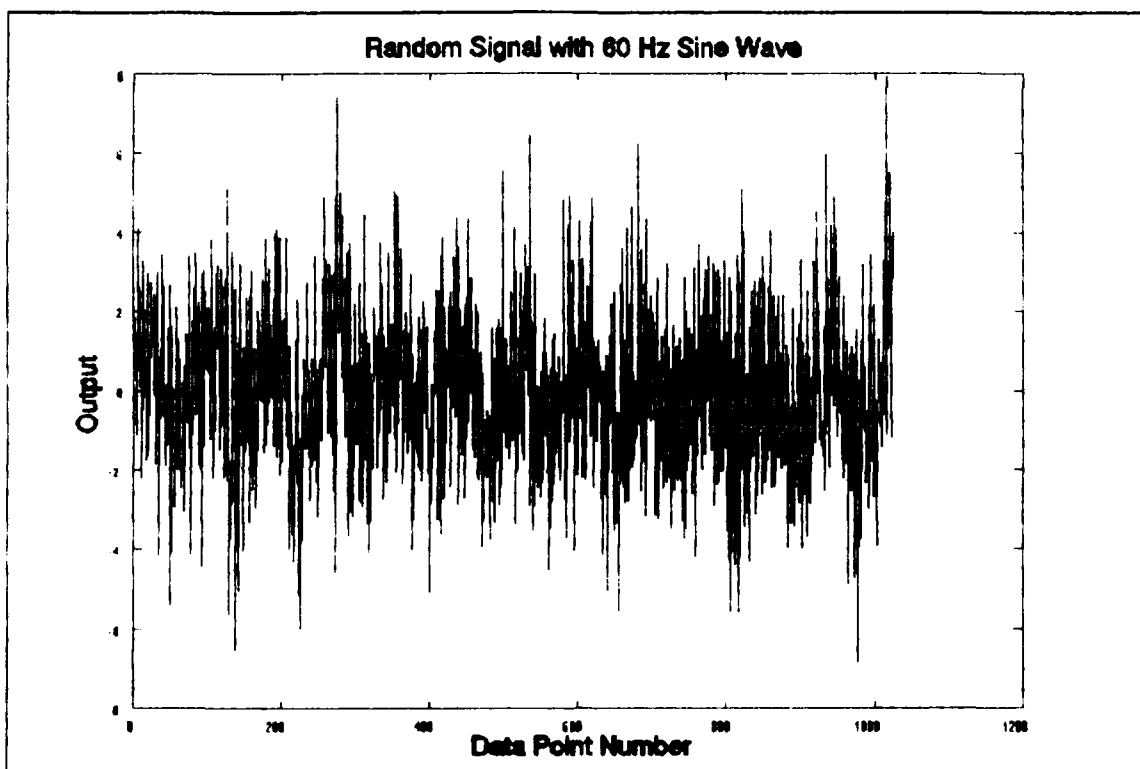


Figure E-1. Random Noise Signal with Embedded 60 Hz Sine Wave.

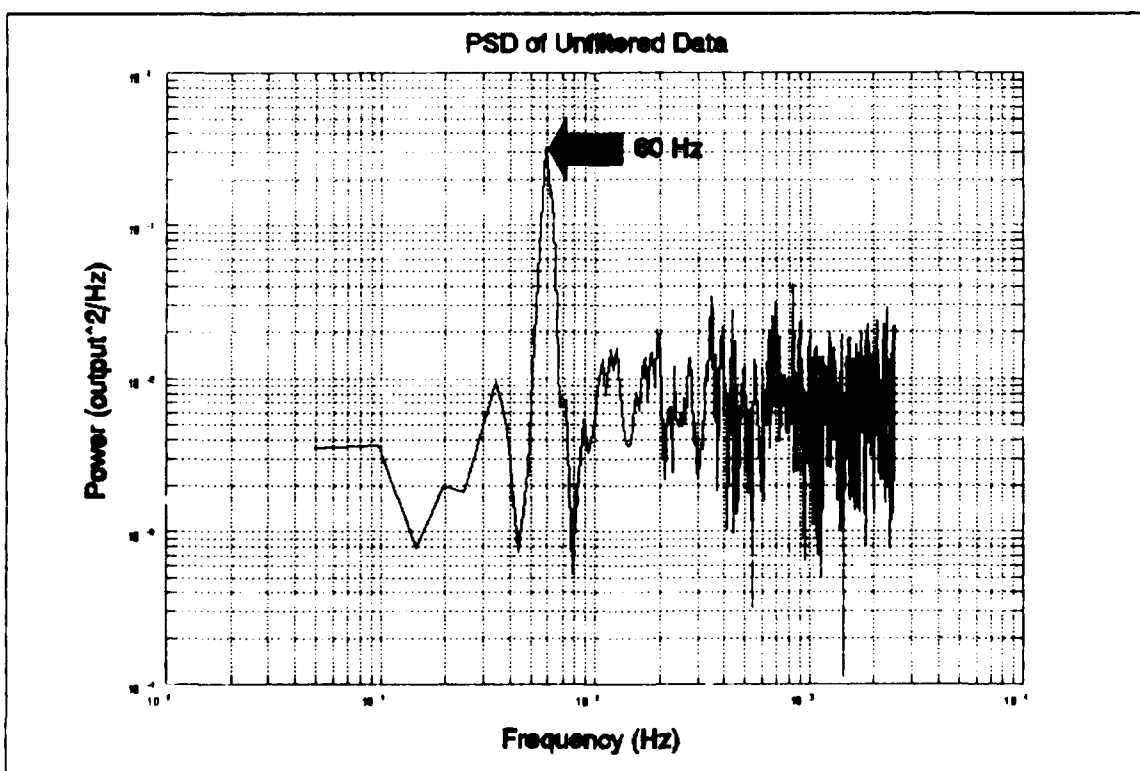


Figure E-2. PSD of the Unfiltered Random Noise Signal.

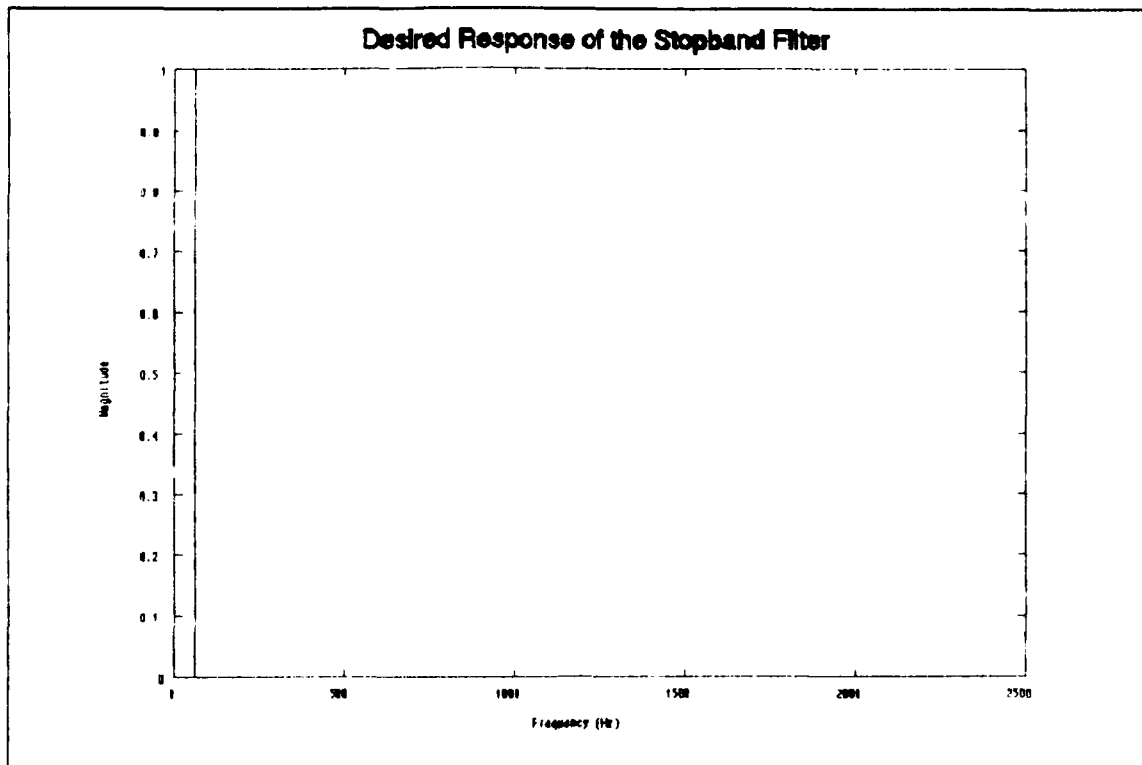


Figure E-3. Desired Frequency Response of the Stopband Filter.

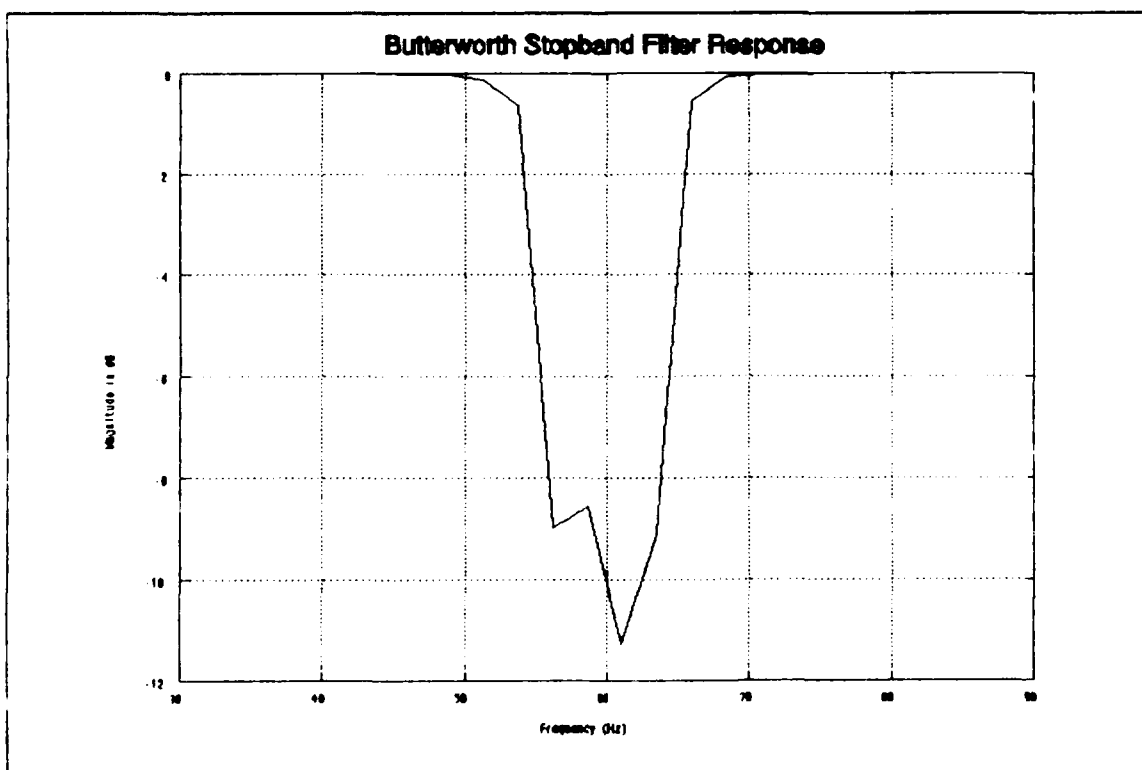


Figure E-4. Response of the Butterworth Stopband Filter.

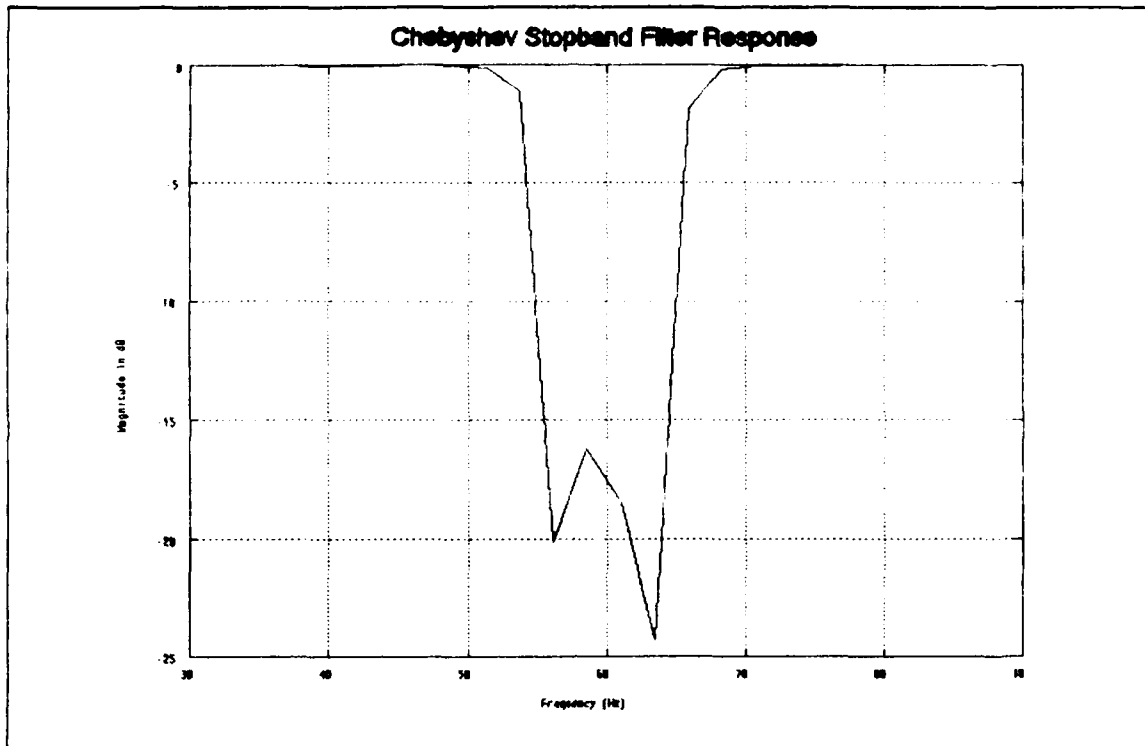


Figure E-5. Response of the Chebyshev Stopband Filter.

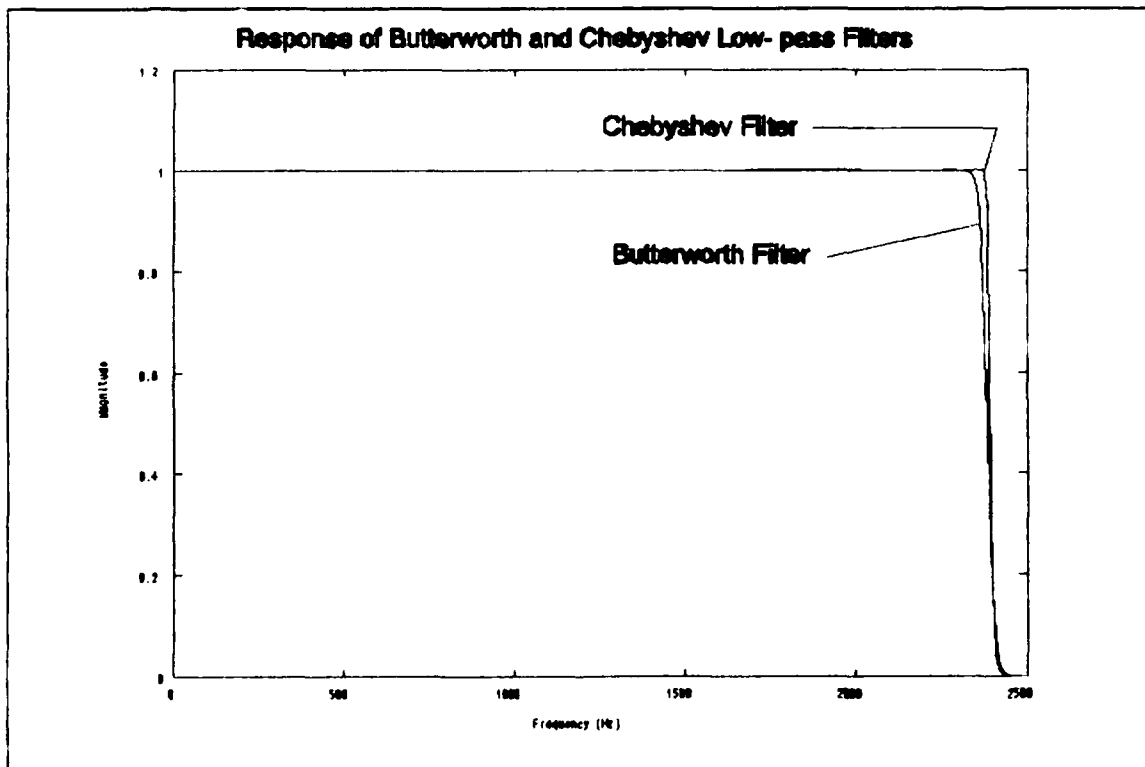


Figure E-6. Response of the Butterworth and Chebyshev Low-pass Filters.



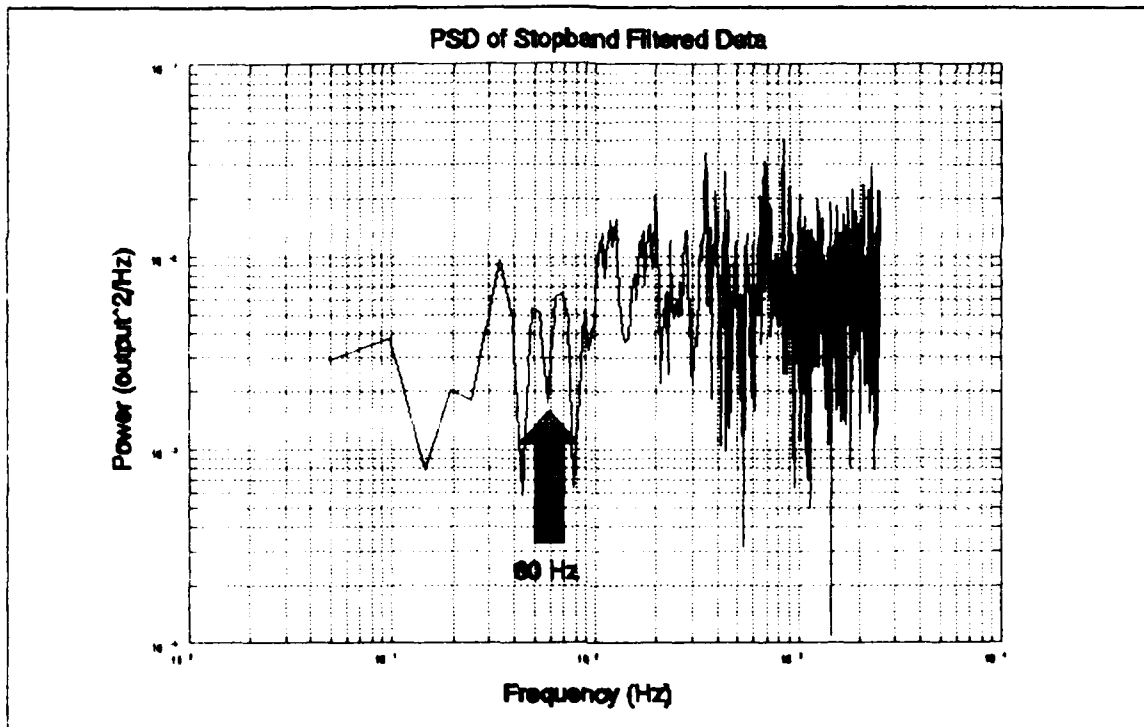


Figure E-7. PSD of the 'Noisy' Data Filtered with the Chebyshev Stopband Filter.

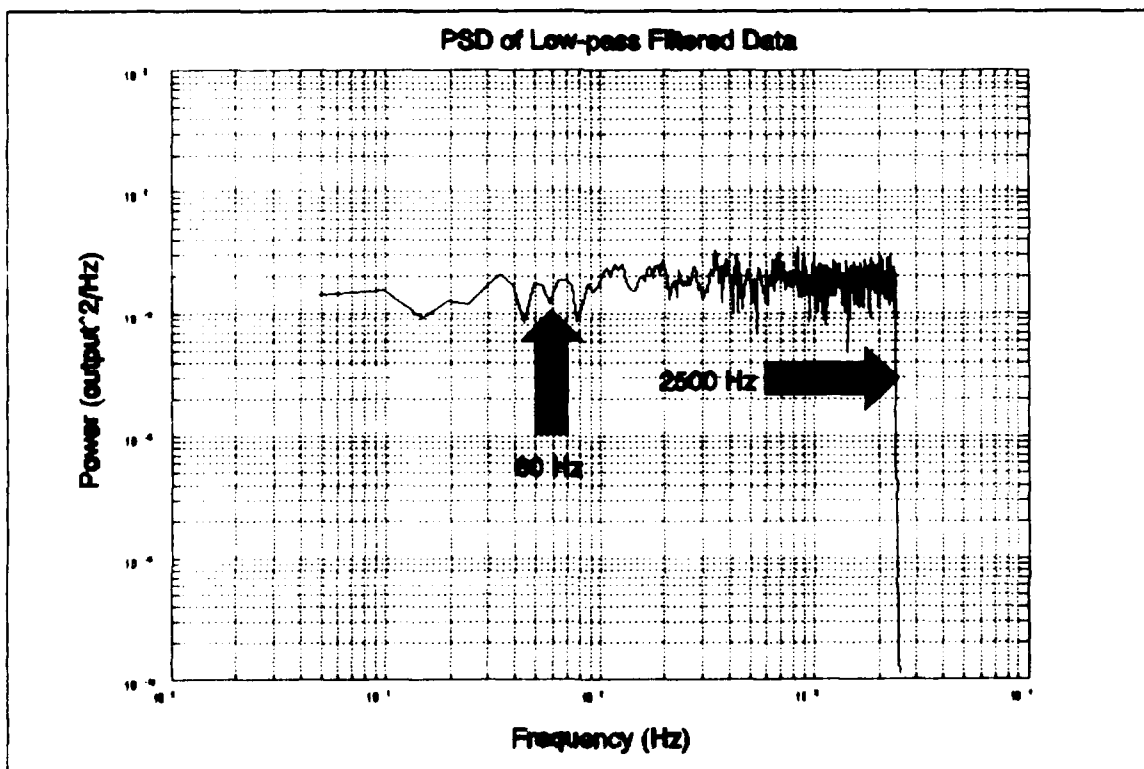


Figure E-8. PSD of the 'Noisy' Data Filtered the Chebyshev Stopband and Low-pass Filters.

## Appendix F: Sample Time History Reconstruction

This appendix gives a sample of how the data was reconstructed for the sine wave shown in Figure 4-6. Before any calculations are done, the offset, due to an improper nulling adjustment on the charge amplifier, is removed. This is done by subtracting the simple mean of all the data points. For point [1:1], the adjusted value is  $0.0055 - 0.0003 = 0.0053$ , where 0.0003 is the mean offset. The first three adjusted data sample periods are shown in the following arrays (see Table F-1 column E). That is,

Array 1 = [0.0055 0.0085 0.0135 0.0205 0.0275 0.0365 0.0475  
0.0595 0.0755 0.0885 0.1075]

Array 2 = [0.0145 0.0325 0.0545 0.0765 0.0985 0.1205 0.1475  
0.1715 0.1945 0.2235 0.2495]

Array 3 = [0.0155 0.0425 0.0725 0.0975 0.1295 0.1555 0.1865  
0.2145 0.2415 0.2685 0.2955].

To create time history, the first point of Array 1 [1:1] is taken as the starting point and set to zero. The rest of the sample points remain unaffected.

The first point in Array 2 [2:1], is a "reset" point and is discarded. It is replaced by a "bridge" point calculated from equation 3-36. That is,

$$[2:1]_{\text{new}} = \frac{x_{n-1} + x_{n-1} + x_{n+1}}{2} = \frac{0.1023 + 0.1023 + 0.0309}{2} = 0.1177$$

where  $x_n$  is the point [2:1],  $x_{n-1}$  is point [1:11], and  $x_{n+1}$  is point [2:2]. The next ten points in Array 2, now need to have the value of point [1:11] added to them. That is,

$$\begin{aligned}
[2:2]_{\text{new}} &= [2:2]_{\text{old}} + [1:11] \\
[2:3]_{\text{new}} &= [2:3]_{\text{old}} + [1:11] \\
&\vdots \\
[2:11]_{\text{new}} &= [2:11]_{\text{old}} + [1:11].
\end{aligned}$$

The "new" points replace the "old" values. This procedure is repeated for the next array of points (see Table F-1 column I). The resulting new points are shown in the following arrays. That is,

Array 1 = [0.0053 0.0081 0.0129 0.0195 0.0262 0.0347 0.0452  
0.0566 0.0718 0.0842 0.1023]

Array 2<sub>new</sub> = [0.1177 0.1332 0.1541 0.1750 0.1960 0.2169 0.2426  
0.2654 0.2875 0.3148 0.3396]

Array 3<sub>new</sub> = [0.3597 0.3800 0.4085 0.4323 0.4627 0.4874 0.5170  
0.5436 0.5693 0.5949 0.6206].

Next, the DC offset is removed by scaling all points with the DC offset factor. For example point [1:2] becomes  $0.95 * 0.0081 = 0.0077$ . All the other points are scaled in the same manner (see Table F-1 column H).

In the case of the sine wave, the rise rate was found by fitting a linear least-squares line through the peak amplitude points of each cycle. These three values (0.916, 0.896, and 0.868) were 0.0196 seconds apart. The least-squares analysis gave a slope of -1.173.

The rise rate error was removed by subtracting the rise or "slope correction factor" from each point. Point [1:1] was the starting point and is assumed to have no error. Point [1:2] was corrected in the following manner:

$$[1:2]_{\text{corrected}} = [1:2] + 1/5555 * n * 1.173 = 0.0079$$

where n is the index beginning with n = 0 for [1:1], n = 12 for [2:1], n = 22 for [3:1], and so forth for the remaining points in the data record. Finally, the sine wave was re-adjusted by subtracting 0.4646 from each point to give a zero mean to the corrected data points (see Table F-1 column J).

For the first thirty three points, the final corrected values are as follows: [-0.4646 -0.4563 -0.4513 -0.4446 -0.4376 -0.4288 -0.4181 -0.4066 -0.3911 -0.3785 -0.3602 -0.3446 -0.3289 -0.3077 -0.2866 -0.2655 -0.2443 -0.2185 -0.1954 -0.1733 -0.1456 -0.1206 -0.1002 -0.0797 -0.0510 -0.0270 0.0036 0.0286 0.0583 0.0851 0.1110 0.1369 0.1628]. These values correspond to the first thirty three points plotted in Figure 4-6.

Table F-1. Sample Numbers Used to Reconstruct Sine Data.

D	E	F	G	H	I	J
0	0.005529	-0.15828	0	0.005258	0	-0.46461
0.00018	0.008529	-0.24528	0	0.008111	0.008111	-0.45629
0.00036	0.013529	-0.33228	0	0.012866	0.012866	-0.45132
0.00054	0.020529	-0.41228	0	0.019523	0.019523	-0.44445
0.00072	0.027529	-0.49728	0	0.02618	0.02618	-0.43759
0.0009	0.036529	-0.57728	0	0.034739	0.034739	-0.42882
0.00108	0.047529	-0.65928	0	0.0452	0.0452	-0.41814
0.00126	0.059529	-0.73828	0	0.056612	0.056612	-0.40652
0.00144	0.075529	-0.81228	0	0.071828	0.071828	-0.39109
0.00162	0.088529	-0.88528	0	0.084191	0.084191	-0.37852
0.001801	0.107529	-0.95728	0	0.10226	0.10226	-0.36024
0.001981	0.014529	-1.02528	1	0	0.117728	-0.34456
0.002161	0.032529	-1.09128	0	0.030935	0.133196	-0.32888
0.002341	0.054529	-1.15028	0	0.051857	0.154118	-0.30775
0.002521	0.076529	-1.20728	0	0.072779	0.17504	-0.28661
0.002701	0.098529	-1.26128	0	0.093701	0.195962	-0.26548
0.002881	0.120529	-1.31028	0	0.114623	0.216884	-0.24435
0.003061	0.147529	-1.35528	0	0.1403	0.242561	-0.21846
0.003241	0.171529	-1.39428	0	0.163124	0.265385	-0.19542
0.003421	0.194529	-1.43128	0	0.184997	0.287258	-0.17334
0.003601	0.223529	-1.46228	0	0.212576	0.314837	-0.14555
0.003781	0.249529	-1.49228	0	0.237302	0.339563	-0.12061
0.003961	0.015529	-1.51428	1	0	0.359785	-0.10018
0.004141	0.042529	-1.52828	0	0.040445	0.380008	-0.07975
0.004321	0.072529	-1.54128	0	0.068975	0.408538	-0.051
0.004501	0.097529	-1.55028	0	0.09275	0.432313	-0.02702
0.004681	0.125529	-1.55828	0	0.123182	0.462745	0.003624
0.004861	0.155529	-1.55028	0	0.147908	0.487471	0.028561
0.005041	0.186529	-1.53928	0	0.177389	0.516952	0.058253
0.005221	0.214529	-1.52728	0	0.204017	0.54358	0.085092
0.005401	0.241529	-1.51328	0	0.229694	0.569257	0.110981
0.005581	0.268529	-1.49228	0	0.255371	0.594934	0.136869
0.005701	0.295529	-1.46228	0	0.281048	0.620611	0.162757
0.005941	0.011529	-1.43228	1	0	0.639407	0.181764

Column A: Not shown - Original time tag.

Column B: Not shown - Original reset data.

Column C: Not shown - Original input data.

Column D: Time adjusted to zero.

Column E: Reset data offset adjusted to zero.

Column F: Input data offset adjusted to zero.

Column G: Reset point logic: 0=not reset, 1=reset.

Column H: DC offset removed from reset data.

Column I: Reset data joined to form time history.

Column J: Reset data corrected for rise rate and zero mean.

# LOTUS 123 Cell Formulas Used to Reconstruct the Sine Data

A1: 0.00324  
 B1: -0.01  
 C1: -0.14  
 D1: (A1-\$A\$1)  
 E1: (B1-\$B\$343)  
 F1: (C1-\$C\$343)  
 G1: 0  
 H1: (@IF(G1=1,0,0.951\*E1))  
 I1: 0  
 J1: (1.17267303\*D1+(I1-0.46461))  
 A2: 0.00342  
 B2: -0.007  
 C2: -0.227  
 D2: (A2-\$A\$1)  
 E2: (B2-\$B\$343)  
 F2: (C2-\$C\$343)  
 G2: (@IF(@ABS(E2-E1)>0.051,@TRUE,@FALSE)=1)  
 H2: (@IF(G2=1,0,0.951\*E2))  
 I2: @IF(G2=0,(H2\*1),(I1+I1+H3)/2))  
 J2: (1.17267303\*D2+(I2-0.46461))  
 A3: 0.0036  
 B3: -0.002  
 C3: -0.314  
 D3: (A3-\$A\$1)  
 E3: (B3-\$B\$343)  
 F3: (C3-\$C\$343)  
 G3: (@IF(@ABS(E3-E2)>0.051,@TRUE,@FALSE)=1)  
 H3: (@IF(G3=1,0,0.951\*E3))  
 I3: @IF(G3=0,(H3\*1),(I2+I2+H4)/2))  
 J3: (1.17267303\*D3+(I3-0.46461))  
 A4: 0.00378  
 B4: 0.005  
 C4: -0.394  
 D4: (A4-\$A\$1)  
 E4: (B4-\$B\$343)  
 F4: (C4-\$C\$343)  
 G4: (@IF(@ABS(E4-E3)>0.051,@TRUE,@FALSE)=1)  
 H4: (@IF(G4=1,0,0.951\*E4))  
 I4: @IF(G4=0,(H4\*1),(I3+I3+H5)/2))  
 J4: (1.17267303\*D4+(I4-0.46461))  
 A5: 0.00396  
 B5: 0.012  
 C5: -0.479  
 D5: (A5-\$A\$1)  
 E5: (B5-\$B\$343)  
 F5: (C5-\$C\$343)  
 G5: (@IF(@ABS(E5-E4)>0.051,@TRUE,@FALSE)=1)  
 H5: (@IF(G5=1,0,0.951\*E5))  
 I5: @IF(G5=0,(H5\*1),(I4+I4+H6)/2))  
 J5: (1.17267303\*D5+(I5-0.46461))

A6: 0.00414  
 B6: 0.021  
 C6: -0.559  
 D6: (A6-\$A\$1)  
 E6: (B6-\$B\$343)  
 F6: (C6-\$C\$343)  
 G6: (@IF(@ABS(E6-E5)>0.051,@TRUE,@FALSE)=1)  
 H6: (@IF(G6=1,0,0.951\*E6))  
 I6: @IF(G6=0,(H6\*1),(I5+I5+H7)/2))  
 J6: (1.17267303\*D6+(I6-0.46461))  
 A7: 0.00432  
 B7: 0.032  
 C7: -0.641  
 D7: (A7-\$A\$1)  
 E7: (B7-\$B\$343)  
 F7: (C7-\$C\$343)  
 G7: (@IF(@ABS(E7-E6)>0.051,@TRUE,@FALSE)=1)  
 H7: (@IF(G7=1,0,0.951\*E7))  
 I7: @IF(G7=0,(H7\*1),(I6+I6+H8)/2))  
 J7: (1.17267303\*D7+(I7-0.46461))  
 A8: 0.0045  
 B8: 0.044  
 C8: -0.72  
 D8: (A8-\$A\$1)  
 E8: (B8-\$B\$343)  
 F8: (C8-\$C\$343)  
 G8: (@IF(@ABS(E8-E7)>0.051,@TRUE,@FALSE)=1)  
 H8: (@IF(G8=1,0,0.951\*E8))  
 I8: @IF(G8=0,(H8\*1),(I7+I7+H9)/2))  
 J8: (1.17267303\*D8+(I8-0.46461))  
 A9: 0.00468  
 B9: 0.06  
 C9: -0.794  
 D9: (A9-\$A\$1)  
 E9: (B9-\$B\$343)  
 F9: (C9-\$C\$343)  
 G9: (@IF(@ABS(E9-E8)>0.051,@TRUE,@FALSE)=1)  
 H9: (@IF(G9=1,0,0.951\*E9))  
 I9: @IF(G9=0,(H9\*1),(I8+I8+H10)/2))  
 J9: (1.17267303\*D9+(I9-0.46461))  
 A10: 0.00486  
 B10: 0.073  
 C10: -0.867  
 D10: (A10-\$A\$1)  
 E10: (B10-\$B\$343)  
 F10: (C10-\$C\$343)  
 G10: (@IF(@ABS(E10-E9)>0.051,@TRUE,@FALSE)=1)  
 H10: (@IF(G10=1,0,0.951\*E10))  
 I10: @IF(G10=0,(H10\*1),(I9+I9+H11)/2))  
 J10: (1.17267303\*D10+(I10-0.46461))  
 A11: 0.005041  
 B11: 0.092  
 C11: -0.939

D11: (A11-\$A\$1)  
 E11: (B11-\$B\$343)  
 F11: (C11-\$C\$343)  
 G11: (@IF(@ABS(E11-E10)>0.051,@TRUE,@FALSE)=1)  
 H11: (@IF(G11=1,0,0.951\*E11))  
 I11: @IF(G11=0,(H11\*1),(I10+I10+H12)/2))  
 J11: (1.17267303\*D11+(I11-0.46461))  
 A12: 0.005221  
 B12: -0.001  
 C12: -1.007  
 D12: (A12-\$A\$1)  
 E12: (B12-\$B\$343)  
 F12: (C12-\$C\$343)  
 G12: (@IF(@ABS(E12-E11)>0.051,@TRUE,@FALSE)=1)  
 H12: (@IF(G12=1,0,0.951\*E12))  
 I12: @IF(G12=0,(H12+\$I\$11),((\$I\$11+I11+H13)/2))  
 J12: (1.17267303\*D12+(I12-0.46461))  
 A13: 0.005401  
 B13: 0.017  
 C13: -1.073  
 D13: (A13-\$A\$1)  
 E13: (B13-\$B\$343)  
 F13: (C13-\$C\$343)  
 G13: (@IF(@ABS(E13-E12)>0.051,@TRUE,@FALSE)=1)  
 H13: (@IF(G13=1,0,0.951\*E13))  
 I13: @IF(G13=0,(H13+\$I\$11),((\$I\$11+I12+H14)/2))  
 J13: (1.17267303\*D13+(I13-0.46461))  
 A14: 0.005581  
 B14: 0.039  
 C14: -1.132  
 D14: (A14-\$A\$1)  
 E14: (B14-\$B\$343)  
 F14: (C14-\$C\$343)  
 G14: (@IF(@ABS(E14-E13)>0.051,@TRUE,@FALSE)=1)  
 H14: (@IF(G14=1,0,0.951\*E14))  
 I14: @IF(G14=0,(H14+\$I\$11),((\$I\$11+I13+H15)/2))  
 J14: (1.17267303\*D14+(I14-0.46461))  
 A15: 0.005761  
 B15: 0.061  
 C15: -1.189  
 D15: (A15-\$A\$1)  
 E15: (B15-\$B\$343)  
 F15: (C15-\$C\$343)  
 G15: (@IF(@ABS(E15-E14)>0.051,@TRUE,@FALSE)=1)  
 H15: (@IF(G15=1,0,0.951\*E15))  
 I15: @IF(G15=0,(H15+\$I\$11),((\$I\$11+I14+H16)/2))  
 J15: (1.17267303\*D15+(I15-0.46461))  
 A16: 0.005941  
 B16: 0.083  
 C16: -1.243  
 D16: (A16-\$A\$1)  
 E16: (B16-\$B\$343)  
 F16: (C16-\$C\$343)



G16: (@IF(@ABS(E16-E15)>0.051,@TRUE,@FALSE)=1)  
 H16: (@IF(G16=1,0,0.951\*E16))  
 I16: @IF(G16=0,(H16+\$I\$11),((\$I\$11+I15+H17)/2))  
 J16: (1.17267303\*D16+(I16-0.46461))  
 A17: 0.006121  
 B17: 0.105  
 C17: -1.292  
 D17: (A17-\$A\$1)  
 E17: (B17-\$B\$343)  
 F17: (C17-\$C\$343)  
 G17: (@IF(@ABS(E17-E16)>0.051,@TRUE,@FALSE)=1)  
 H17: (@IF(G17=1,0,0.951\*E17))  
 I17: @IF(G17=0,(H17+\$I\$11),((\$I\$11+I16+H18)/2))  
 J17: (1.17267303\*D17+(I17-0.46461))  
 A18: 0.006301  
 B18: 0.132  
 C18: -1.337  
 D18: (A18-\$A\$1)  
 E18: (B18-\$B\$343)  
 F18: (C18-\$C\$343)  
 G18: (@IF(@ABS(E18-E17)>0.051,@TRUE,@FALSE)=1)  
 H18: (@IF(G18=1,0,0.951\*E18))  
 I18: @IF(G18=0,(H18+\$I\$11),((\$I\$11+I17+H19)/2))  
 J18: (1.17267303\*D18+(I18-0.46461))  
 A19: 0.006481  
 B19: 0.156  
 C19: -1.376  
 D19: (A19-\$A\$1)  
 E19: (B19-\$B\$343)  
 F19: (C19-\$C\$343)  
 G19: (@IF(@ABS(E19-E18)>0.051,@TRUE,@FALSE)=1)  
 H19: (@IF(G19=1,0,0.951\*E19))  
 I19: @IF(G19=0,(H19+\$I\$11),((\$I\$11+I18+H20)/2))  
 J19: (1.17267303\*D19+(I19-0.46461))  
 A20: 0.006661  
 B20: 0.179  
 C20: -1.413  
 D20: (A20-\$A\$1)  
 E20: (B20-\$B\$343)  
 F20: (C20-\$C\$343)  
 G20: (@IF(@ABS(E20-E19)>0.051,@TRUE,@FALSE)=1)  
 H20: (@IF(G20=1,0,0.951\*E20))  
 I20: @IF(G20=0,(H20+\$I\$11),((\$I\$11+I19+H21)/2))  
 J20: (1.17267303\*D20+(I20-0.46461))  
 A21: 0.006841  
 B21: 0.208  
 C21: -1.444  
 D21: (A21-\$A\$1)  
 E21: (B21-\$B\$343)  
 F21: (C21-\$C\$343)  
 G21: (@IF(@ABS(E21-E20)>0.051,@TRUE,@FALSE)=1)  
 H21: (@IF(G21=1,0,0.951\*E21))  
 I21: @IF(G21=0,(H21+\$I\$11),((\$I\$11+I20+H22)/2))

J21: (1.17267303\*D21+(I21-0.46461))  
 A22: 0.007021  
 B22: 0.234  
 C22: -1.474  
 D22: (A22-\$A\$1)  
 E22: (B22-\$B\$343)  
 F22: (C22-\$C\$343)  
 G22: (@IF(@ABS(E22-E21)>0.051,@TRUE,@FALSE)=1)  
 H22: (@IF(G22=1,0,0.951\*E22))  
 I22: @IF(G22=0,(H22+\$I\$11),((\$I\$11+I21+H23)/2))  
 J22: (1.17267303\*D22+(I22-0.46461))  
 A23: 0.007201  
 B23: 0  
 C23: -1.496  
 D23: (A23-\$A\$1)  
 E23: (B23-\$B\$343)  
 F23: (C23-\$C\$343)  
 G23: (@IF(@ABS(E23-E22)>0.051,@TRUE,@FALSE)=1)  
 H23: (@IF(G23=1,0,0.951\*E23))  
 I23: @IF(G23=0,(H23+\$I\$22),((\$I\$22+I22+H24)/2))  
 J23: (1.17267303\*D23+(I23-0.46461))  
 A24: 0.007381  
 B24: 0.027  
 C24: -1.51  
 D24: (A24-\$A\$1)  
 E24: (B24-\$B\$343)  
 F24: (C24-\$C\$343)  
 G24: (@IF(@ABS(E24-E23)>0.051,@TRUE,@FALSE)=1)  
 H24: (@IF(G24=1,0,0.951\*E24))  
 I24: @IF(G24=0,(H24+\$I\$22),((\$I\$22+I23+H25)/2))  
 J24: (1.17267303\*D24+(I24-0.46461))  
 A25: 0.007561  
 B25: 0.057  
 C25: -1.523  
 D25: (A25-\$A\$1)  
 E25: (B25-\$B\$343)  
 F25: (C25-\$C\$343)  
 G25: (@IF(@ABS(E25-E24)>0.051,@TRUE,@FALSE)=1)  
 H25: (@IF(G25=1,0,0.951\*E25))  
 I25: @IF(G25=0,(H25+\$I\$22),((\$I\$22+I24+H26)/2))  
 J25: (1.17267303\*D25+(I25-0.46461))  
 A26: 0.007741  
 B26: 0.082  
 C26: -1.532  
 D26: (A26-\$A\$1)  
 E26: (B26-\$B\$343)  
 F26: (C26-\$C\$343)  
 G26: (@IF(@ABS(E26-E25)>0.051,@TRUE,@FALSE)=1)  
 H26: (@IF(G26=1,0,0.951\*E26))  
 I26: @IF(G26=0,(H26+\$I\$22),((\$I\$22+I25+H27)/2))  
 J26: (1.17267303\*D26+(I26-0.46461))  
 A27: 0.007921  
 B27: 0.114

C27: -1.54  
 D27: (A27-\$A\$1)  
 E27: (B27-\$B\$343)  
 F27: (C27-\$C\$343)  
 G27: (@IF(@ABS(E27-E26)>0.051,@TRUE,@FALSE)=1)  
 H27: (@IF(G27=1,0,0.951\*E27))  
 I27: @IF(G27=0,(H27+\$I\$22),((\$I\$22+I26+H28)/2))  
 J27: (1.17267303\*D27+(I27-0.46461))  
 A28: 0.008101  
 B28: 0.14  
 C28: -1.532  
 D28: (A28-\$A\$1)  
 E28: (B28-\$B\$343)  
 F28: (C28-\$C\$343)  
 G28: (@IF(@ABS(E28-E27)>0.051,@TRUE,@FALSE)=1)  
 H28: (@IF(G28=1,0,0.951\*E28))  
 I28: @IF(G28=0,(H28+\$I\$22),((\$I\$22+I27+H29)/2))  
 J28: (1.17267303\*D28+(I28-0.46461))  
 A29: 0.008281  
 B29: 0.171  
 C29: -1.521  
 D29: (A29-\$A\$1)  
 E29: (B29-\$B\$343)  
 F29: (C29-\$C\$343)  
 G29: (@IF(@ABS(E29-E28)>0.051,@TRUE,@FALSE)=1)  
 H29: (@IF(G29=1,0,0.951\*E29))  
 I29: @IF(G29=0,(H29+\$I\$22),((\$I\$22+I28+H30)/2))  
 J29: (1.17267303\*D29+(I29-0.46461))  
 A30: 0.008461  
 B30: 0.199  
 C30: -1.509  
 D30: (A30-\$A\$1)  
 E30: (B30-\$B\$343)  
 F30: (C30-\$C\$343)  
 G30: (@IF(@ABS(E30-E29)>0.051,@TRUE,@FALSE)=1)  
 H30: (@IF(G30=1,0,0.951\*E30))  
 I30: @IF(G30=0,(H30+\$I\$22),((\$I\$22+I29+H31)/2))  
 J30: (1.17267303\*D30+(I30-0.46461))  
 A31: 0.008641  
 B31: 0.226  
 C31: -1.495  
 D31: (A31-\$A\$1)  
 E31: (B31-\$B\$343)  
 F31: (C31-\$C\$343)  
 G31: (@IF(@ABS(E31-E30)>0.051,@TRUE,@FALSE)=1)  
 H31: (@IF(G31=1,0,0.951\*E31))  
 I31: @IF(G31=0,(H31+\$I\$22),((\$I\$22+I30+H32)/2))  
 J31: (1.17267303\*D31+(I31-0.46461))  
 A32: 0.008821  
 B32: 0.253  
 C32: -1.474  
 D32: (A32-\$A\$1)  
 E32: (B32-\$B\$343)

F32: (C32-\$C\$343)  
 G32: (@IF(@ABS(E32-E31)>0.051,@TRUE,@FALSE)=1)  
 H32: (@IF(G32=1,0,0.951\*E32))  
 I32: @IF(G32=0,(H32+\$I\$22),((\$I\$22+I31+H33)/2))  
 J32: (1.17267303\*D32+(I32-0.46461))  
 A33: 0.009001  
 B33: 0.28  
 C33: -1.444  
 D33: (A33-\$A\$1)  
 E33: (B33-\$B\$343)  
 F33: (C33-\$C\$343)  
 G33: (@IF(@ABS(E33-E32)>0.051,@TRUE,@FALSE)=1)  
 H33: (@IF(G33=1,0,0.951\*E33))  
 I33: @IF(G33=0,(H33+\$I\$22),((\$I\$22+I32+H34)/2))  
 J33: (1.17267303\*D33+(I33-0.46461))  
 A34: 0.009181  
 B34: -0.004  
 C34: -1.414  
 D34: (A34-\$A\$1)  
 E34: (B34-\$B\$343)  
 F34: (C34-\$C\$343)  
 G34: (@IF(@ABS(E34-E33)>0.051,@TRUE,@FALSE)=1)  
 H34: (@IF(G34=1,0,0.951\*E34))  
 I34: @IF(G34=0,(H34+\$I\$33),((\$I\$33+I33+H35)/2))  
 J34: (1.17267303\*D34+(I34-0.46461))

### References

1. Amato, I. "Fantastic Plastic, " *Science News*, 136: 328 - 329 (Nov 1989).
2. Carraway, D.L. and A. Bertelrud. "Use of Piezoelectric Foil for Flow Diagnostics," *IEEE Instrumentation In Aerospace Simulation Facilities*. 613 - 626. Piscataway NJ: IEEE, 1989.
3. DeReggi, A.S. and others. *Piezoelectric Polymer Transducers for Dynamic Pressure Measurements: Final Report*, April - December 1975. Contract DOT-HS-4-00835 1A. Washington DC: Department of Transportation, August 1977.
4. "Kynar Piezo Film - a novel transducer," *Scottish Schools Science Equipment Research Centre*, 155: 22-33 (Jan 87).
5. KYNAR Piezo Film Department. *Kynar Piezo Film Technical Manual*. Pennwalt Corporation, Valley Forge PA, 1987.
6. Mitsche, W. and others. "Application of Piezoelectric Foils in Experimental Aerodynamics," *IEEE Instrumentation In Aerospace Simulation Facilities*. 57-65. Piscataway NJ: IEEE, 1989.
7. Park, K.T. and others. "A Charge Readout Algorithm for Piezoelectric Force Transducers," *IEEE International Symposium on the Applications of Ferroelectrics*, (1988). Piscataway NJ: IEEE, 1988.
8. Cady, Walter G. *Piezoelectricity, An Introduction to the Theory and Applications of Electromechanical Phenomena in Crystals*, Volumes I and II (Second Edition). New York: Dover Publications, Inc., 1964.

9. *The Illustrated Science and Invention Encyclopedia*. New York: H. S. Stuttman Company, 1977.
10. Cowan, Eugene W. *Basic Electromagnetism*. New York: Academic Press, Inc., 1968.
11. Kittel, Charles *Introduction to Solid State Physics* (Sixth Edition). New York: John Wiley and Sons, Inc., 1986.
12. Doebelin, Ernest O. *Measurement Systems: Application and Design*. New York: McGraw-Hill, Inc., 1983.
13. Horowitz, Paul and Winfield Hill. *The Art of Electronics* (Second Edition). New York: Cambridge University Press, 1989.
14. Park, K.T. *Analysis and Design of a Novel Robotic Tactile Sensor Utilizing Polyvinylidene Fluoride*. PhD dissertation. Drexel University, 1986.
15. Pettit, Joseph M. and Malcolm M. McWhorter. *Electronic Switching, Timing, and Pulse Circuits*. New York: McGraw-Hill, Inc., 1970.
16. Kraus, John D. *Electromagnetics* (Third Edition). New York: McGraw-Hill, Inc., 1984.
17. Kanzig, Werner. *Ferroelectrics and Antiferroelectrics*. New York: Academic Press, Inc., 1957.
18. Mason. Warren P. *Piezoelectric Crystals and Their Application to Ultrasonics*. New York: D. Van Nostrand Company, Inc., 1950.
19. Megaw, Helen D. *Ferroelectricity in Crystals*. London: Methuen and Company, Ltd., 1957.
20. Jaffe, Bernard and others. *Piezoelectric Ceramics*. New York: Academic Press, Inc., 1971.

21. Kawai, Heiji. "Piezoelectricity of Poly(vinylidene fluoride)," *Japan Journal of Applied Physics*, 8: 975-976 (May 1969).
22. Furukawa, Takeo. "Piezoelectricity and Pyroelectricity in Polymers," *IEEE Transactions on Electrical Insulation*, 24: 375-393. New York: IEEE Press, 1989.
23. Carlisle, Ben H. "Piezoelectric Plastics Promise New Sensors," *Machine Design*, 10: (Reprint) 1-6 (October 1986).
24. Omar, M. Ali. *Elementary Solid State Physics: Principles and Applications*. Reading MA: Addison-Wesley Publishing Company, Inc., 1975.
25. Analog Devices. *Linear Products Databook*. Norwood MA: Analog Devices, Inc., 1988.

## Vita

Captain Ted H. Halley was born on 6 October 1958 in Norwalk, California. He graduated from Opelika High School in Opelika, Alabama in 1977 and attended Auburn University, graduating with a Bachelor of Mechanical Engineer degree in 1982. After graduating, he received a reserve commission in the USAF and was assigned to the Armament Division of AFSC at Eglin AFB, Florida. He worked there as an AMRAAM (Advanced Medium Range Air-to-Air Missile) Mechanical Engineer in the 3246th Test Wing. His primary responsibilities on the AMRAAM program included: 1) All captive carry vibration analysis, 2) fuse and endgame analysis, and 3) seeker analysis. In January 1987 he was assigned to the Ballistic Missile Office (BMO) at Norton AFB, California. At BMO, he served as a project officer on the Peacekeeper Rail Garrison program. He was responsible for the mechanical integration of the entire train and development of the Launch Control Car and Security Car. In May 1989 Captain Halley entered the Air Force Institute of Technology to pursue a Masters Degree in Aeronautical Engineering.

Permanent Address: 633 Overbrook Circle

Ft Walton Beach, FL 32548



December 1990      Master's Thesis

Development of a Piezoelectric Polymer Film  
Pressure Transducer for Low Frequency and  
Dynamic Pressure Measurement

Ted H. Halley, B.M.E., Captain, USAF

Air Force Institute of Technology  
WPAFB OH 45433-6583

AFIT/GAE/ENY/90D-09

Approved for public release;  
distribution unlimited

The purpose of this research was to investigate the characteristics of a small and inexpensive pressure transducer made from piezoelectric film. The pressure transducer was designed to be small and surface mountable so that the pressure distribution could be measured on an aerodynamic body. A charge reset technique was used to overcome the traditional limitations, low frequency measurements and charge decay, of a piezoelectric device. The resulting time history had to be integrated, so a method was developed to integrate the data and remove sources of error. The time history reconstruction technique was tested with a known input and found to accurately reassemble the original input. The piezoelectric film pressure transducer was tested in a flow field along side a commercial pressure transducer. The piezoelectric transducer's frequency response showed agreement with the frequency response of the commercial transducer. Also, the time history response of the piezoelectric transducer gave evidence that low frequency pressure measurements are possible with a piezoelectric pressure transducer.

Pressure Transducer, Pressure Gage, Piezoelectric Film,  
PVDF, Aerodynamic Testing, Pressure Measurement

143